University of Alberta

Microbial Cell Surface Reactivity and Silicification

by

Stefan Victor Lalonde 

A thesis submitted to the Faculty of Graduate Studies and Research
in partial fulfillment of the requirements for the degree of

Master of Science

Department of Earth and Atmospheric Sciences

Edmonton, Alberta
Fall 2006

Your file Votre référence
ISBN: 978-0-494-22301-7
Our file Notre référence
ISBN: 978-0-494-22301-7

Abstract

Some of the oldest physical evidence for life on Earth is preserved in siliceous sediments as microfossiliferous remains. In order to better understand the earliest fossil record, thermophilic *Aquificales* and mesophilic cyanobacterial genera were experimentally silicified. Silica adsorption to cyanobacterial surfaces was undetectable under all conditions investigated, while cultures of *Aquificales* adsorbed significant amounts of colloidal silica, and only under conditions of silica supersaturation. For both organisms, a biological response to the silicification processes was observed, manifest by qualitative and quantitative changes in chemistry at the interface between the cell and the aqueous phase. Using mesophilic cyanobacteria, surface chemical changes were further explored as a function of diverse growth conditions. It is demonstrated that the bacterial surface is dynamic, such that surface chemical properties may be altered as a survival strategy in response to nutritional or geochemical stress, with implications for microbial silicification and microbe-mineral interactions in general.

Acknowledgments

The realization of this thesis could not have been possible without the generous support of my family, friends, and colleagues. In particular, I would like to thank Dr. Anna-Louise Reysenbach, Dr. Scott Smith, and Dr. George Owttrim for their critical technical contributions, logistical support, and most importantly, sincere personal encouragements. Friends such as Dr. Paula Aguiar, Larry Amskold, and most especially, Kati Kovacs, helped me through difficult times with their companionship.

I am hugely grateful for the unwavering confidence of Dr. Kurt Konhauser. He accepted me as a summer undergraduate student on faith alone, and has treated me as a colleague, and a friend, ever since. Through his guidance and trust, he provided me with the means to develop and express my passion for Geomicrobiology, and for that I shall always remain indebted to him.

Lastly, I would like to thank my immediate family for their lifelong support; my brother Andre for his limitless kinship, and my mother Lucille for her unconditional love. With utmost gratitude, I dedicate this thesis to them.

Table of Contents

List of Tables

List of Figures

CHAPTER 1

An introduction to microbial silicification and cell surface chemistry

1.1 Background[1]

Microorganisms are the most ubiquitous forms of life on Earth. They are capable of surviving conditions ranging from high vacuum to thousands of atmospheres, from below freezing to above boiling, in the absence of sunlight or under heavy flux of ionizing radiation. It is not surprising that microorganisms are found in nearly every surface environment, including locations where the chemical or physical environment is hostile enough to preclude all other forms of life. In aquatic systems, microorganisms are typically present in concentrations of 10^5 -10^6 cells/ml, and in environments where their growth is largely unchecked by grazing, such as the case at hydrothermal vents, concentrations can reach 10^9 cells

[1] See Konhauser (2006) for a comprehensive review.

per ml. Microbial biomass on Earth represents upwards of 100% of the total organic carbon sequestered by plants, and may in fact be even more important if microbial communities are confirmed to be extensive in the Earth's subsurface (Teske, 2005).

Microorganisms were also the first life forms to inhabit the Earth, and thrived in the absence of macrobiota for the greater part of Earth history, from their origin over 3.5 Gya to as recently as ~1 Gya. They were responsible for affecting the global biogeochemical processes that shaped the atmosphere, hydrosphere, and lithosphere into their present states, and to this day they continue to exert significant control over the chemical state of surface environments. The study of life's antiquity on Earth not only provides a context for understanding the modern microbial processes shaping the planet, but also has profound scientific and philosophical implications for the existence of extraterrestrial life.

The majority of Precambrian cellular microfossils are preserved in siliceous sediments. In this thesis, the preservation of microbial fossils by silicification is examined in consideration of preservation biases that may exist in the rock record. Such biases may arise as the result of species-specific patterns of preservation, which are inextricably a function of the chemical reactions occurring on a microbial surface during exposure to mineralizing silica solutions. In this regard, a diversity of microbial surface chemistry is explored within a quantitative framework that is directly applicable to models accounting for surface chemical reactions.

1.2 Microbial silicification

The inorganic precipitation of silica is often an inevitable process occurring in many modern hydrothermal systems, most of which host diverse microbial communities. The interaction between the various microbes and the mineralizing solutions they inhabit is of particular scientific interest because of the extremely high preservation potential of microbial remains in such environments. In particular, ancient chert deposits often retain chemical, isotopic, and

morphological fossil remnants of microbes, as well as their growth patterns (i.e., laminations, morphology, etc.), over geological time scales. Indeed, chert-rich formations in Australia and South Africa provide some of the oldest records of life on Earth, extending back at least 3.5 Gya (see Chapter 2).

The geochemical conditions favoring the precipitation of amorphous silica and preceding its alteration to chert are observed in natural hot spring waters today. When hot fluids originating at equilibrium with quartz from deep reservoirs are discharged at the surface, they are quickly rendered supersaturated with respect to amorphous silica by the combined actions of degassing, rapid cooling, decompression, and pH change (Konhauser et al., 2004). The processes of silica polymerization and precipitation, while induced by inorganic factors, are frequently observed to result in the complete encrustation of microbial assemblages *in situ*. Modern hot spring systems have been used as analogues for the study of microfossilization as it pertains to the Precambrian (Schultze-Lam et al., 1995, Konhauser et al., 2001, Konhauser et al., 2003), and similar conditions have been reproduced *in vitro* for controlled silicification experiments (See Konhauser et al., 2004, for review). Carefully designed experiments aimed at expanding our knowledge of the microbial silicification process, such as those described in Chapter 2, are absolutely necessary in order to identify variables influencing the long-term preservation of life's signatures.

Laboratory silicification studies have been limited to date despite their importance; for example, it has only recently been demonstrated using laboratory cultures that cyanobacteria remain viable and photosynthetically active despite complete silica encrustation, and that UV-absorbing silica sinter may even have afforded protection from the sterilizing UV radiation thought to be prevalent at the surface of the early Earth (>2.2 Gya) (Phoenix et al., 2000; Phoenix et al., 2001). Other microbial silicification experiments performed *in vitro* have revealed that species-specific patterns of silicification exist (Horogyski et al., 1992, Westall et al., 1995, Westall, 1997, Toporski et al., 2002) and have alluded to

possible roles in silicification for the various surface biomaterials[1] that bacteria expose to their extracellular milieu (Westall, 1997, Urrutia and Beveridge, 1993, Benning et al., 2004). In other words, microorganisms silicify at different rates, with different degrees of fidelity, and silicification proceeds as a function of the chemical composition of their outermost surfaces (Konhauser et al., 2004).

Microbial surfaces exposed to silica-supersaturated solutions appear to mineralize by the adsorption of preformed silica colloids, a physico-chemical process that may be described by a combination of inorganic chemical and physical processes that are inherently dictated by the surface chemistry of the microbe of interest (Chapter 2). In turn, differential surface chemistry between microbial genera results in preservation biases that determine which microorganisms are preferentially fossilized in the rock record. Complicating the matter is the fact that species-specific biological responses to the silicification process, such as cyanobacterial sheath thickening (Benning et al., 2004), increased biofilm extrusion (Chapter 2), and cell surface functional group redistribution (Chapter 4), are now being reported. Such biological responses to the silicification processes provide the potential for preservation bias beyond that inherent to the initial silica-cell wall interaction. Furthermore, the modification of bacterial surface chemical properties in response to a geochemical stressor, such as silica, has important ramifications beyond the silicification process, as discussed below (Chapter 1.3).

In Chapter 2, the experimental silicification of a chemolithoautotrophic, biofilm-forming thermophile (*Sulfurihydrogenibium azorense*) confirms previous hypotheses regarding specific interactions between various aqueous silica phases (silica monomers, polymers, and colloids) and the bacterial surface. It is further revealed in Chapter 2 that there exists a biological response to silicification on the behalf of this deeply-branching thermophile, manifest by changes in biofilm production as measured by soluble protein concentrations, and dependent on the nutrient source utilized by this metabolically-versatile organism. It appears that

[1] Including sheaths, capsules, polysaccharidic and proteinaceous extracellular polymeric substances (EPS), and Gram-negative and Gram-positive cell walls.

the abnormally cationic nature of the biofilm surface is, in part, responsible for its propensity to adsorb negatively-charged silica colloids from solution.

Similar experiments performed using the cyanobacterium *Anabaena* sp. strain PCC 7120 indicates a much different scenario; despite the cyanobacteria becoming effectively silicified after repeated and prolonged exposure (up to 30 days) to polymerizing silica solutions (Fig. 1-1), the affinity for monomeric and colloidal silica to the cyanobacterial Gram-negative cell wall is so low that it cannot be measured at realistic silica:biomass concentration ratios. Figure 1-2 demonstrates that any silica adsorbed to the Gram-negative cyanobacterial surface at biomass concentrations up to 5 g/L is within the limits of experimental error. Consequently, the quantitative assessment of this microbial surface in terms of reactivity towards silica must be done using a proxy indicator. Chapters 3 and 4 assess surface proton sorptive capacity rather than silica sorptive capacity, and by doing so, allow for the complete characterization of this cyanobacterial species in terms of cell wall chemical reactivity, surface charging behavior, and specific biological responses, chemically manifested at the microbial surface, to various nutritional and geochemical stressors. Such a molecular-scale understanding of the microbial surface is vital in order to fully evaluate the mechanisms and diversity of microbe-mineral interactions, including those involving silica.

1.3 Bacterial cell surface chemistry

Chemical reactions occurring at any solid-water interface, including hydrolysis, adsorption, precipitation, dissolution, ion-exchange, polymerization, and oxidation-reduction, are largely dependant upon surface electrical charging behavior, which is, in turn, determined by the properties and concentrations of chemical functional groups exposed to the aqueous environment (Davis and Kent, 1990). Some minerals, such as micas, zeolites, and clay minerals, possess permanent structural surface charges that arise from cationic substitution within their crystal lattice, while others, such as metal oxyhydroxides and complex organic macromolecules, develop charge solely as the result of surface functional group protonation/deprotonation reactions (Langmuir, 1997). For example, the

typical negative charge associated with the cell walls and extracellular layers of microorganisms develops as a function of pH, primarily via the following four functional group deprotonation reactions:

$$R\text{-}COOH \rightarrow R\text{-}COO^- + H^+ \qquad (1)$$

$$R\text{-}PO_4H_2 \rightarrow R\text{-}PO_4H^- + H^+ \qquad (2)$$

$$R\text{-}NH_3^+ \rightarrow R\text{-}NH_2 + H^+ \qquad (3)$$

$$R\text{-}OH \rightarrow R\text{-}O^- + H^+ \qquad (4)$$

Reactions (1) and (2) proceed spontaneously at neutral pH, and the deprotonated ligands are responsible for the bulk of the overall cell surface negative charge typical of microbial surfaces at pH values greater than ~3 (Bayer and Sloyer, 1990). Reaction (3) occurs at pH values between 8-11 (Hunt, 1986), and reaction (4) only becomes significant at pH values around 11 (Martell and Smith, 1989), thus negligibly affecting microbial surface charge under most conditions. In addition to determining overall surface charge, these functional groups also act as highly efficient ligands for the complexation of various metal cations and as nucleation sites for a variety of authigenic mineral phases (see Chapters 3.1 and 4.1). In other words, these proton-active surface sites, highly reactive to many aqueous geochemical solutes, serve as the primary biological components in the initial stages of microbe-mineral interaction. Considering the large surface area to volume ratios of most microorganisms, their ubiquity in the environment, and their high cell densities (10^5 – 10^6 cells/ml in most aquatic environments (Fenchel et al., 2000)), it becomes clear how microorganisms have come to be responsible for effecting global biogeochemical cycles (see Konhauser (2006) for review).

The ability to accurately describe their reactive surfaces in a quantitative framework is paramount to any mechanistic understanding of their geochemical influence. Metal adsorption to a biological or mineral surface is largely an electrostatic phenomenon, dictated by the structural and compositional nature of the exposed functional groups, as well as the unique physico-chemical properties of each sorbate forming a surface complex (Langmuir, 1997). Quantitative

constraints regarding the availability (in terms of concentration) of surface sites where adsorption reactions may occur is readily assessed by potentiometric titration; the desorption of surface functional group protons can be quantified as a function of pH, and to this data, concentrations and stability constants of discrete surface functional groups may be fitted for bacterial (e.g., Fein et al., 1997; Cox et al., 1999) and mineral surfaces (e.g., Kennedy et al., 2003; Smith and Ferris, 2003). The result is a set of parameters quantitatively describing a surface, which may be extrapolated to predict interactions between the ligands of this surface and competing aqueous species in complex solutions in a surface complexation model approach (e.g., Fowle and Fein, 1999).

While chemical descriptions of the microbial surface are paramount for the mechanistic understanding of its role in various microbe-mineral interactions, only recently has microbial surface reactivity been considered in a biological, rather than geochemical, paradigm. Biological systems are inherently dynamic, responding to a variety of stimuli that range in scale from molecular to global. However, chemical and mathematical methods in the field of interface chemistry have largely been developed for application towards inorganic, mineral surfaces. In a seminal study, Fein et al. (1997) applied such methods to describe the surface of the Gram-positive bacterium *Bacillus subtilis* within a quantitative surface chemistry framework that allows for the extrapolation of "inherent" surface properties to predict ion sorption behavior under geochemically diverse conditions. Daughney et al. (2001) first highlighted the possibility that the microbial surface, for a single species, may vary with regards to chemical reactivity as a function of biological parameters. Using potentiometric titration data, they demonstrate that surface chemical reactivity varies as a function of growth phase in batch culture. Since then, studies by Borrok et al. (2004) and Haas (2004) similarly investigated variability in bacterial surface chemical parameters as a function of nutrient supply in addition to culture age (See Chapters 3.1 and 4.1).

In Chapter 3, the surface chemistry of *Anabaena* sp. is investigated as a function of growth phase and nitrogen acquisition pathway in order to contribute

to current knowledge of metabolic controls on bacterial surface chemistry with special regard to biological factors that are inherent to batch culture techniques employed in microbiology (and geomicrobiology) laboratories worldwide. In Chapter 4, a cyanobacterial reaction to the silicification processes is assessed in a surface chemical context that allows for the direct comparison of geochemical stressors and batch culture growth conditions as potential determinants of cell surface reactivity.

Over the course of this MSc and to facilitate the discrete site modeling of surface chemical data by linear programming (Chapters 3 and 4), a computer script was written for the MATLAB environment (version 6.5.1, The Mathworks, Inc., Natick, MA) and is included in Appendix 1.

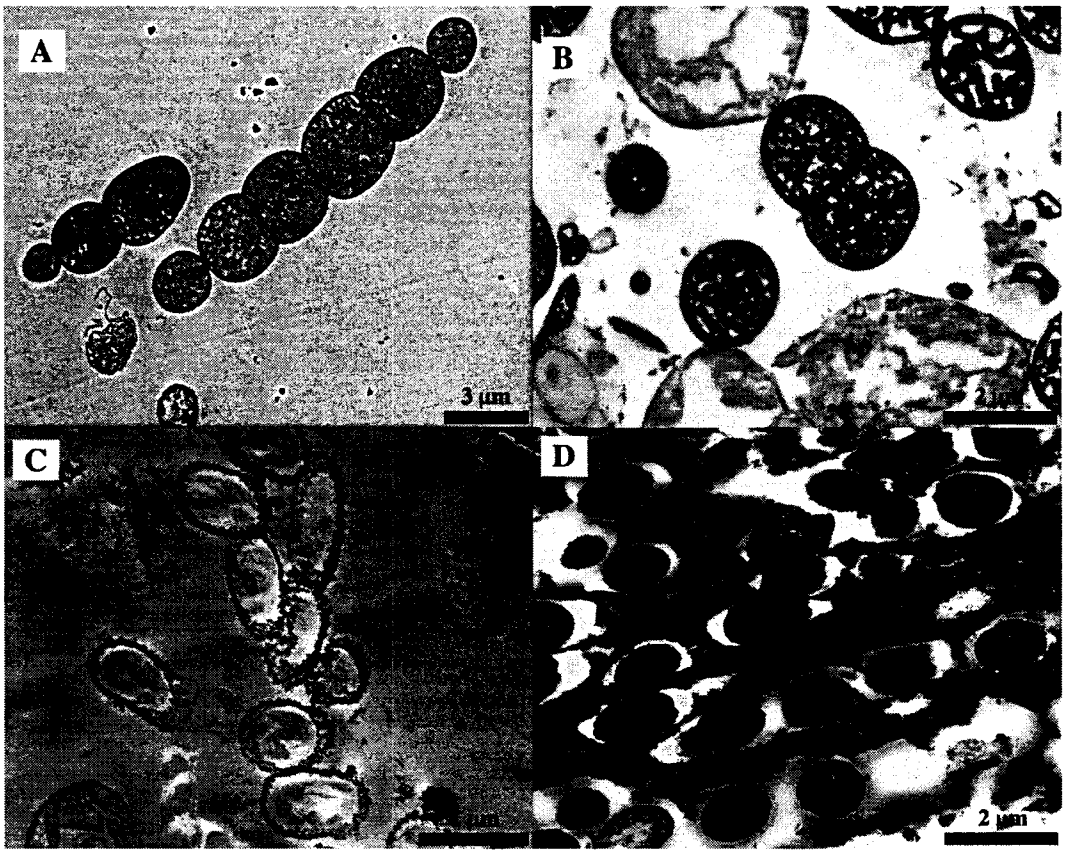

Figure 1-1. TEM micrographs[1] depicting the progressive silicification of *Anabaena*: (A) Intact filaments prior to silica exposure, (B) after 14 days of repeated exposure to polymerizing silica solutions, extensive cell lysis is evident, (C) after 21 days of exposure, cytoplasmic contents are lost and cell wall permineralization occurs, and (D) upon desiccation after 30 days of exposure, cells are imbedded in a matrix of amorphous silica.

[1] TEM preparation and imaging were performed according to methodology outlined in Chapter 2.2

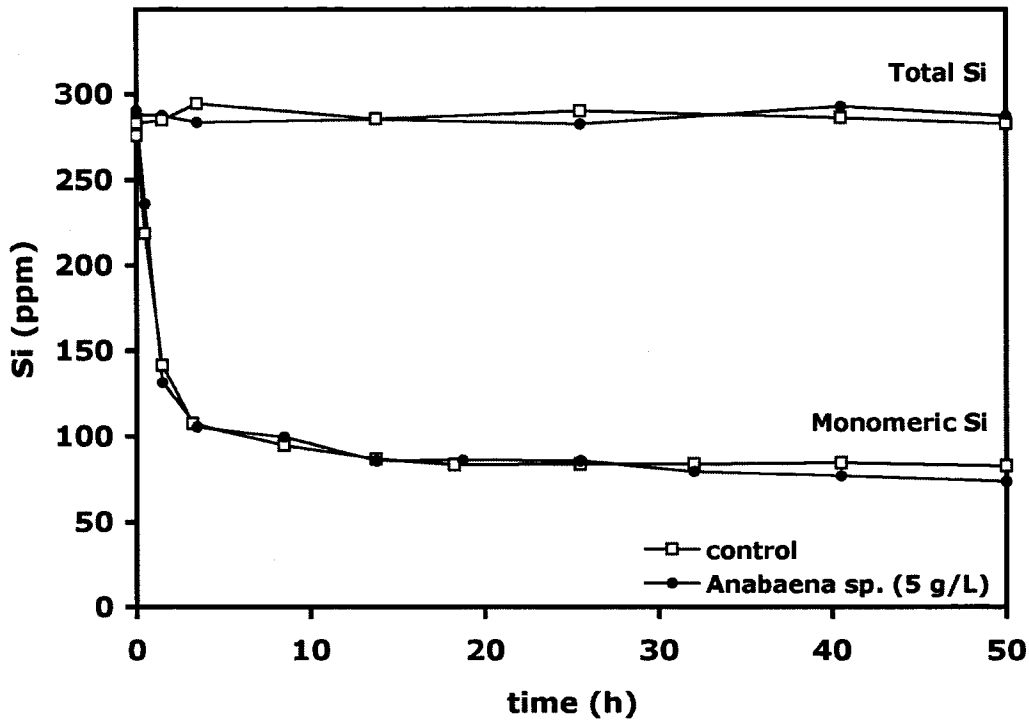

Figure 1-2. Silicification of a concentrated suspension (5 g/L) of *Anabaena* sp. strain PCC 7120 cells. Cells were concentrated by centrifugation and exposed to 300 ppm Si circumneutral silica solution (pH 8) that was rendered supersaturated with respect to amorphous silica by pH neutralization.[1] Monomeric silica condenses to form polymers and colloids, approaching silica saturation (~55 ppm) within 50 hours in both experiment and control. Similarly, the unchanging total Si concentration demonstrates that any adsorption of polymeric and colloidal silica is undetectable in this system.

[1] Silicification was performed according to methodology outlined in Chapter 2.2 and cyanobacterial culture methods outlined in Chapter 3.2

1.4 References

Bayer ME and Sloyer Jr. JL (1990) The electrophoretic mobility of Gram-negative and Gram-positive bacteria: an electrokinetic analysis. *Journal of General Microbiology* 136, 867-874.

Benning LG, Phoenix VR, Yee N, and Konhauser KO (2004) The dynamics of cyanobacterial silicification: an infrared micro-spectroscopic investigation. *Geochimica et Cosmochimica Acta* 68, 743-757.

Borrok D, Fein JB, Tischler M, O'Loughlin E, Meyer, H, Liss M, and Kemner KM (2004) The Effect of Acidic Solutions and Growth Conditions on the Adsorptive Properties of Bacterial Surfaces. *Chemical Geology* 209, 107-109.

Cox JS, Smith DS, Warren LA, and Ferris FG (1999) Characterizing heterogeneous bacterial surface functional groups using discrete affinity spectra for proton binding. *Environmental Science and Technology* 33, 4514–4521.

Daughney CJ, Fowle DA, and Fortin DF (2001) The effect of growth phase on proton and metal adsorption by Bacillus subtilis. *Geochimica et Cosmochimica Acta* 65, 1025-1035.

Davis JA and Kent DB (1990) Surface complexation modeling in aqueous geochemistry. *In* Mineral-water interface geochemistry (eds. Hochell MF and White AF). *Reviews in Mineralogy* 23, 177-260.

Fein JB, Daughney CJ, Yee N, and Davis TA (1997) A chemical equilibrium model for metal adsorption onto bacterial surfaces. *Geochimica et Cosmochimica Acta* 61, 3319-3328.

Fenchel T, King GM, and Blackburn TH (2000) *Bacterial Biogeochemistry. The*

ecophysiology of mineral cycling, 2nd edition. Academic Press, San Diego, CA.

Fowle DA and Fein JB (1999) Competitive adsorption of metal cations onto two Gram positive bacteria: testing the chemical equilibrium model. *Geochimica et Cosmochimica Acta* 63, 3059-3067.

Haas,JR (2004) Effects of cultivation conditions on acid-base titration properties of *Shewanella putrefaciens. Chemical Geology* 209, 67-81.

Horodyski RJ, Bauld J, Lipps JH, and Mendelson CV (1992) Preservation of prokaryotes and organic-walled and calcareous and siliceous protists. In: Schopf JW and Klein C (eds), *The Proterozoic Biosphere.* Cambridge University Press, Cambridge, pp. 185-193.

Hunt S (1986) Diversity of biopolymer structure and its potential for ion-binding applications. In: Eccles H and Hunt S (eds), *Immobilization of Ions by Bio-Sorption.* Ellis Harwood, Chichester, UK, pp. 15–46.

Kennedy CB, Martinez RE. Scott SD, and Ferris FG (2003) Surface chemistry and reactivity of bacteriogenic iron oxides from Axial Volcano, Juan de Fuca Ridge, north-east Pacific Ocean. *Geobiology* 1, 59-69.

Konhauser KO, Phoenix VR, Bottrell SH, Adams DG, and Head IM (2001) Microbial-silica interactions in modern hot spring sinter: Possible analogues for Precambrian siliceous stromatolites. *Sedimentology* 48, 415-435.

Konhauser KO, Jones B, Reysenbach AL, and Renaut RW (2003) Hot spring sinters: keys to understanding Earth's earliest life forms. *Canadian Journal of Earth Sciences* 40, 1713-1724.

Konhauser KO, Jones B, Phoenix VR, Ferris FG, and Renaut RW (2004) The microbial role in hot spring silicification. *Ambio*, 33, 552-558.

Konhauser KO (2006) *Introduction to Geomicrobiology.* Blackwell Scientific Publications, Oxford, England.

Langmuir D (1997) *Aqueous Environmental Geochemistry.* Prentice Hall, Upper Saddle River, NJ.

Martell AE and Smith RM (1977) *Critical stability constants.* Plenum Press, New York, NY.

Phoenix VR, Adams DG, and Konhauser KO (2000) Cyanobacterial viability during hydrothermal biomineralization. *Chemical Geology* 169, 329-338.

Phoenix VR, Konhauser KO, Adams DG, and Bottrell SH (2001) Role of biomineralisation as an ultraviolet shield: Implications for Archean life. *Geology* 29, 823-826.

Schultze-Lam S, Ferris FG, Konhauser KO, and Wiese RG (1995) In situ silicification of an Icelandic hot spring microbial mat: Implications for microfossil formation. *Canadian Journal of Earth Sciences* 32, 2021-2026.

Smith DS and Ferris FG (2001) Proton binding by hydrous ferric oxide and aluminum oxide surfaces interpreted using fully optimized continuous pK_a spectra. *Environmental Science and Technology* 35, 4637-4642.

Teske AP (2005) The deep subsurface is alive and well. *Trends in Microiology* 13, 402-404.

Toporski JKW, Steele A, Westall F, Thomas-Keprta KL, and McKay DS (2002) The simulated silicification of bacteria – new clues to the modes and timing of bacterial preservation and implications for the search for extraterrestrial microfossils. *Astrobiology* 2, 1-26.

Urrutia MM and Beveridge TJ (1993) Mechanism of silicate binding to the bacterial cell wall in Bacillus subtilis. *Journal of Bacteriology* 175, 1936-1945.

Westall F, Boni L, and Guerzoni E (1995) The experimental silicification of microorganisms. *Palaeontology* 38, 495-528.

Westall F (1997) The influence of cell wall composition on the fossilization of bacteria and the implications for the search for early life forms. In: Cosmovici C, Bowyer S, Werthimer D (eds) *Astronomical and Biochemical Origins and the Search for Life in the Universe*. Editori Compositrici, Bologna, pp. 491-504.

CHAPTER 2

The experimental silicification of *Aquificales* and their role in hot spring sinter formation[1]

2.1 Introduction

Much of what we understand about the early evolution of life comes from the examination of bacterial structures preserved in chert and cherty metasediments. The majority of the oldest Archean microfossils have filamentous or coccoid morphologies and appear to have grown as microbial mats in semi-restricted basins where a combination of high productivity, limited water circulation and high salinity facilitated greater cellular preservation (Horodyski et al., 1992). Additionally, rapid mineralisation was necessary to limit post-mortem degradation, a condition most commonly met by silicification in shallow, silica-supersaturated waters (Knauth and Lowe, 2003). The microfossils consist exclusively of the remains of cell sheath and cell wall material, while the

[1] Lalonde SV, Konhauser KO, Reysenbach A-L, and Ferris FG. *Geobiology* **3**, 41-52.

cytoplasm and other cellular content have either completely decayed or formed remnant structures unrelated to the original structure (e.g., Knoll et al., 1988). As a consequence of the poor preservation, comparisons between microfossils and modern microbes have largely been based on size and morphology. This has led to the suggestion that many of the Archean microfossils represent cyanobacteria (e.g., Schopf and Packer, 1987; Awramik, 1992) or alternatively, anoxygenic photosynthetic bacteria, e.g., *Chloroflexus* (Walter et al., 1972).

A number of experimental studies have attempted to determine the physical changes associated with various bacteria during silicification (e.g., Oehler and Schopf 1971; Oehler 1976; Francis et al. 1978; Westall et al. 1995; Westall 1997; Toporski et al. 2002). These studies show that species-specific patterns of silicification exist, and that different microbes are capable of being silicified with different degrees of fidelity. Interestingly, all of the studies have focused on phototrophic or heterotrophic mesophilic bacteria, with an emphasis on cyanobacterial species. Surprisingly, no studies that we are aware of have attempted to silicify thermophilic or chemolithoautotrophic bacteria.

There are a number of reasons why the earliest microfossils could represent microorganisms that grew bathed in hot, silica-supersaturated fluids, perhaps sheltered from surface UV exposure (e.g., Nisbet and Sleep, 2001):

(1) It is believed that the early oceans were warm (Knauth et al., 2003) and supersaturated with respect to amorphous silica (Siever, 1992; Tice and Lowe, 2004). At present, microorganisms adapted to life at high temperatures and high silica concentrations are restricted to modern hot springs and hydrothermal vent systems, environments presumed to be much more prevalent in the early Archean (Farmer, 2000). Importantly, re-interpretation of the 3.46 Gyr Apex Chert 'microfossils' of the Warrawoona Group, Western Australia, has led to the suggestion that the chert 'clasts' are not riverine, but instead hydrothermal deposits, and that if these structures are actually biogenic, they would likely have been thermophilic (Brasier et al., 2002). Similarly, the recent discovery of pyritic, thread-like filaments in 3.2 Gyr volcanogenic massive sulphides from the Pilbara

Craton of Australia indicates that chemolithoautotrophic thermophiles lived in, or around, hydrothermal systems at that time (Rasmussen, 2000).

(2) In the high-temperature regimes around hot spring vents, photosynthesis is inhibited by elevated temperatures, and chemolithoautotrophic bacteria dominate microbial assemblages (Reysenbach and Shock, 2002). Many thermophilic bacteria and archaea survive by oxidizing reduced gases emitted from the vents (e.g., H_2, H_2S). Despite a general preference for O_2 as the terminal electron acceptor, many species of the *Aquificales* are tolerant of, or even dependent on, reducing conditions where the oxidation of H_2 is coupled to S^0-reduction (Reysenbach and Shock, 2002). Such organisms likely thrived in the early Archean, and not surprisingly, phylogenetic evidence generally places such chemolithoautotrophic species as more deeply divergent than photosynthetic species, in accordance with a "hot" early Earth and hydrothermal origin of life (Bochetta et al., 2000).

(3) Regardless of the potentially high sulfur gas concentrations in the Archean atmosphere, without the presence of oxygen absorbing radiation at wavelengths 220 to 300 nm early photoautotrophs would have been subject to detrimental levels of solar radiation at ultraviolet wavelengths (Kasting, 1987). Conversely, an independence from sunlight meant that chemolithoautotrophs could have grown either as mats in deeper waters or under thick mineral crusts that would have sheltered the cells from the harmful UV rays (Pierson et al., 1993).

(4) Experimental silicification studies have confirmed that silicification appears to be an inevitable consequence of microbes growing in polymerizing, silica-supersaturated solutions, and that conditions favoring the precipitation of amorphous silica are induced by rapid pH or temperature changes (Phoenix et al., 2000; Yee et al., 2003). Modern analogues exist at hot spring vents where hot, pressurized, silica-rich geothermal fluids are rapidly exposed to surface conditions (Fournier, 1985). At this interface, thermophilic chemolithoautotrophs thrive at

the near-exclusion of other biota, where the geochemical conditions of their habitat render them more likely to be silicified.

Given the points above, it seems that interpretations of ancient microfossil assemblages based on experimental studies using only mesophilic species could be severely flawed. Additionally, little is known about the role of extracellular polymeric substances (EPS) secreted by many prokaryotes during the formation of biofilm, despite the fact that they may be more readily preserved than the bacteria that secreted them (Westall et al., 2000). As a result, in this study a preliminary attempt was made to address the above issues by experimentally silicifying *Sulfurihydrogenibium azorense,* a thermophilic, biofilm-forming, chemolithoautotrophic, anaerobic to microaerophilic member (Aguiar et al., 2004) of what has been considered the most deeply branching order of life characterized to date, the *Aquificales* (Bochetta et al., 2000). The role of two important chemolithoautotrophic metabolisms in silicification was assessed, and constraints are placed on potential interactions between silica species and the surfaces of *S. azorense*. The response of *S. azorense* to the initial stages of the mineralisation process affects its cellular preservation potential as well as potential roles in hot spring sinter formation.

2.2 Materials and Methods

2.2.1 Organisms and cultivation

Pure cultures of *S. azorense* Az-Fu1 were obtained from liquid nitrogen storage at the Oregon collection of methanogens (OCM 825) and are also available from Deutsche Sammlung von Mikroorganismen, Braunschweig, Germany (DSMZ 15241). Recently recognized as a new terrestrial species of the *Aquificales*, the biofilm-forming *Sulfurihydrogenibium azorense* strain Az-Fu1 was isolated from a terrestrial hot spring (68.4°C, pH 5.9) on São Miguel Island, Azores, in January 2001 (Aguiar et al., 2004). Initial cultures were grown in modified MSH media previously described by Aguiar et al. (2004). While the controlled-atmosphere conditions necessitated the use of borosilicate glass

Hungate tubes and serum bottles, the use of glassware was avoided wherever possible. Sodium hydroxide was used to adjust the pH of the media and was freshly prepared in order to prevent the introduction of leached silica during media preparation.

A final gas phase of CO_2:O_2:H_2 (41.6:1.8:56.6, v/v, 138 KPa) was established to contain O_2 (added after autoclaving) and H_2 (added upon inoculation) as the sole electron acceptor and donor, respectively. Constitutive metabolic limitation to H_2-oxidation was chosen for the starting cultures because *S. azorense* has been observed to grow in this combination of single electron donor and acceptor better than the other possible singular combinations (unpublished data). Small cultures were repeatedly transferred in mid-exponential phase under these conditions to establish cell populations that have consistently metabolized via H_2-oxidation. To establish adequate biomass, cultivation was initially performed in 15 ml Hungate tubes containing 8 ml of media and then transferred to 120 ml glass serum bottles containing 60 ml of media,

Cultures consistently limited to metabolism by S°-oxidation were established by inoculation and successive transfer into modified MSH media to which approximately 4 g S^0 had been added per liter. Insoluble S^0 was added directly to serum bottles prior to dispensing and autoclaving to ensure equal distribution. Oxygen was added prior to inoculation for a final gas phase of CO_2:O_2 (95:5, v/v, 106.4 KPa). The inoculum for S°-oxidizing cultures was initially obtained from the established H_2-oxidizing cultures. All cultivation and experiments were performed at 68° C.

2.2.2 Experimental silicification

Silicification experiments were performed in 120 ml serum bottles with an initial volume of 60 ml. Actively growing cultures (10 ml derived from the cultures established in modified MSH media) were inoculated into 40 ml solutions consisting of a combination of sterile water and appropriate electron

donors and acceptors, with 10 ml of a concentrated silica solution injected at initiation. All silicification experiments were performed at this 1/6 dilution of the modified MSH media to reduce interference with the molybdosilicate assay described in the next section. The initial concentrations of electron donors and acceptors remain fixed between cultivation and experiments, and growth during the experiments was uninhibited by the media dilution.

During preparation, glassware and other extraneous sources of silica were avoided wherever possible. Forty ml of anoxic 18MΩ water was dispensed into the serum bottles under a CO_2 atmosphere. Experiments established for S°-oxidation received 0.2 mg S° directly into the serum bottle prior to the dispensing of the water, and 3 ml O_2 was added after autoclaving.

The solubility of amorphous silica (SiO_2) was calculated to be 96 ppm Si at 68°C and pH 6.0 using the software package Geochemist's Workbench. A concentration of 90 ppm Si was chosen to evaluate the potential for bacterial silica adsorption slightly below the saturation state for amorphous silica at 68°C (i.e., at undersaturated conditions). An initial Si concentration of 300 ppm was chosen to ensure supersaturation while investigating the microbial response to silica polymerization. Such high concentrations have been documented in silica-rich natural hot spring effluents (e.g., Jones et al., 2003; Mountain et al., 2003). To attain these concentrations, silica solutions of 540 ppm and 1800 ppm Si, respectively, were prepared by the addition of $Na_2SiO_3 \cdot 5H_20$ to anoxic 18MΩ water (with an equilibrium pH >11). The silica solutions were stored alkaline at 90°C until the moment of initiation, to ensure that the silica remained entirely monomeric and molybdate-reactive.

Experiments were initiated by the injection of 10 ml of the appropriate concentrated silica solution, and were immediately adjusted to pH 6.0 by the addition of 1M HCl (1M NaOH for silica free controls) in an amount predetermined for each combination of silica solution and media. Biotic experiments received 10 ml of inoculum from the appropriate cell lines grown in modified MSH media. Conditions established for H_2-oxidation received H_2 gas to a pressure of 138 KPa as a final step. Experiments were performed in two ways:

(i) with initiation occurring immediately upon inoculation, and (ii) with initiation occurring approximately 20 h after inoculation, to characterize behavior for both actively growing and stationary phase cultures, respectively. Heat-killed experiments were similarly prepared, but were autoclaved for 25 min at 121 °C approximately 20 h after inoculation, and immediately initiated upon cooling to 68 °C.

Abiotic controls received an injection of the appropriate sterile media preheated to 68°C, and silica-free controls received injections of anoxic 18MΩ water preheated to 90°C. All media were preheated to 68°C prior to inoculation, and all experiments were performed in triplicate. Samples (2.5 ml) were removed by syringe after gentle inversion at various intervals for (i) visualization by transmission electron microscopy (TEM), (ii) analysis by modified Coomassie protein assay, and (iii) analysis using two molybdosilicate assays. Eight hundred µl of subsamples were preserved in 3% glutaraldehyde and stored at 4°C until preparation for TEM. Additional experiments were terminated mid-experiment to evaluate pH change over time, and for all experiments the final pH was recorded. For all graphs, error bars representing 95% confidence intervals were calculated as Z=1.96 multiplied by the standard error of the mean about each triplicate data point.

2.2.3 Colorimetric techniques

Colorimetry was performed using a Beckman DU520 UV/VIS spectrophotometer and plastic cuvettes with a 1 cm path length. Molybdate-reactive silica determinations were performed at the time of sampling.

The heteropoly-blue molybdosilicate method (Fannin et al., 1973) was used to measure molybdate-reactive silica concentrations. This technique was chosen because it provides increased sensitivity and resistance to interfering substances over the traditional molybdosilicate yellow technique (Fannin et al., 1973). Immediately upon sampling, 100 µl of sample was serially diluted to a factor of 200, and 2 ml of diluted sample was acidified with 40 µl of 2M HCl.

Eighty µl of 0.3 M ammonium molybdate solution (pH 8) was added simultaneously, followed 6 minutes later by the addition of 80 µl 0.6M oxalic acid solution to eliminate interference from phosphate. Twelve minutes after the addition of the ammonium molybdate reagent, 80 µl of reducing agent solution (containing 0.01M 1-amino-2-naphthol-4-sulfonic acid, 0.04M Na_2SO_3, and 1.44M $NaHSO_3$) was added, and the absorbance was read at 815 nm after 18 minutes.

In order to assess total silica concentrations, molybdate-unreactive silica was rendered molybdate-reactive by heated digestion with $NaHCO_3$ and H_2SO_4 (using methodology of Fanning and Pilson, 1973), and analyzed using the heteropoly blue technique as above. The two methods were standardized against a 1000 ppm Si atomic absorption reference standard (Fisher Chemicals, Fairlawn, NJ), and the analytical uncertainties (2σ) for the two silica determinations were ±2.6% and ±2.9%, respectively.

Protein concentrations were determined using the Coomassie Plus protein assay reagent kit (Pierce Biotechnology, Rockford, IL) and standardized to known concentrations of bovine serum albumin diluted into the medium of interest. A 0.5 ml aliquot of room temperature reagent was added to 1.0 ml of undiluted sample, incubated for 10 minutes, and the absorbance was read at 595 nm. This protocol produced linear absorbance values over a 1 – 25 µg ml^{-1} range for bovine serum albumin, and proved more sensitive for the experimental conditions than the suggested reagent to sample ratio of 1:1.

2.2.4 Sample preparation for TEM

Samples stored in 3% glutaraldehyde were washed three times in PBS buffer, remaining in the buffer for 10 minutes between each wash. Samples were then stained with 2% osmic acid for 2 hours, after which the PBS washes were repeated. Serial dehydration was performed using ethanol concentrations increasing in 10% increments, from 20% to 100%, with an incubation of 15 minutes at each increment. Samples were further incubated in 1:1 propylene oxide/100% ethanol, followed by propylene oxide, for 15 minutes each, after

which they were left in 1:1 propylene oxide/spurr resin for 12 hours. Samples were embedded in spurr resin and cured in a vacuum oven at 60°C for 24 hours, after which they were sectioned using a Reichert-Jung ultracut microtome, collected on copper grids and examined with a Morgani 268 Philips electron microscope. Selected grids were subsequently stained with 1% uranyl acetate to enhance the contrast of cell material.

2.2.5 Acid-base titrations

A 50 ml aliquot of *S. azorense* culture, grown under silica-free conditions limited to H_2-oxidation, was centrifuged at 20° C for 8 minutes at 10,400 *g*, and washed four times in 100 ml of 18MΩ water with similar centrifugation. The pellet was resuspended in 0.01M KNO_3 (pH ~ 5.5), transferred to a 100 ml titration flask containing 200 µl of 0.2M HNO_3, and diluted with 0.01 M KNO_3 to a final volume of 50 ml. An airtight lid, prefitted with an N_2 gas line and a precalibrated pH electrode connected to an autotitrator (Metrohm Titrino GP 736), was installed on the titration flask and the system was henceforth continuously purged with N_2 to prevent carbonate formation from CO_2 dissolution. The system was allowed to equilibrate until fluctuations in the pH reading were less than 0.5 mV min^{-1} for at least 25 minutes. Titrations were performed using the autotitrator's burette containing carbonate-free 0.01 M NaOH, delivered into the acidified suspension to increase the pH by increments of approximately 0.1 unit, over a range of 3 to 12 pH units. Discrete pK_a spectra were generated from the titration data using the Linear Programming Method (LPM) (Sokolov et al., 2001), and control titrations were performed in the absence of *S. azorense*.

2.3 Results

2.3.1 Growth under hydrogen-oxidizing conditions

2.3.1.1 Conditions undersaturated with respect to amorphous silica

In solutions with 90 ppm Si, the stability of monomeric silica and the absence of bacterial adsorption is illustrated by unchanging molybdate-reactive Si concentrations (Fig. 2-1). Although molybdosilicate colorimetry is often used to infer monomeric silica concentrations, silica polymers of low molecular weight may also remain molybdate-reactive upon polymerization, and therefore, such assays cannot yield true monomeric concentrations (Fannin et al., 1973). Results obtained reflect the speciation between monomers and small polymers that are molybdate-reactive, and larger polymers, colloids and precipitates that are rendered molybdate-unreactive by increased polymer length. As a result, the proportion of molybdate-reactive to molybdate-unreactive Si species is not only dependent on the conditions governing polymerization, but to some degree on the assay protocol itself (i.e., reagent concentrations, sample dilutions). A pH change over the course of the experiment was observed in the biotic experiments, corresponding to an average increase of approximately 0.3 pH units after 48 h.

The abiotic controls mimic the biological experiments in that they show no removal of molybdate-reactive Si from undersaturated solutions. The slight co-variations of Si concentration observed only in Fig. 2-1 were likely due to an inconsistency in the molybdosilicate technique specific to the time of sampling, as each culture and respective abiotic control were initiated, sampled and analyzed in parallel.

2.3.1.2 Conditions supersaturated with respect to amorphous silica

In the 300 ppm Si experiments, spontaneous polymerization occurred in both abiotic and biotic experiments after the addition of silica and pH neutralization. This is indicated by the decrease in the molybdate-reactive Si concentrations over time in both sets of experiments (Fig. 2-2). In the abiotic experiments, approximately 50% of the monomeric silica was rendered unreactive to the molydosilicate technique within 15 hours, after which changes in the

molybdate-reactive Si concentrations occurred slowly. These results highlight the strong chemical driving force for silica polymerization at high silica concentrations.

H_2-oxidizing cells of *S. azorense*, either growing exponentially (Fig. 2-2) or in stationary phase (results not shown) had a negligible effect on both the rate and extent of silica polymerization. Nonetheless, exponentially growing cells did immobilize up to 29 ppm Si (~12%) of the molybdate-unreactive silica, corresponding to approximately 7% of the total silica, after 50 hours of exposure (Fig. 2-3). By comparison, any silica retained on the serum bottles in the abiotic experiments was within the experimental error of the molybdosilicate technique.

2.3.1.3 Protein concentrations

While difficult to quantify, EPS production was visually observed to be most extensive under the conditions of H_2-oxidation, with biofilm completely covering the area of the liquid-gas interface (230 cm^2) after 24 h. With experimental conditions of S°-oxidation, however, the production of EPS appeared less important and was largely limited to association with the insoluble elemental sulfur. Under these conditions, the protein concentrations often fell outside the linear range of the Coomassie assay, hence, there was no accurate means of protein quantification in these experiments. In all cases growth was confirmed by light microscopy, although the biofilm-forming nature of growth made the monitoring of growth by cell counting unreliable.

Protein concentrations were monitored in the H_2-oxidizing experiments after the addition of silica solution. Experiments initiated during stationary phase growth were also monitored for protein concentrations after the injection of silica solution, with no increase in protein concentration or significant difference relative to silica-free controls observed (results not shown). For all exponentially growing cultures, a rapid increase in protein concentration was measured (Fig. 2-4), corresponding temporally to the onset of visible biofilm accumulation.

For experiments containing 0 and 90 ppm Si, exponential growth began approximately 12 hours after inoculation, resulting in similar maximum protein

concentrations (Fig. 2-4). The highest protein concentrations attained in the 0 ppm Si cultures occurred slightly later compared to those containing 90 ppm Si. This corresponded to a more rapid increase in protein concentration in the 90 ppm Si cultures. For cultures containing 300 ppm Si, an even more rapid increase in protein concentration was observed, occurring approximately 4 hours earlier than for cultures containing either 90 or 0 ppm Si. The unusual decrease and subsequent increase in protein concentration beginning at 14 h was observed for all of the triplicates containing 300 ppm Si. It was determined that such high silica concentrations had a negligible effect on the linear response of the Coomassie assay as performed. Specific growth rates based on protein concentrations were calculated as follows:

$$\text{Specific growth rate } (h^{-1}) = \frac{\ln c_1 - \ln c_2}{t_1 - t_2}$$

where c represents the concentration (in this case, μg/ml BSA protein equivalent) at time t.

A plot of the maximum growth rate achieved *vs* Si concentration (Fig. 2-5) revealed a linear relationship between growth rate and Si concentration of good fit (R^2=0.9997), although on the basis of three silica concentrations confidence in the relationship should be reserved.

2.3.2 Growth under sulfur-oxidizing conditions

2.3.2.1 Conditions undersaturated with respect to amorphous silica

Neither exponentially growing cells of *S. azorense* metabolizing by S°-oxidation nor their abiotic controls promoted the adsorption or polymerization of monomeric silica from solutions undersaturated with respect to amorphous silica (Fig. 2-6). The pH decreased a maximum of 0.3 pH units in concordance with the equation for metabolism by S°-oxidation:

$$S^0 + 3/2\ O_2 + H_20 \Leftrightarrow SO^{2-}_4 + 2H^+$$

2.3.2.2 Conditions supersaturated with respect to amorphous silica

The rate and extent of polymerization, as evaluated by the decrease in molybdate-reactive Si, was not affected by the presence of *S. azorense* growing in either stationary phase (unpublished) or exponential phase (Fig. 2-7). In both the biotic and abiotic experiments, silica polymerization occurred spontaneously with a rate and magnitude comparable to those observed under conditions of H_2-oxidation. Again, a maximum pH decrease of 0.3 pH units was observed in experiments containing *S. azorense* passing through exponential phase growth, with apparently little affect on the depletion of molybdate-reactive Si. Growth of *S. azorense* occurs between pH 5.5 and 7 (Aguiar et al., 2004).

Unlike the case of H_2-oxidation, no biological removal of silica outside of the experimental uncertainty was observed 50 hours after the injection of concentrated silica solution into cultures containing exponential phase or stationary phase cultures of *S. azorense* grown via S°-oxidation.

2.3.3 Acid-base titration

The acid-base titrations were performed on whole cells, without discrimination between EPS and cell surface functional groups, through a pH range of 3 to 12. The discrete pKa plot generated by LPM has a number of distinct pKa clusters (Fig. 2-8) to which functional groups may be assigned following the criteria outlined by Phoenix et al. (2002). Cluster A falls within the pH range over which carboxylic functional groups deprotonate. Clusters B and C may represent either carboxylic or phosphoryl groups, although cluster B is closer to the former's range, and cluster C, the latter. Cluster D likely represents phosphoryl groups, and cluster E, amine groups, as in Phoenix et al. (2002). Although hydroxyl groups are an abundant component of the hydrated polysaccharides that comprise EPS (Whitefield and Keenleyside, 1995), they would not have contributed to the titration profiles because they do not deprotonate at pH values <11, with the exception of phenolic sites (Perdue, 1985).

The most striking pKa peak (cluster F) can be assigned to amine functional groups. It appears that this functional group is present in greater

abundance relative to any other group, as evident from the height of the site density peaks. This observation is interesting in that the amine peak is somewhat more pronounced than that observed with either *Bacillus subtilis* or *Calothrix* sp. Overall, the titration data indicates that on a dry weight basis, the surfaces of *S. azorense* are less reactive than those of *Calothrix* sp. whole filaments. This is not surprising considering that the hydroxyl-rich EPS would contribute significant weight while not contributing exchangeable protons over the pH range of the titrations.

2.4 Discussion

2.4.1 The role of *S. azorense* during silicification

In recent years a number of experimental studies have attempted to elucidate the bacterial role in silicification (see Konhauser et al., 2004 for references). In this case, by considering both molybdate-reactive and total silica concentrations in the absence of silica flocculation, the extent of microbial silicification under the experimental conditions is be constrained to the adsorption of homogenously nucleated silica polymers and colloids, as discussed below.

2.4.1.1 Adsorption from silica-undersaturated conditions

Urrutia and Beveridge (1993) proposed that microbially-mediated silica precipitation might occur by silicate anion adsorption onto specific organic surface sites, such as positively-charged amine functional groups. This has been proven unlikely to occur from silica-undersaturated solution, as monomeric silica exists primarily as neutrally-charged H_4SiO_4 at circum-neutral pH conditions (Iler, 1979). Under alkaline (approximately pH > 9.5) conditions, where anionic silica species may dominate the aqueous Si phase (Iler, 1979), bacterial cell walls are highly electronegative due to the deprotonation of carboxyl and phosphoryl groups, which invariably would inhibit electrostatic attraction between aqueous $H_4SiO_3^-$ and any positively-charged amine groups that might exist under these conditions. The absence of monomeric silica adsorption to bacterial cell surfaces has recently been confirmed by several papers. Using *B. subtilis* (Fein et al., 2002;

Phoenix et al., 2003) and *Calothrix sp.* (Yee et al., 2003; Benning et al., 2004), it was shown that adsorption at circum-neutral pH is unlikely to remove significant quantities of soluble silica, as the affinity of monomeric silica for these bacterial surfaces was found to be negligible under these conditions.

In a near-neutral hot spring environment, higher temperatures allow for elevated concentrations of silica to be achieved, while still maintaining silica-undersaturated conditions; the solubility of amorphous silica at pH 6 is 96 ppm Si at 68°C *vs.* ~60 ppm Si at 30°C. By investigating the adsorption of silica from only slightly undersaturated solutions, reactions of even weaker affinity (at a very slight cost of colorimetric resolution) between monomeric silica species and bacterial cell surfaces could potentially be revealed. The use of the heteropoly blue molybdosilicate method in this study provided increased resolution over the molybdate yellow technique used in similar studies (e.g., Yee et al., 2003). With the increased sensitivity, the results confirm earlier observations; the adsorption of monomeric silica from undersaturated solutions does not significantly contribute to the bacterial silicification process.

2.4.1.2 Polymerization and precipitation in silica-supersaturated solutions

At hot springs, the sudden cooling of ascending hydrothermal fluids, decompressional boiling and degassing, fluid mixing, pH changes, and evaporation all contribute to a sudden increase in saturation state with respect to amorphous silica, leading to homogeneous nucleation (Fournier, 1985). In addition, it has been suggested that the high reactivity of microbial surfaces can lower activation energy barriers and promote the heterogeneous nucleation of amorphous silica (Schultze-Lam et al., 1995; Konhauser and Ferris, 1996; Konhauser et al., 2001). Indeed, the separation of microbial and inorganic influences on basic geochemical processes remains a primary goal of geomicrobiology. From our results, it might appear that species such *S. azorense* would have a limited role in this regard because they do not affect the rate or magnitude of silica polymerization outside of experimental uncertainty, regardless of metabolism or growth phase. This is not surprising; in many hot springs, the

high silica concentrations, continuous effluent flow, and rapid changes in silica solubility will result in the predominance of homogenous nucleation. Silica species heterogeneously nucleated on bacterial surfaces would be quantitatively insignificant, and such was the case during this study, where silica polymerization rates were unaffected by the presence of bacteria.

Without affecting the kinetics of polymerization, the biological immobilization of silica under the experimental conditions must have been limited to silica phases that are molybdate-unreactive (i.e., the large polymer, colloidal, and/or precipitate phases). Westall et al. (1995) have suggested that it is the polymeric/colloidal fraction that is bound to bacterial surfaces, and Heaney and Yates (1998) have discussed relations to hydrogen-bonding. Colloidal interaction is supported by frequent observations by electron microscopy that *in situ* bacterial silicification occurs by the immobilization of preformed nanosize siliceous spherules (Schultz-Lam et al., 1995; Konhauser and Ferris, 1996; Phoenix et al., 2000). The factors driving changes in saturation state will ultimately control the distribution of silica between monomeric, polymeric/colloidal, and precipitate phases, and therefore determine the proportion available for biomineralisation. For example, visual precipitate accumulation was not noted in the experiments containing 300 ppm Si after 50 h, allowing for a greater polymeric/colloidal silica fraction. Correspondingly, TEM images (Fig. 2-9, discussed below) indicate that silicification occurred by the adsorption of nanosize silica spheres. Colorimetric and visual observation indicates that the biologically removed silica was neither molybdate-reactive nor precipitate at the time of adsorption, and that the silica must have been in the polymeric/colloidal form.

In the absence of significant heterogeneous nucleation, it follows that the immobilization of negatively charged, molybdate-unreactive silica species by bacterial surfaces is decoupled from the initial polymerization process. Although Yee et al (2003) did not consider silica immobilization independent of polymerization, it has been subsequently demonstrated that in silica-supersaturated solutions, *Calothrix sp.* removed only ~3% more silica than bacteria-free systems, at the same time becoming encrusted in amorphous silica

precipitate (Benning et al., 2004). However, Phoenix et al (2003) found that *B. subtilis* failed to remove significant quantities of Si from silica-supersaturated solutions without the aid of cation bridging. With an apparent silica removal of ~7% for cells metabolizing via H_2-oxidation, our results indicate that *S. azorense* immobilized slightly more silica than *Calothrix sp.* from a 300 ppm Si solution, albeit at lower pH, lower biomass and higher temperature. The ability of a single bacterial cell to immobilize numerous large, preformed colloids, especially with the aid of the increased surface area offered by various exopolymers secreted by a wide range of thermophiles and mesophiles, might serve to explain potential discrepancies between *in situ* microbial silicification rates and laboratory simulations.

While the differing factors of pH and temperature between the Benning et al. (2004) study and our own experimental conditions undoubtedly yielded a colloidal fraction of different size and charge that is difficult to compare, at higher temperatures more silica will remain in solution. At concentrations supersaturated with respect to amorphous silica, the partitioning of the silica phases will favor the polymeric/colloidal rather than precipitate fraction, relative to lower temperature systems. The obvious implication is that, with interactions between microbes and silica initially limited to the colloidal phase, the silicification of microorganisms at higher temperatures would be accelerated relative to their counterparts inhabiting mesophilic niches, and even appear spontaneous at conditions where silica flocculation or precipitation is insignificant. Importantly, if the forces driving bacterial silicification are more important at higher temperatures, then microorganisms inhabiting such niches (i.e., thermophiles) would need to tolerant of the mineralisation process relative to mesophilic counterparts.

2.4.1.3 The effects of chemolithoautotrophic metabolism.

The different combinations of electron donors and acceptors used by *S. azorense* affected the amount of silica retained in the biomass. As discussed above, cells grown as H_2-oxidizers removed 7% of silica from solution, while the S°-oxidizers showed no significant quantity of silica removed from solution. This pattern may reflect a number of factors.

(1) *S. azorense* was observed to produce negligible EPS while metabolizing via S°-oxidation, and grew largely attached to the insoluble elemental sulfur particles. It appeared as though growth was less favorable under S°-oxidizing conditions, as indicated by unpublished cell counts and lower to undetectable protein concentrations.

(2) Cell surface functional groups, and hence surface charge, may be characteristically different for cells grown under different metabolisms. The cyanobacterium *Calothrix sp.* varies sheath production under different growth conditions (Benning et al., 2004), and the sheath and cell wall ligands contribute differently to overall surface charge (Phoenix et al., 2002). It is also known that surface charge can respond to changes in growth phase (Daughney et al., 2001), and it would be surprising if changes in metabolic conditions did not exert a similar effect.

(3) Proton extrusion (see equation 1) altered the pH of the batch culture, thereby potentially inhibiting silica adsorption to *S. azorense*. The pH differences between experiments containing *S. azorense* metabolizing via H_2-oxidation and S°-oxidation are indeed significant, with the H^+ concentration increased by a factor of 4 in the S°-oxidizing cultures, relative to H_2-oxidizing cultures. In highly acidic solutions, protons inhibit the silica polymerization process (Rothbaum et al., 1979), but our experiments were run at pH 6.0 and thus it is unlikely that protons inhibited the bulk polymerization. No effect on silica polymerization could be attributed to the pH difference between abiotic and bacterial experiments.

However, we cannot be certain that despite minimal changes to the bulk pH, there may have been immeasurable but drastic effects in the local microenvironment around the cell as the result of proton extrusion.

Irrespective of whether surface area, surface chemistry, or pH were the most significant factors in the metabolic effect, TEM micrographs of *S. azorense* grown by S°-oxidation in solutions supersaturated with respect to amorphous silica did not reveal silica aggregates on the cell surfaces. This result suggests that polymerization in those experiments did not lead to mineral formation. It is interesting to note that a phylogenetic survey of seven silica-depositing hot springs in Yellowstone National Park indicated that H_2-oxidation was the primary means of productivity (Hugenholtz et al., 1998). It is possible that the retention of silica associated with *S. azorense* during growth by H_2-oxidation may represent acclimatization to the increased silica deposition rates associated with conditions favoring that metabolism. However, further surveys of the primary means of productivity in silica-depositing hot springs is required for any correlation to be stated with confidence. Regardless, it appears that H_2-oxidation in silica-supersaturated springs will allow for a microbial contribution towards siliceous sinter formation. Our results suggest that specific study of microenvironmental regulations by chemolithoautotrophs, which we have demonstrated here to be viable in heavily mineralizing fluids, would undoubtedly yield important insights regarding ancient silicification.

2.4.2 The response of *S. azorense* to silicification

It has previously been demonstrated that *Calothrix sp.* can perform photosynthesis and remain viable when encrusted in a matrix of amorphous silica (Phoenix et al., 2000). It can do so because it produces a thick, electroneutral sheath that restricts silicification to the cell's outer periphery, and prevents cytoplasmic mineralisation (Phoenix et al., 2002). Sheath thickening during silicification has been implicated using synchrotron radiation Fourier-transform infra-red (SR-FTIR) studies on individual silicifying *Calothrix* filaments

(Benning et al., 2004). We present here preliminary findings that the EPS extruded by *S. azorense* could potentially serve to restrict silicification in an analogous fashion.

2.4.2.1 The restriction of silicification to EPS

Transmission electron micrographs of *S. azorense*, grown under conditions limited to H_2-oxidation and supersaturated with respect to amorphous silica, reveal the accumulation of spheroidal silica aggregates of ~20 nm in diameter after 50 hours. The close proximity of the cells (Fig. 2-9A) illustrates their aggregation in the biofilm matrix, yet the silica spheres were generally not observed in direct association with the cell wall. Instead, silicification is limited to the EPS surrounding the cells (Fig. 2-9B). In some cases, the accumulation of silica spheres could be observed to follow the shape of cell contours, while restricted to a distance of ~70 nm from the cell wall. The influence of preparatory procedures on TEM representation of the initial stages of laboratory silicification is unknown, although it is unlikely that such preparation resulted in the removal of silica from bacterial cell walls as various studies have demonstrated colloidal silica in association with cell walls using similar preparatory techniques (Konhauser and Ferris, 1996, Phoenix et al., 2000). Despite being permeable to soluble ions, the lack of silica accumulation on the cell wall suggests that the cell proper has the means of protecting itself from silicification, possibly via the continual secretion of a protective EPS.

2.4.2.2 Fluxes in Protein concentration during batch growth

Protein concentrations were observed to increase earlier, more rapidly, and achieve higher maximum values in cultures containing 300 ppm Si. Visually and in light micrographs, more extensive biofilm was also produced in those cultures. How the two observations are related cannot be demonstrated with our methods and results, but involves either (i) the cell doubling times being accelerated in the presence of silica or (ii) individual cells producing more protein-containing product(s) without altering cell division rates. The answer likely lies in a

combination of the two possibilities. While we are not aware of any nutritional role for Si during chemoautotrophic growth, the stress-induced production of biofilm has been documented for hyperthermophilic archaea and bacteria. For example, *Thermococcus litoralis* and *Thermotoga maritima* increase their production of exopolysaccharides with increasing dilution rates in continuous culture (Rinker and Kelly, 2000). *Archaeoglobus fulgidus* extrudes additional polysaccharides during pH, temperature, and metal/solute stress (LaPaglia and Hartzell, 1997). Furthermore, the relationship between growth rate and Si concentration does not appear to follow Monod kinetics at high Si concentrations (i.e., the plot remains first order at high Si), suggesting that the increased protein production at high Si concentration is not due to any nutritional role.

As biofilms are chemically heterogeneous assemblages containing and, in some cases, dominated by acidic polypeptides (Beveridge, 1981), we propose that the increased protein concentrations observed may be attributed in some part to increased EPS production. Importantly, a protein-rich EPS is supported by the potentiometric titrations; amine functional groups are overly abundant on a dry weight basis, and the EPS contributes a significant portion of that weight. Differential protein expression (Oosthuizen et al., 2002) as well as differential gene expression (Whiteley et al., 2001; Prigent-Combaret et al., 1999) have been previously indicated during biofilm formation. If EPS extrusion is a coping mechanism against cell silicification, biofilm-forming microorganisms would be able to tolerate environments where silica is precipitated more rapidly, relative to species with exposed cell walls.

2.4.2.3 A potential mechanism of polymeric/colloidal silica immobilization

To date, two mechanisms for microbial silicification have been invoked. In the first instance, *B. subtilis* has been used to illustrate the case for cation-bridging, where the carboxyl-dominated cell wall of *B. subtilis* makes it unable to bind silica in the absence of a cation bridge due to electrostatic repulsion (Fein et al., 2002; Phoenix et al., 2003). Second, immobilization by hydrogen-bonding has been implicated for cyanobacterial silicification. For example, acid-base titrations

of *Calothrix* reveal that the sheath is largely electroneutral, and the polysaccharides it contains provide abundant hydroxylgroups sites to hydrogen-bond with the hydroxyl groups of polymeric/colloidal silica (Phoenix et al., 2002).

The immobilization of silica as colloids, as well the increase in protein concentration observed during growth at states of silica supersaturation, point toward a mechanism for silica-microbe interaction previously considered unimportant. Urrutia and Beveridge (1993) originally proposed that microorganisms remove anionic silica by adsorption onto positively charged amine groups. For monomeric silica species, this has proven unlikely due to the lack of silicate anions at pH values below 9, and no experiments to date have revealed a bacterial removal of monomeric silica in the absence of a cation bridge. In the case of *S. azorense,* hydrogen-bonding between a polysaccharidic EPS and the electronegative and neutral silica species cannot be discounted in explaining the silica immobilization observed. However, binding is electrostatically favored by the abundant, positively charged amine groups inferred for surfaces of *S. azorense.*

As thermophilic organisms have evolved in niches with solute concentrations typically higher than those of their mesophilic counterparts, and since they have been observed growing in heavily mineralizing hot spring systems, it would be surprising if thermophilic organisms did not employ a more active system for coping with silicification, relative to their mesophilic counterparts. Such a system is implied by the titration and protein concentration data herein, whereby proteins inherently amine-rich, and potentially comprising a significant component of the biofilm matrix, serve to ensure the prevention of cell wall mineralisation by providing highly reactive sites where silica can be immobilized and removed in a manner under biological control. While such interaction may ultimately lead to increased silica immobilization, and by deduction, increased rates of sinter formation, it also ultimately prevents the interactions between reactive silica species and the cell surface proper. While experiments ultimately leading to complete permineralization are desirable, our results imply that microorganisms preventing the silicification of their cell wall,

such as *S. azorense*, will less readily become encrusted in a fossilizing silica matrix and therefore will not be preserved in the ancient rock record.

2.5 Conclusion

In this study, we have found that *S. azorense* remains viable, and can grow exponentially, in the presence of high concentrations of silica. We also demonstrated that *S. azorense* does not adsorb monomeric silica from undersaturated solution, nor does it accelerate the rate or magnitude of polymerization of silica from supersaturated solution during growth by any of its metabolic pathways. There is, however, a metabolic role in silicification, that being exponentially-growing, H_2-oxidizing cultures of *S. azorense* remove small amounts of colloidal silica, while those cultures growing by S°-oxidation do not. Moreover, *S. azorense* remained viable in solutions supersaturated with respect to amorphous silica and yielded higher and more rapidly increasing protein concentrations in batch cultures with increasing Si concentration, possibly as a stress response. Although not confirmed quantitatively, biofilm production was visually noted to be more important in such cultures. Acid-base titrations indicate that amine functional groups are highly prominent on the surfaces of *S. azorense*, and likely serve as the ligands involved in silica colloid adsorption within the protein-rich biofilm matrix. Since silicification was observed to be restricted to the EPS, we propose that *S. azorense* may prevent cellular silicification to some degree by producing abundant reactive sites in the biofilm matrix and regulating EPS production appropriately. Finally, while we indicate that microbial silicification may lead to increased rates of sinter formation, we speculate that this does not necessarily equate to morphological fossil preservation, and propose that organisms such as *S. azorense* would not be preserved in the fossil record as a consequence of protection from cellular silicification.

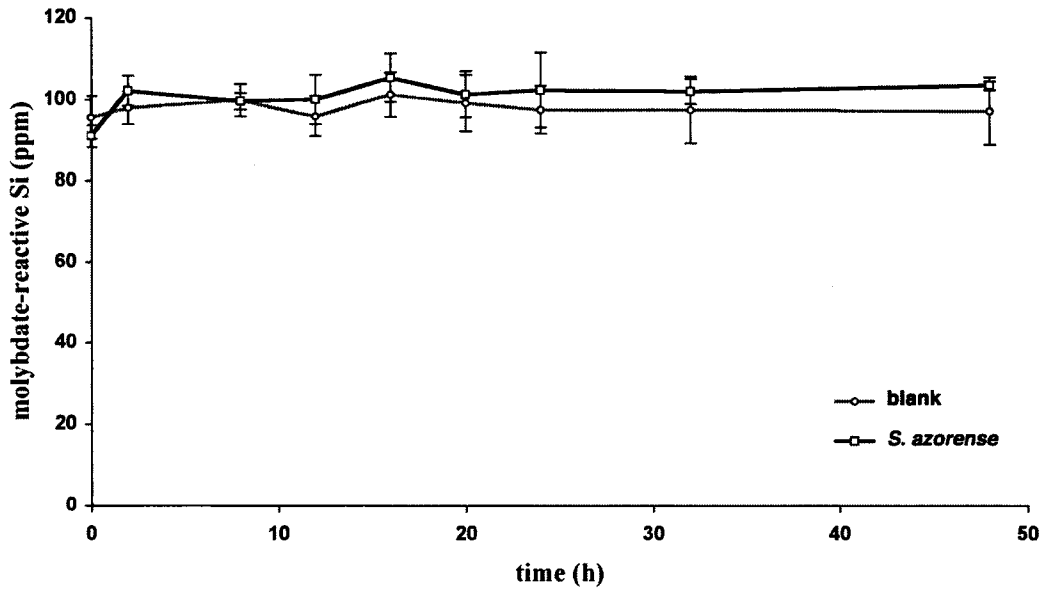

Figure 2-1. Si concentrations in silica undersaturated solutions. The blank controls contain no bacteria, and *S. azorense* was grown under hydrogen-oxidizing conditions and passed through exponential phase growth during the course of the experiment. Points are the average of triplicates, and error bars represent 95% confidence intervals.

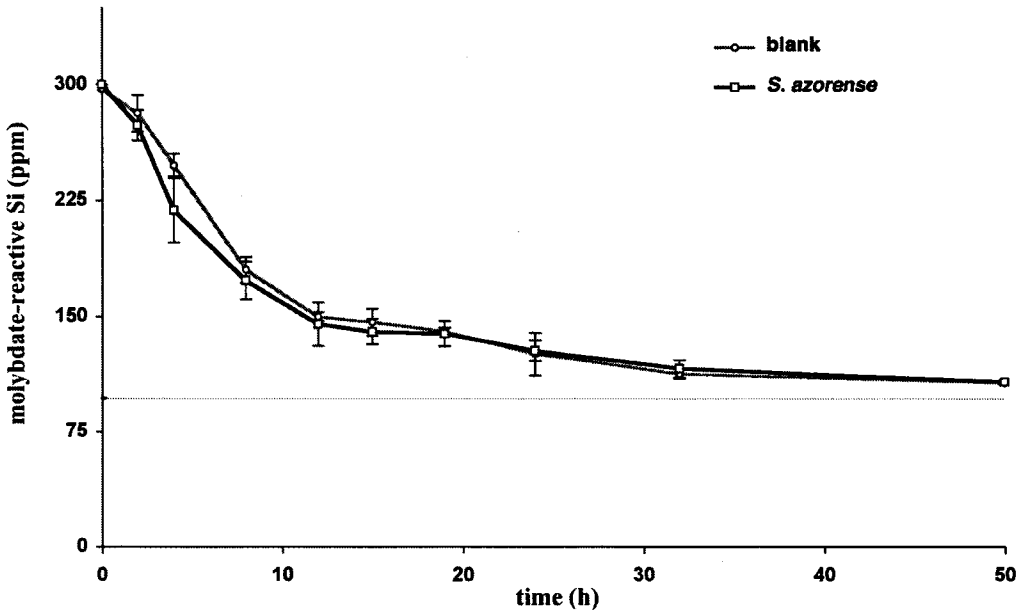

Figure 2-2. Molybdate-reactive Si concentrations in silica supersaturated solution. The blank controls (without bacteria) illustrate spontaneous polymerization. *S. azorense* grew exponentially by hydrogen oxidation during the course of the experiment. Points are the average of triplicates, error bars represent 95% confidence intervals, and the grey line indicates the solubility of silica for the experimental conditions.

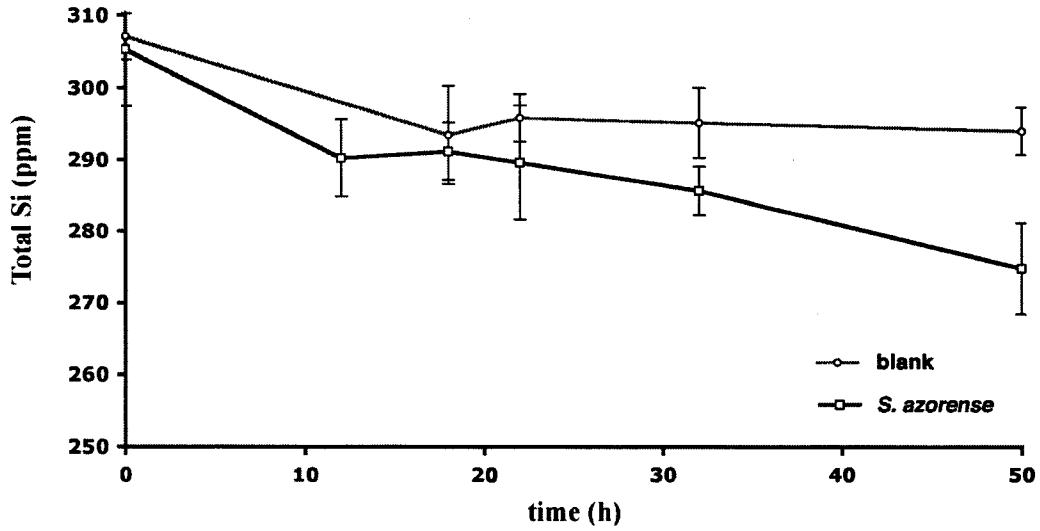

Figure 2-3. Total silica concentrations over time in silica supersaturated experiments containing *S. azorense* grown by hydrogen oxidation. Points are the average of triplicates, and error bars reflect 95% confidence intervals.

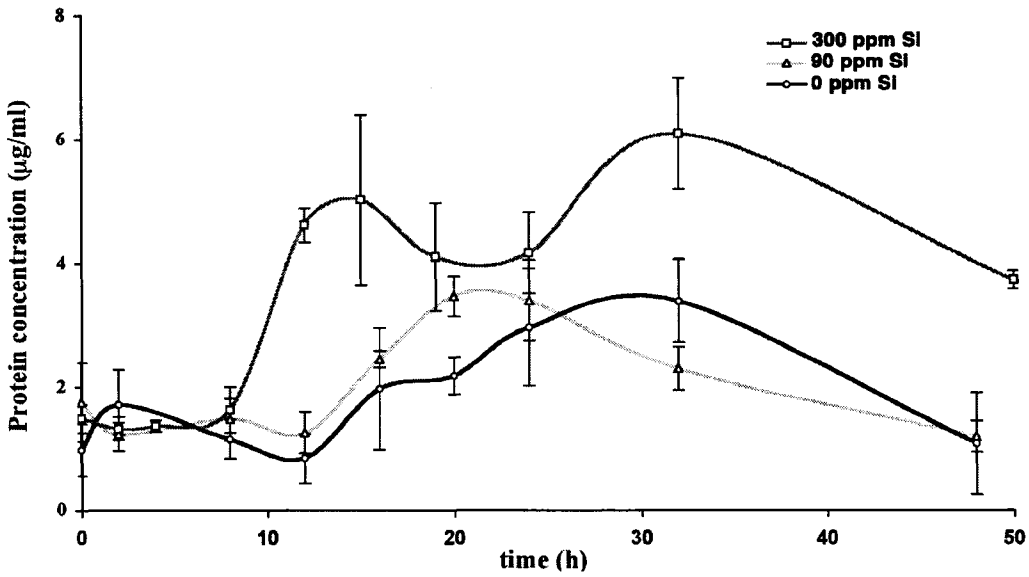

Figure 2-4. Protein concentrations in hydrogen-oxidizing batch cultures of *S. azorense*, plotted as a function of time and at various Si concentrations. Graph begins with the simultaneous inoculation and silica solution injection. Points are the average of triplicates, and error bars indicate the 95% confidence intervals.

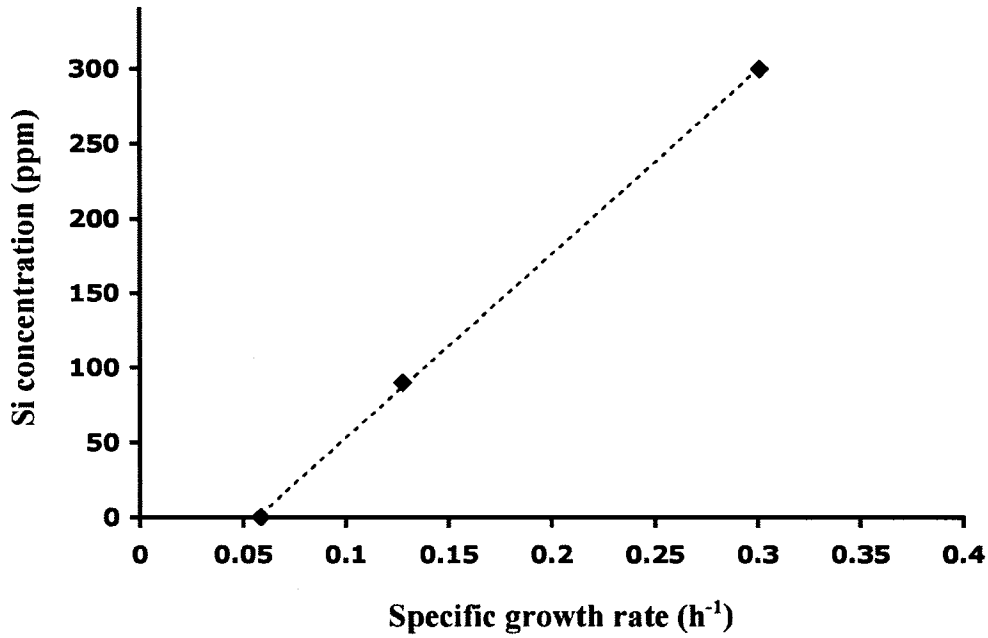

Figure 2-5. The relationship of maximum growth rate achieved to Si concentration. The highest growth rate between two data points was chosen for any Si concentration, and fit is $R^2 = 0.9997$.

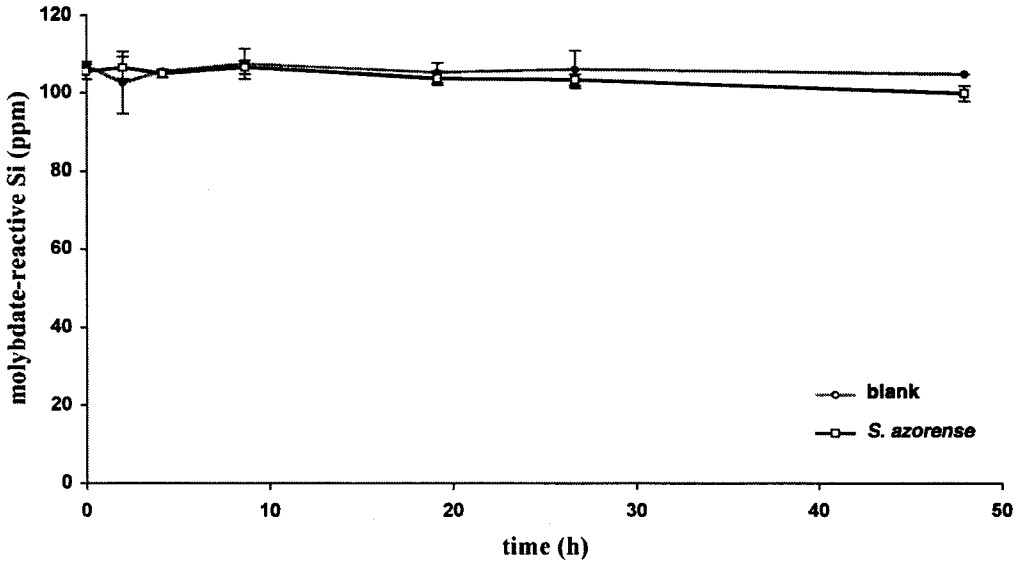

Figure 2-6. Si concentrations in silica undersaturated solution. The blank experiments contain no bacteria, and *S. azorense* grew by sulfur-oxidation through exponential phase during the course of the experiment. Points are the average of triplicates, and error bars represent 95% confidence intervals.

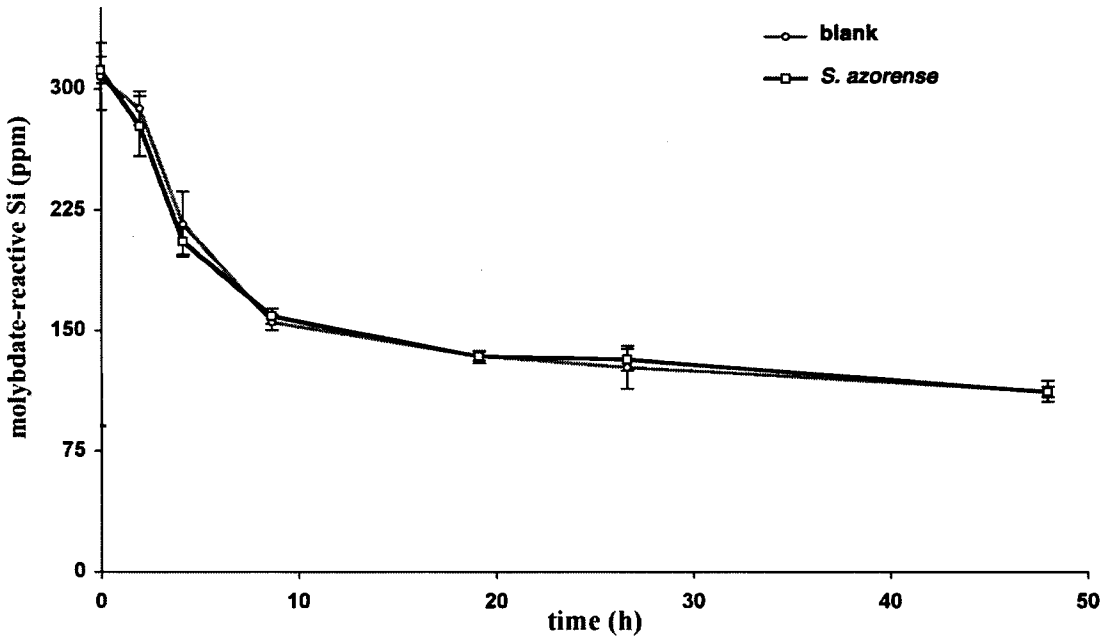

Figure 2-7. Molybdate-reactive Si concentrations in silica supersaturated solution. *S. azorense* grew exponentially by sulfur-oxidation during the course of the experiment, and yielded silica polymerization comparable to the bacteria-free blanks. Points are the average of triplicates, error bars represent 95% confidence intervals, and the grey line indicates the solubility of silica for the experimental conditions.

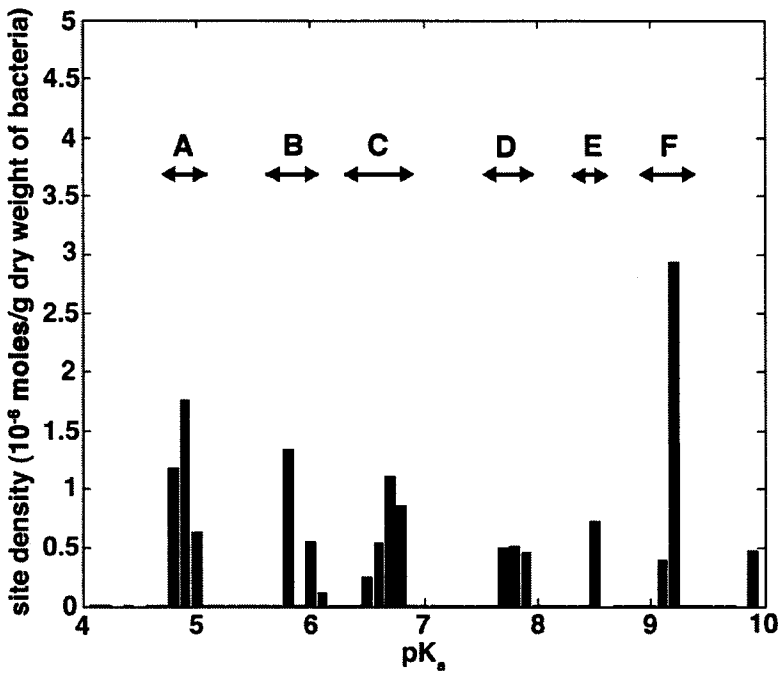

Figure 2-8. Acid-base titration of *S. azorense* whole culture (cells+biofilm) grown in silica-free media under hydrogen-oxidizing conditions. Cluster A is suggested to represent carboxyl groups, clusters B and C, carboxyl or phosphoryl groups, cluster D, phosphoryl groups, and clusters E and F, amine groups.

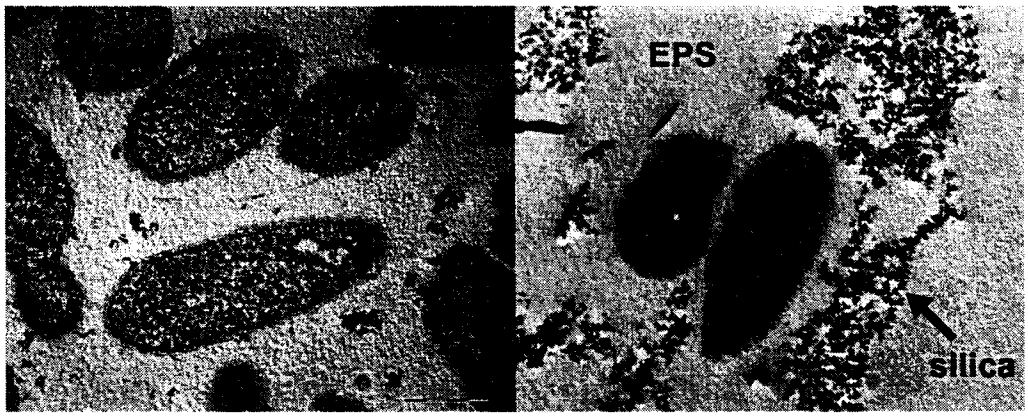

(A) **(B)**

Figure 2-9. TEM images of *S. azorense* grown metabolising by hydrogen oxidation in silica supersaturated solution. Scale bars represent 500 nm. **(a)** Cells are observed at high density encased in the biofilm matrix. Siliceous spheres are have no significant cell association. **(b)** After 50 hours in silica-supersaturated solution, nanoscale silica spheres had been restricted from cell surfaces. Colloidal silica, EPS, and cells are labeled. Staining with uranyl acetate was not performed for the preparation imaged in **(b)**.

2.6 References

Aguiar P, Beveridge TJ, and Reysenbach AL (2004) *Sulfurihydrogenibium azorense,* sp. nov., a thermophilic hydrogen-oxidizing microaerophile from terrestrial hot springs in the Azores. *International Journal of Systematic and Evolutionary Microbiology* 54, 33-39.

Awramik SM (1992) The oldest records of photosynthesis. *Photosynthesis Research* 33, 75-89.

Benning LG, Phoenix VR, Yee N, and Konhauser KO (2004) The dynamics of cyanobacterial silicification: an infrared micro-spectroscopic investigation. *Geochimica et Cosmochimica Acta* 68, 743-757.

Blank CE, Cady SL, and Pace NR (2002) Microbial composition of near-boiling silica depositing thermal springs throughout Yellowstone National Park. *Applied and Environmental Microbiology* 6, 5123-5135.

Bocchetta M, Gribaldo S, Sanagelantoni A, and Cammarano P (2000) Phylogenetic depth of the bacterial genera Aquifex and Thermotoga inferred from analysis of ribosomal protein, elongation factor, and RNA polymerase subunit sequences. *Journal of Molecular Evolution* 50, 366–380.

Brasier MD, Green OR, Jephcoat AP, Kleppe AK, Van Kranendonk MJ, Lindsay JF, Steele A, and Grassineau NV (2002) Questioning the evidence for Earth's oldest fossils. *Nature* 416, 76-81.

Daughney CJ, Fowle DA, and Fortin DF (2001) The effect of growth phase on proton and metal adsorption by *Bacillus subtilis. Geochimica et Cosmochimica Acta* 65,1025-1035.

Fanning KA and Pilson MEQ (1973) On the spectrophotometric determination of dissolved silica in natural waters. *Analytical Chemistry* 45, 135-140.

Farmer J (2000) Hydrothermal systems: Doorways to early biosphere evolution. GSA Today Vol 10, No. 7, 1-9.

Fein JB, Scott S, and Rivera N (2002) The effect of Fe and Si adsorption by *Bacillus subtilis* cell walls: insights into non-metabolic bacterial precipitation of silicate minerals. *Chemical Geology* 182, 265-273.

Fournier RO (1985) The behaviour of silica in hydrothermal solutions. In: Berger BR, Bethke PM (eds), *Geology and Geochemistry of Epithermal Systems. Reviews in Economic Geology* 2, 45-61.

Francis S, Margulis L, and Barghoorn ES (1978) On the experimental silicification of microorganisms. II. On the time of appearance of eukaryotic organisms in the fossil record. *Precambrian Research* 6, 65-100.

Heaney PJ and Yates DM (1998) Solution chemistry of wood silicification. *Geological Sociey of America Annual Meeting Abstracts.* Program 30, A-375.

Horodyski RJ, Bauld J, Lipps' JH, and Mendelson CV (1992) Preservation of prokaryotes and organic-walled and calcareous and siliceous protists. In: Schopf JW, Klein C (eds), *The Proterozoic Biosphere.* Cambridge University Press, Cambridge, pp. 185-193.

Hugenholtz P, Pitulle C, Hershberger KL, and Pace NR (1998) Novel division level bacterial diversity in a Yellowstone hot spring. *Journal of Bacteriology* 180, 336-376.

Iler RK (1979) *The Chemistry of Silica.* Wiley-Interscience, New York.

Jones B and Renaut RW (2003) Hot spring and geyser sinters – the integrated product of precipitation, replacement, and deposition. *Can. J. Earth Sci.* **40**, 1549-1569.

Kasting JF (1987) Theoretical constraints on oxygen and carbon dioxide concentrations in the Precambrian atmosphere. *Precambrian Research* 34, 205-229.

Knauth LP and Lowe DR (2003) High Archean climatic temperatures inferred from oxygen isotope geochemistry of cherts in the 3.5 Ga Swaziland Supergroup, South Africa. *Geological Society of America Bulletin* 155, 566-580.

Knoll AH, Strother PK, and Rossi S (1988) Distribution and diagenesis of microfossils from the Lower Proterozoic Duck Creek Dolomite, Western Australia. *Precambrian Research* 38, 257-279.

Konhauser KO and Ferris FG (1996) Diversity of iron and silica precipitation by microbial mats in hydrothermal waters, Iceland: Implications for Precambrian iron formations. *Geology* 24, 323-326.

Konhauser KO, Phoenix VR, Bottrell SH, Adams DG, and Head IM (2001) Microbial-silica interactions in modern hot spring sinter: Possible analogues for Precambrian siliceous stromatolites. *Sedimentology* 48, 415-435.

Konhauser KO, Jones B, Reysenbach A-L, and Renaut RW (2003) Hot spring sinters: keys to understanding Earth's earliest life forms. *Canadian Journal of Earth Sciences* 40, 1713-1724.

Konhauser KO, Jones B, Phoenix VR, Ferris FG, and Renaut RW (2004) The microbial role in hot spring silicification. *Ambio*, 33, 552-558.

LaPaglia C and Hartzell PL (1997) Stress-induced production of biofilm in the hyperthermophile *Archaeoglobus fulgidus*. *Applied and Environmental Microbiology*. 63, 3158-3163.

Leo RF and Barghoorn ES (1976) Silicification of wood. *Botanical Museum leaflets, Harvard University* 25, 1-29.

Mountain BW, Benning LG, and Boerema JA (2003) Experimental studies on New Zealand hot spring sinters: rates of growth and textural development. *Canadian Journal of Earth Sciences* 40, 1643-1667.

Nisbet EG and Sleep NH (2001) The habitat and nature of early life. *Nature* 409, 1083-1091.

Oehler JH (1976) Experimental studies in Precambrian paleontology: Structural and chemical changes in blue-green algae during simulated fossilization in synthetic chert. *Geological Society of America Bulletin* 87, 117-129.

Oehler JH and Schopf JW (1971) Artificial microfossils: Experimental studies of permineralization of blue-green algae in silica. *Science* 174, 1229-1231.

Oosthuizen MC, Steyn B, Theron J, Cosette P, Lindsay D, von Holy A, and Brözel VS (2002) Proteomic analysis reveals differential protein expression by

Bacillus cereus during biofilm formation. *Applied and Environmental Microbiology* 68, 2770-2780.

Pace NR (1997) A molecular view of microbial diversity and the biosphere. *Science* 276, 734-740.

Perdue ME (1985) In *Humic Substances in soil, sediment and water* (ed. Aiken RG, McKnight DM, Wershaw RL, MacCarthy P) Wiley-Interscience, New York, pp 493-526.

Pierson BK, Mitchell HK, and Ruff-Roberts AL (1993) *Chloroflexus aurantiacus* and ultraviolet radiation: Implications for Archean shallow-water stromatolites. *Origins of Life and Evolution of the Biosphere* 23,243-260.

Phoenix VR, Adams DG, and Konhauser KO (2000) Cyanobacterial viability during hydrothermal biomineralization. *Chemical Geology* 169, 329-338.

Phoenix VR, Konhauser KO, Adams DG, and Bottrell SH (2001) Role of biomineralization as an ultraviolet shield: Implications for Archean life. *Geology* 29, 823-826.

Phoenix VR, Martinez RE, Konhauser KO, and Ferris FG (2002) Characterization and implications of the cell surface reactivity of the cyanobacteria *Calothrix* sp. *Applied and Environmental Microbiology* 68, 4827-4834.

Phoenix VR, Konhauser KO, and Ferris FG (2003) Experimental study of iron and silica immobilization by bacteria in mixed Fe-Si systems: Implications for microbial silicification in hot-springs. *Canadian Journal of Earth Sciences* 40, 1669-1678.

Prigent-Combaret C, Vidal O, Dorel C, and Lejeune P (1999) Abiotic surface sensing and bio-film dependent regulation of gene expression in *Escherichia coli*. *Journal of Bacteriology* 191, 5993-6002.

Rasmussen B (2000) Filamentous microfossils in a 3,235-million-year-old volcanogenic massive sulphide deposit. *Nature* 405,676-679.

Reysenbach AL and Shock E (2002) Merging genomes with geochemistry at hydrothermal ecosystems. *Science* 296, 1077-1082.

Rinker KD and Kelly RM (2000) Effect of carbon and nitrogen sources on growth dynamics and exopolysaccharide production for the hyperthermophilic archaeon *Thermococcus litoralis* and bacterium *Thermotoga maritime*. *Biotechnology and Bioengineering* 69, 537-547.

Rothbaum HP, Anderton BH, Harrison RF, Rohde AG, and Slatter A (1979) Effect of silica polymerization and pH on geothermal scaling. *Geothermics* 8, 1-20.

Schopf JW and Packer BM (1987) Early Archean (3.3-billion to 3.5-billion-year-old) microfossils from Warrawoona Group, Australia. *Science*, 237, 70-72.

Schultze-Lam S, Ferris FG, Konhauser KO, and Wiese RG (1995) *In situ* silicification of an Icelandic hot spring microbial mat: Implications for microfossil formation. *Canadian Journal of Earth Sciences* 32, 2021-2026.

Siever R (1992) The silica cycle in the Precambrian. *Geochimica et Cosmochimica Acta*, 56, 3265-3272.

Sokolov I, Smith DS, Henderson GS, Gorby YA, and Ferris FG (2001) Cell surface electrochemical heterogeneity of the Fe(III)-reducing bacteria *Shewanella putrefaciens*. *Environmental Science and Technology* 35, 341–347.

Swedlund PJ and Webster JG (1999) Adsorption and polymerization of silicic acid on ferrihydrite, and its effect on arsenic adsorption. *Water Research* 33, 3413-3422.

Tice MM and Lowe DR (2004) Photosynthetic microbial mats in the 3,416-Myr-old ocean. *Nature* 431, 549-552.

Toporski JKW, Steele A, Westall F, Thomas-Keprta KL, and McKay DS (2002) The simulated silicification of bacteria – new clues to the modes and timing of bacterial preservation and implications for the search for extraterrestrial microfossils. *Astrobiology* 2, 1-26.

Urrutia MM and Beveridge TJ (1993) Mechanism of silicate binding to the bacterial cell wall in *Bacillus subtilis*. *Journal of Bacteriology* 175, 1936-1945.

Urrutia MM and Beveridge TJ (1994) Formation of fine-grained metal and silicate precipitates on a bacterial surface (*Bacillus subtilis*). *Chemical Geology* 116, 261-280.

Walter MR, Bauld J, and Brock TD (1972) Siliceous algal and bacterial stromatolites in hot spring and geyser effluents of Yellowstone National Park. *Science* 178, 402-405.

Warren LA and Ferris FG (1998) Continuum between sorption and precipitation of Fe(III) on microbial surfaces. *Environmental Science and Technology* 32, 2331-2337.

Westall F, Boni L, and Guerzoni E (1995) The experimental silicification of microorganisms. *Palaeontology* 38, 495-528.

Westall F (1997) The influence of cell wall composition on the fossilization of bacteria and the implications for the search for early life forms. In: Cosmovici C, Bowyer S, Werthimer D (eds), *Astronomical and Biochemical Origins and the Search for Life in the Universe.* Editori Compositrici, Bologna, pp. 491-504.

Westall F, Steele A, Toporski J, Walsh M, Allen C, Guidry S, McKay D, Gibson E, and Chaftez H (2000) Polymeric substances and biofilms as biomarkers in terrestrial materials: Implications for extraterrestrial samples. *Journal of Geophysical Research 105, 24,511-24,527.*

Whiteley M, Bangera MG, Lory S, and Greenberg EP (2001) Gene expression in *Pseudomonas aeruginosa* biofilms. *Nature* 413, 860-864.

Whitfield C and Keenleyside WJ (1995) Regulation of expression of group IA capsular polysaccharides in *Escherichia coli* and related extracellular polysaccharides in other bacteria. *Journal of Industrial Microbiology* 15, 361–371.

Yee N, Phoenix VR, Konhauser KO, Benning LG, and Ferris FG (2003) The effect of cyanobacteria on silica precipitation at neutral pH: Implications for bacterial silicification in geothermal hot springs. *Chemical Geology* 199, 83-90.

CHAPTER 3

Acid-base properties of cyanobacterial surfaces I: influences of growth phase and nitrogen metabolism on cell surface reactivity[1]

3.1 Introduction

The ubiquitous presence of bacteria in surface environments, along with their chemical reactivity, make them important factors in driving elemental cycling on the Earth's surface. In particular, organic functional groups located in the bacterial cell wall act as highly efficient ligands for the sorption of metals (e.g., Beveridge and Murray, 1980; Beveridge et al., 1982; Daughney and Fein, 1998; Daunghney et al., 1998) and/or organic compounds (Baughman and Paris,

[1] Lalonde SV, Smith DS, Owttrim GW, and Konhauser KO (2006) *Geochimica et Cosmochimica Acta* submission W4104, in review as of April 11th, 2006.

1981; Fein and Delea, 1999). Those ligands also determine the overall cell surface charge governing bacterial adherence to solid substrata (Van Loosdrecht et al., 1989, 1990; Yee et al., 2000), which in turn, impacts on metal mobility in many fluid-rock systems (e.g., McCarthy and Zachara, 1989; Lindqvist and Enfield, 1992; Corpcioglu and Kim, 1995). The sorptive capacity of bacteria additionally alters mineral precipitation and dissolution rates at the bacterial surface (Konhauser et al., 1993; Fortin et al., 1997; Warren and Ferris, 1998).

Potentiometric titrations have been employed to determine discrete proton-exchanging surface ligands for an increasing number of bacterial strains (e.g., Plette et al., 1995; Fein et al., 1997; Cox et al., 1999; Haas et al., 2001; 2004; Sokolov et al., 2001; Martinez et al., 2002; Phoenix et al., 2002; Ngwenya et al., 2003; Yee et al., 2004; Borrok et al, 2004; 2005) using a diverse selection of modeling techniques (reviewed by Fein et al., 2005). While these may vary in mathematical approach and assumptions made regarding electrostatic phenomena at the bacterial surface, they are unified in their goal of providing parameters, such as ligand concentrations and proton-ligand stability constants, that quantitatively describe the bacterial surface. These modeled parameters are considered constants that, when applied to artificial or natural geochemical systems using a chemical surface complexation approach, successfully enable quantitative predictions of mass balance with respect to those surfaces under a variety of conditions (e.g., Fowle and Fein, 1999). Daughney et al. (2001) first pointed out that while surface complexation models may accurately account for the influence of abiotic variables on the bacterial metal adsorption process, biotic variables have been largely ignored. The bacterial surface is a highly dynamic interface where new cell wall material and/or extracellular layers are added, proteins are inserted, signals are transduced, adherence to solid substrata occurs, flocculation and motility are controlled, and nutrients and metabolites are exchanged.

Preliminary studies have only begun to reveal biological processes affecting ligand distribution on Gram-positive (Daughney et al., 2001) and Gram-negative (Haas, 2004; Borrok et al., 2004) bacterial surfaces, and there exists

some evidence indicating that for a single bacterial species, metal adsorption may be controlled by variations in ligand distributions that ultimately arise as a consequence of the diversity of conditions under which the bacteria may grow. Previously reported bacterial metal binding constants indicate an important role for proton-exchanging (i.e., carboxyl) ligands in metal sorption (Fein et al., 1997; Daughney et al., 1998; Fowle et al., 2000; Daughney et al., 2001), and variability in the concentration of some ligand-bearing organic components of the cell wall (i.e., techoic and teichuronic acids) has been shown to influence the metal sorption process (Beveridge and Murray, 1980; Beveridge et al., 1982). Efforts to reveal biological controls on the extent of metal sorption have focused largely on the life cycle of a laboratory batch culture; at high nutrient and/or low metabolite concentrations, cells proliferate exponentially to the point where growth is limited by the total consumption of one or more nutrients, or metabolites reach toxic levels, and cell populations remain stationary (Madigan et al., 1997).

Growth phase has been implicated as a factor in metal sorption for a variety of bacteria with mixed results (Friis et al., 1986; Chang et al., 1997; Daughney et al., 2001), and it is likely that the effects of growth phase are species-specific (Daughney et al., 2001). For example, Daughney et al. (2001) indicated that such growth effects can be of sufficient significance as to strongly affect the outcome of surface complexation models employing the Gram-positive *Bacillus subtilis*, while Haas (2004) concluded that growth phase had negligable influence on the ligand distributions of the Gram-negative *Shewanella putrefaciens*. Both Haas (2004) and Borrok et al. (2004) have further assessed the role of nutrient concentration on *S. putrefaciens* and *Psuedomonas fluorecens*, respectively, and they accepted the null hypothesis in this respect. As progression through growth phases is dictated in part by nutrient concentration, it is not surprising that any variability associated with growth phase might also include variability attributable to nutrient concentration.

The situation becomes much more complex with the consideration of facultative metabolic pathways. For bacteria that are capable of switching between multiple metabolic pathways, the presence or absence of specific

nutrients may dictate the expression of nutrient-specific chelation agents and membrane transport proteins (e.g., Wandersman and Delepelaire, 2004), the production of extracellular polymers (Rinker and Kelly, 2000), adhesion in biofilm communities (Thormann et al., 2005), and cellular differentiation such as heterocyst formation (see Wolk, 1996 for review). Both Haas (2004) and Borrok et al. (2004) considered facultative aerobic and anaerobic dissimilatory metabolism in their investigations, with mixed results. While Borrok et al. (2004) found that the metabolic pathway of growth had negligible effect on Co adsorption by *Shewanella oneidensis* MR-1, Haas (2004) found sufficient variability by potentiometric titration of *S. putrefaciens* as to warrant two distinct sets of surface parameters, each specific to a particular metabolic pathway, for the accurate description of this microbial surface. Clearly, controversy remains regarding metabolic determinants of microbial surface reactivity, and facultative variation has only been assessed between microbes of the same genus and metabolic pathways.

In this study, we consider the potential role that assimilatory metabolism may play in determining surface ligand distributions. Specifically, we evaluate:

(1) the acid-base properties of a well-characterized, unsheathed cyanobacterium (*Anabaena* sp. strain PCC 7120) in order to contribute to the collection of chemical parameters describing the surfaces of diverse bacteria,

(2) proton sorption by the same cyanobacterium grown under conditions ensuring assimilatory nitrate reduction, ammonium assimilation, and nitrogen fixation, with the goal of revealing variability in surface chemistry as a reflection of compositional differences in cell wall architecture as dictated by specific N availability,

(3) the role of growth phase, complimenting data previously reported for variability in the surface chemistry of a Gram-positive bacterium (Daughney et al., 2001) and Gram-negative bacteria (Haas, 2004; Borrok et al., 2004).

We report a set of average surface chemical parameters modeled from replicate potentiometric titrations of cells over two growth phases and three nitrogen metabolisms, and statistically evaluate the ability of the average parameters to

account for the variations in surface chemical parameters observed between individual conditions.

3.2 Methods

3.2.1 Growth procedures

The cyanobacterial strain *Anabaena* sp. PCC 7120 (henceforth referred to as *Anabaena*) was chosen for its lack of sheath or S-layer (Rippka et al., 1979), ability to fix atmospheric nitrogen via heterocyst formation, and well characterized genome (Kaneko et al., 2001). Axenic cultures were grown under constant illumination of ~100 microeinsteins/m^2/s in liquid BG-11 media (Rippka et al., 1979) at 30 °C with aeration provided by shaking at 150 rpm and bubbling with filtered and humidified air (Chamot and Owttrim, 2000). Separate populations consistently limited, over at least 3 transfers, to growth on either nitrate, ammonium, or dinitrogen as the sole nitrogen source were maintained in nitrogen-free BG-11(0) media to which 17.6 mM of nitrate as $NaNO_3$, 17.6 mM ammonium as NH_4Cl, or 17.6 mM NaCl (no fixed nitrogen source) was added, respectively. For *Anabaena* species, heterocyst formation, and therefore nitrogen fixation, is inhibited by the addition of a fixed nitrogen source (Wolk, 1996). For all media, the BG-11 ingredients containing fixed nitrogen (ferric ammonium citrate and cobaltous nitrate hexahydrate) were replaced with nitrogen-free equivalents (ferric citrate and cobaltous chloride hexahydrate), and the media was buffered around pH 8 by the addition of 10 mM Tricine.

The three cell populations were maintained as stock cultures by successive transfers into 50 ml of media with 10% v/v inoculations. In order to obtain sufficient biomass for potentiometric titration, 3L cultures were established in 6L Erlenmeyer flasks, magnetically stirred, and bubbled with filtered air. The 10% inoculum used to establish the large cultures was derived from 300 ml cultures prepared from, and supplementary to, the 50 ml stock cultures. Growth was monitored by optical density measurements at 595 nm, and cultures were harvested at an absorbance of 0.3 ± 0.03(~ 0.13 g dry weight/L) for exponential phase cells, and 0.6 ± 0.03 (~ 0.24 g dry weight/L) for stationary phase cells.

Growth rates varied according to nitrogen assimilatory pathway, and therefore the time of harvest varied for each condition.

Cells were harvested by centrifugation at room temperature (10,000 rpm, 10 min) and washed three times with 200 ml of 18 MΩ water, followed by four washes with 50 ml of 0.01 M KNO_3 titration electrolyte. Between washes, the cells were incubated for 10 min, pelleted by centrifugation as above, and the supernatant discarded. After the last wash, the concentrated biomass deriving from 1 L of culture was suspended in 0.01M KNO_3 to a final volume of 50 ml. Cell suspensions were stored at room temperature until titration.

3.2.2 Potentiometric titrations

All plastic and glassware used for solution preparation and potentiometric titration were soaked in 10% v/v nitric acid for 24 hours and subsequently in 18 MΩ sterile water for 48 hours (Cox et al., 1999). All solutions were prepared according to standard analytical methods (Harris, 1995) using sterile 18MΩ water purged of dissolved CO_2 with $N_2(g)$ for at least 30 minutes and stored under a nitrogen atmosphere. The 0.01 M KNO_3 titration electrolyte was prepared volumetrically by the addition of weighed KNO_3 salt, and 0.2 M HNO_3 as well as 0.01 M NaOH were similarly prepared using 50% NaOH solution and concentrated trace-metal nitric acid, respectively. Solutions were standardized by titration against dried potassium hydrogen phthalate prior to titration according to the methodology of Cox et al. (1999).

Before each titration, 10 g of concentrated (2.6 - 4.8 g dry weight/L) biomass suspension was added to 40 g of KNO_3 electrolyte solution in a titration flask prefitted with a Ross-type glass pH electrode (Man-Tech Associates Inc., Guelph, ON), reduced to pH ~3.2 with 200 µl 0.2 M HNO_3, and allowed to equilibrate for 30 minutes under a constant purge of N_2 gas. Titrations were performed alkalimetrically from pH ~3.2 to pH 11 using a QC-Titrate autotitrator (Man-Tech Associates Inc., Guelph, Ontario) variably delivering CO_2-free 0.01 M NaOH for 0.1 pH increments and maintaining electrode stability criteria of <1 mV/s. The system was continuously purged with N_2 gas and magnetically stirred.

The pH electrode was calibrated daily using three commercial buffers, and assessed for drift between titrations using the same buffers. A thermocouple was used to compensate pH calibration as well as verify that temperature remained within 1 degree of 23 °C throughout titration.

Immediately following titration, biomass was filtered onto preweighed Whatman GF/C #42 filters (Whatman Inc, Florham park, New Jersey) and oven dried at 70 °C for 48 hours prior to weighing. Each condition tested was represented by one liter of culture that yielded concentrated biomass for 5 replicate and consecutive titrations. The exponential and stationary phase biomass for titration was harvested at different times from the same 3L culture, for each nitrogen metabolism. Heat-killed biomass was similarly harvested as stationary phase biomass, but autoclaved at 121 °C for 20 minutes after the final resuspension in KNO_3 electrolyte, and titrated upon cooling. All titrations were performed within 18 hours of biomass harvesting, and after titration cellular integrity was confirmed by pigment autofluorescence using a Zeiss Axioskop 2 epi-fluorescent light microscope.

3.2.3 Modeling of ligand concentrations

Bacterial ligand concentrations and acid-neutralizing capacity were fit to the titration data using a pK_a spectrum approach; pK_a values were fixed in a chosen interval (in this case, 3 to 11 in intervals of 0.2) and ligand concentrations at each pK_a value were fit using a linear-programming approach (Brassard et al., 1990; Smith and Kramer, 1999; Smith et al., 1999; Cox et al., 1999; Martinez and Ferris, 2001; Martinez et al., 2002; Phoenix et al., 2002; Fein et al., 2005). The linear-programming method determines by iteration the ligand concentrations that minimize the absolute of the error between the charge excess measured by titration and the charge excess resulting from the iteratively proposed ligand concentrations. In order to calculate charge excess, the charge balance of the system is first expressed as:

$$Cb + [H^+] + [ANC] = Ca + [OH^-] + \sum_{j=1}^{n} [L_j^-]$$

where Cb and Ca are the concentrations of base and acid, respectively, $[H^+]$ and $[OH^-]$ are measured by the pH electrode, $[L_j^-]$ is the concentration of deprotonated functional groups for the j^{th} monoprotic site of n possible sites set by the pKa spectrum, and the acid-neutralizing capacity [ANC] is a constant offset representing the difference between functional groups that remain protonated and those that remain deprotonated over the titration range (Smith and Ferris, 2001). Blank titrations were performed to confirm that the electrolyte solution and experimental error contributed negligibly to charge excess over the modeled pH range. Charge excess due to experimental error (discussed below) became significant below pH ~3.5 and above pH ~10.4.

The charge balance can be rewritten such that, for the i^{th} addition of titrant, charge excess $b_{i\ fit}$ represents the contribution of bacterial functional groups to the charge balance as fit by linear programming. Similarly, this rearrangement allows for $b_{i\ measured}$ to be assessed in terms of measured parameters:

$$b_{i\ fit} = \sum_{j=1}^{n} [L_j^-] - [ANC]$$

$$b_{i\ measured} = Cb_i - Ca_i + [H^+]_i - [OH^-]_i$$

The set of ligand concentrations that best fit the titration data is obtained when $b_{i\ fit}$ approaches $b_{i\ measured}$. This method implicitly assigns a value of zero to $b_{i\ measured}$ at the pH of the suspension prior to acidification.

For the j^{th} site with a value of K_{aj} provided by the chosen pK_a spectrum, at the i^{th} addition of titrant, the deprotonated site concentration $[L_j^-]$ is related to the total site concentration $[L_{Tj}]$ by the expression:

$$[L_j^-] = \frac{K_{aj}\,[L_{Tj}]}{[H^+]_i + K_{aj}}$$

After fixing the possible pK_a values using the spectrum approach, $[L_{Tj}]$ and [ANC] are readily fit to the measured excess charge $b_{i\ measured}$. The linear-programming method iteratively calculates the charge excess deriving from a proposed set of positive ligand concentrations ($b_{i\ fit}$) as:

$$b_{i\ fit} = \sum_{j=1}^{n} \frac{K_{aj}\,[L_{Tj}]}{[H^+]_i + K_{aj}} - [ANC]$$

and fits the data by minimizing the difference between $b_{i\ measured}$ and the $b_{i\ fit}$. This non-electrostatic means of modeling ligand concentrations emphasizes zero as a possible solution, minimizing the number of distinct-pK_a sites that are required to describe the data. All pK_a values reported here are apparent; electrostatic potential corrections are not applied.

3.3 Results and Discussion

3.3.1 Charge excess data

In order to assess the variance of model parameters using replicates of a single condition, each individual titration was modeled and plotted independently. The measured and fitted charge excess curves for live cultures are plotted as a function of growth phase and nitrogen metabolism in Figure 3-1. On the charge excess curves, the slope at any given point corresponds to the buffer capacity at the point. In other words, the slope indicates the rate of ligand deprotonation, per unit of pH, at that point.

It is immediately evident from Figure 3-1 that rapid changes in charge excess occurred at extreme pH values in all cases, suggesting the presence of significant concentrations of ligands with dissociation constants that lie outside of the titration range. Similar buffering at pH extremes has been reported for potentiometric titration of *Shewanella putrefaciens* (Haas et al., 2001; Haas, 2004), indicating that this may be characteristic of Gram-negative bacterial surfaces. Careful consideration of the system behavior and model limitations is required to fully explain the relevance of these hypothesized ligands to the model parameters reported below. Titrations were performed over a pH range of ~3.2 to 11 and modeled using data from pH 4 to 10, as uncertainty in measured charge excess increases at pH extremes due a combination of uncertainty in electrode calibration and the decreasing importance of bacterial ligands in the charge balance expression (Smith et al., 1999). Using data from pH 4 to 10, ligand concentrations were then fit to a pK_a spectrum of 3 to 11 in order to allow for ligands outside of the selected data range to affect the charge excess curve within the selected data range. Without this approach, the model is forced to assign large

ligand concentrations to the upper and lower limits of the pKa spectrum, and the resultant fit is very poor as the lack of charge excess inflection at extreme pH indicates that the ligands of extreme pK_a do not lie within the titration range. The selection of titration data between pH 4 and 10 minimized the absolute error of the fitted charge excess while having a negligible effect on the concentrations and pKa distributions of ligands with pK_a values between 4 and 10 (data not shown).

The indicated point of zero charge (PZC) (Fig. 3-1) ranges from 8.8 to 9.6, in significant discrepancy with previously reported values determined by electrophoremetry for various Gram-negative bacteria (Bayer and Sloyer, 1990). This is expected as the point of zero charge is inherently set to zero at the pH of the cell suspension prior to acidification, and as discussed above, the titration range excludes charge contribution from ligands with extreme dissociation constants. However, it should be noted that because the charge balance is established to be zero at the pH of the final wash (~7), considerable hysteresis has occurred; non-reversible sorption or desorption processes take place during the titration procedure to result in a PZC that differs from ~7. While this may, in part, be attributed to the irreversible desorption of structurally bound Mg and Ca from the bacterial surface during low pH equilibration at the start of titration (Borrok et al., 2004), this alone is insufficient to account for the degree of hysteresis consistently observed (Fig. 3-1). Reverse titration of selected samples (data not shown) confirmed that hysteretic effects were incurred during the initial, rapid acidification, and that the alkalimetric titration profiles, and therefore modeled ligand concentrations, were unaffected by the observed hysteresis.

Electrophoretic measurements performed on *Anabaena* (data not shown) confirm that the surface charge at the shear plane remains negative at pH values greater than ~4 for all conditions investigated here; however the large filament size of *Anabaena* introduced sufficient random error as to preclude further conclusions regarding effective surface charge.

It should be noted that Fein et al. (2005) highlighted an important parameter as often overlooked in potentiometric titration studies, that of the zero proton condition ($T_H°$). Assuming a fully protonated zero proton condition, $T_H°$

corresponds to the difference between the surface proton concentration at the pH of immersion and the proton concentration of a fully protonated surface. Knowledge of $T_H°$ is only required for the modeling consideration of sites with pK_a values outside of the titration range, and is therefore independent of the modeled parameters presented here. We present the charge excess curves (Fig. 3-1) for qualitative assessment of condition-specific charging profile and replicate repeatability only.

3.3.2 Discrete site modeling

The modeled parameters for all conditions investigated in this study are presented in Table 3-1. Also included in Table 3-1 are parameters previously reported for titrations of *Shewanella putrefaciens* (Haas, 2004), grown by aerobic and anaerobic metabolic pathways. It is evident that the values between these two Gram-negative bacteria are in close agreement, despite different preparation and titration methods, and that variability in ligand concentrations between *Anabaena* growth conditions exceeds that observed for *Shewanella putrefaciens.* Also included in Table 3-1 are data pertaining to heat-killed cell suspensions, discussed below.

For the purposes of statistical comparison, ligands were grouped according to broad pK_a ranges (4-7 and 7-10). This proved necessary due to the heterogeneity in the pK_a distribution of individual ligands between conditions; variation between conditions was sufficient to preclude the confident assignment of ligands that were equivalent between conditions. While statistical comparisons based on the two broad groupings eliminates the power to resolve differences on a ligand-by-ligand basis, it also greatly reduces the chance of type I statistical errors and increases the chance of type II errors. In other words, it decreases the chance of incorrectly finding statistical significance, and increases that chance of incorrectly rejecting statistical significance. Conclusions of difference based on these groupings are more robust by the conservative nature of this statistical approach.

Composite plots for each condition are presented in Figure 3-2. In order to account for the number of occurrences of each ligand across replicates of a single condition, the composite plots were generated by summing the concentration of sites inferred for all replicates at each pK_a interval, and then dividing by the total sum of the biomass titrated over all replicates for that condition. In this manner, the composite plots present site concentrations that are weighted by their occurrence across all 5 replicates.

It is clear from Figure 3-2 that there exists variation across conditions in the modeled number of sites, their concentrations, pK_a distributions, and in the variance between replicates. In all cases, at least three sites were required to describe the titration data, and given the range of pK_a values observed, a variety of functional groups may be ascribed to the results. As functional group classification cannot be wholly confirmed without additional (i.e., spectroscopic) evidence (Fein et al., 2005), and such classification is secondary to the purpose of this paper, a classification scheme will not be outlined here; we consider the pK_a classifications of Cox et al. (1999) as sufficient for discussion purposes.

Irrespective of growth phase, cultures grown by ammonium (NH_4^+) assimilation and by nitrogen fixation showed similar total ligand concentrations in the range of 3 – 4.5 mmol/g (Table 3-1), while those cultures grown on nitrate yielded concentrations approximately 50% lower. With respect to growth phase, those grown on ammonium or by nitrogen fixation both showed a decrease in total ligand concentrations in stationary phase relative to exponential phase cells, while nitrate (NO_3^-) grown cultures display the opposite trend. The former case is in concurrence with findings by Daughney et al. (2001), who found that the concentration of proton-exchanging ligands on the surface of *B. subtilis* decreased from exponential to stationary phase. Previous studies of bacterial metal sorption (see introduction) have likewise indicated changes in surface chemistry between growth phases. As the surfaces of *Anabaena* and *B. subtilis* possess distinctly different architecture (Gram-negative vs. Gram-positive), the concurrence must be either coincidental, or the result of microbial success strategy that for unknown reasons has been selected for across distant positions, and between varying

surface chemistries, within the bacterial domain. It is possible that ligand concentrations are increased for exponential phase cells to facilitate the rapid acquisition of nutrients, and decreased for stationary phase cells to minimize interactions with toxic metabolites, or by the fact that the cells are no longer as metabolically active. Similar trends were observed by Haas (2004) for *Shewanella putrefaciens*, who invoked changes in cell size to explain decreases on a per weight basis, and proposed that site concentrations increased on a per cell basis as a result of reserve polymer production and the expression of nutrient acquisition proteins. The filamentous nature of *Anabaena* prevented evaluation of our results on a per cell basis.

All conditions showed a greater concentration of ligands with pK_a values in the 4 to 7 range than in the 7 to 10 range, with an average acidic to basic ligand ratio of 3.15. Individual ligand pK_a values appear affected less by growth phase than by growth condition; hence, it would seem that growth conditions dictate the types of ligands expressed, while growth phase affects their relative concentrations. In order to determine the ability of one set of modeled parameters to describe all of the conditions with confidence, as well as distinguish trends that are statistically significant, one-way ANOVA as well as Tukey's post-hoc comparisons were performed using the modeled parameters, as described below.

3.3.3 Titrations of heat-killed cell suspensions

Heat-killed cell suspensions were prepared with the intent of releasing all cytoplasmic contents, as well as fully exposing membranes, for characterization by titration. Cell suspensions, prepared with concentrations of biomass equivalent to stationary phase titrations, were autoclaved for 20 minutes at 121 °C after the harvesting and washing procedure, and titrated upon cooling to room temperature. Plots of excess charge and composite ligand profiles, categorized by growth condition, are presented in Figure 3-3.

Excess charge curves (Fig. 3-3) clearly show that the cellular lysates provide considerably increased buffering capacity relative to intact cells. This is to be expected as many cytoplasmic contents, including both organic (e.g.,

cytosolic proteins, carbohydrates, nucleic acids) and inorganic (e.g., intracellular NH_4^+ and HCO_3^-) components, possess functional groups that deprotonate over the titration range. A two-fold increase in buffering capacity might be expected from exposure of the cytoplasmic membrane's inner leaflet alone.

Overall, modeled total site densities were increased 2 to 6 fold by the sterilization process (Table 3-2). Composite plots (Fig. 3-3) reveal that the number of peaks invoked to fit the charge excess curves is increased relative to live cells, concordant with an increased diversity of exposed compounds. Again, cells grown by assimilatory nitrate reduction displayed overall ligand concentrations that were significantly (3 to 4 times) lower than those grown on other nitrogen sources. Such an important difference is difficult to reconcile; significant variation in the intracellular pools of organic compounds may be partially responsible. For example, the cyanobacterium *Synechocystis* sp. strain PCC6803 has been shown to increase intracellular glutamine concentrations by 30 to 40 fold within seconds of exposure to ammonium, although levels return to normal within ~30 minutes (Mérida et al., 1991). Variations in inorganic nitrogen pools (as a consequence of nitrogen metabolism) are unlikely to account for the observed results; in the case of the marine cyanobacterium *Synechococcus subsalsus*, non-protein-associated nitrogen constitutes less than 1% of total cellular nitrogen (Lourenço et al., 2004). This also implies that the reduced ligand concentrations inferred for the live nitrate-reducing cultures are a byproduct of cell wall compositional changes associated with growth by that metabolism. Interestingly, the most important ligands postulated for stationary phase cells grown by nitrogen fixation and ammonium assimilation are also most prominent for their heat-killed counterparts.

3.3.4 Statistical significance

In order to quantitatively assess the ability for the average modeled parameters (Table 3-1) to describe each condition investigated herein, statistical evaluations of confidence were performed in a pair-wise manner using the Tukey-Kramer test, a variant of the Tukey HSD (Honestly Significant Difference) test

(Hsu, 1996). The Tukey-Kramer test is a post-hoc comparison used to supplement one-way ANOVA and provide pair-wise measures of confidence between means of different group sizes while controlling the rate of type I statistical error. For the pair-wise comparison of a large number of means, this is necessary as the probability of making a type I error (incorrectly assigning statistical significance) increases significantly with an increasing number of comparisons. For example, Daughney et al. (2001) performed 30 pair-wise comparisons based on 6 modeled parameters and 5 pairs using independent pair-wise one-way ANOVA. By this method, comparisons are independent of each other, and although the probability of incorrectly assigning significance is 0.05 for each comparison, the large number of individual comparisons increases the probability of incorrectly assigning significance at least once to over 50%. Haas (2004) performed multiple pair-wise comparisons using the student's t test, which similarily suffers from a type I error rate that increases with the number of comparisons made. Tukey's HSD test accounts for this by employing a variation of the t distribution that accounts for the number of means being compared (the studentized range distribution) and maintains the overall type I error rate, rather than the individual comparison type I error rate, at the desired level of significance (0.05 in this case). The Tukey-Kramer test employs corrections for unequal replicate sizes, as the average parameters were determined from all 30 titrations and compared with conditions represented by 5 replicates. One major assumption of this test is that of equal variance between conditions, even though the apparent group variances are summed in the calculation of the mean squared error.

Two-tailed confidence intervals for all pair-wise comparisons are presented in Table 3-2. As mentioned above, the classification of ligands into broad groups rather than treatment on an individual basis serves to increase the importance of any variability that is deemed to be statistically significant. From Table 3-2, it is clearly apparent that the average model parameters are unable to describe the majority of conditions with confidence; in fact, with regards to total ligand concentration, the average parameters only describe stationary phase nitrogen fixing cells with confidence greater than 95%. Exponential nitrate-

reducing and ammonium-assimilating cultures reject the average parameters with greater than 95% confidence, and the remainder are described with varying degrees of confidence. The situation is similar for comparison within ligand classes, with the average parameters providing weak support for the majority of conditions. These findings do not indicate that other investigations providing parameters describing bacterial surfaces are incorrect, but rather that previously reported parameters may be, to some degree and certainly in the case of Gram-negative surfaces, dependent on culturing conditions. Due to large differences in architecture between the surfaces of Gram-positive and Gram-negative bacteria, the variability reported here for the surface of a gram-negative bacterium does not likely extrapolate to Gram-positive bacterial surfaces. Additional investigation using Gram-positive bacteria, employing diversity in both dissimilatory and assimilatory metabolic pathways, is required to fully assess the variability of that surface type. From these results, we concur with Haas (2004) that future characterizations of Gram-negative surface chemistry need to account for variability introduced as a consequence of batch culture conditions. We conclude with statistical confidence that the average parameters alone are inadequate in the accurate chemical description of the surface of *Anabaena* for the majority of batch culture growth conditions investigated herein.

In order to ascertain the sources of variability, pair-wise probabilities were grouped according to metabolism and growth phase, and plotted in Figure 3-4. It is evident that while confidence is generally poor in comparisons between cultures of different metabolism harvested at the same phase of growth, confidence in comparisons between growth phases of the same metabolism is higher (Figure 3-4). We conclude that metabolic pathway is a greater determinant of ligand concentration than growth phase, in concurrance with Haas (2004). It should also be noted that variability in the distribution of ligands between acidic and basic pK_a values may result in largely unchanged total concentrations, as is the case between stationary and exponential ammonium-assimilating cells, as well as between stationary phase ammonium-assimilating and nitrogen fixing cells (Figure 3-4). High confidence in comparisons of total ligand concentrations

between ammonium-assimilating and nitrogen-fixing cultures indicates that they possesses similar overall reactivity summed over the titration range, despite possessing different distributions of individual ligands.

3.4 Conclusion

Ligand concentrations and pK_a distributions describing acid-base properties of the Gram-negative surface of the cyanobacterium *Anabaena* sp. strain PCC 7120 are reported and used to assess variability in surface chemistry as a function of batch culture growth conditions. It was determined that the observed variations in ligand concentration cannot be adequately accounted for using one set of parameters describing this bacterial surface. Future potentiometric evaluations of Gram-negative bacterial surface chemistry should report deviations with respect to both growth phase and potential metabolic pathways. Furthermore, it was concluded that metabolic pathway was a greater determinant of ligand variability than growth phase. These results support the idea that, at least in the case of Gram-negative bacterial surfaces, the bacterial surface is a dynamic one where ligand distributions may evolve, for a single bacterial strain and over short (non-evolutionary) timescales, in response to nutritional or environmental demand.

pK_a class	4 to 7	7 to 10	Ratio (acidic to basic)	Total
NO_3 exp.	0.63±0.08	0.06±0.04	9.99	0.69±0.07
NO_3 stat.	1.24±0.08	0.30±0.05	4.11	1.55±0.10
N_2 exp.	2.75±0.40	0.82±0.15	3.35	3.57±0.54
N_2 stat.	2.85±0.49	0.18±0.18	16.19	3.02±0.65
NH_4^+ exp.	3.34±0.18	1.06±0.13	3.25	4.44±0.25
NH_4^+ stat.	2.18±0.23	1.70±0.10	1.28	3.88±0.31
Average[1]	2.15±0.24	0.68±0.08	3.15	2.84±0.45
S. putrefaciens Aerobic (Haas, 2004)[2]	0.99	0.79	1.24	1.78
S. putrefaciens Anaerobic (Haas, 2004)[2]	0.55	0.15	3.63	0.70
NO_3 heat-killed	3.18±0.07	0.92±0.04	3.46	4.10±0.09
N_2 heat-killed	12.31±0.67	6.39±0.58	1.93	18.70±0.59
NH_4 heat-killed	6.02±1.13	7.67±0.89	0.78	13.69±1.01

Table 3-1. Modeled site concentrations (in mmol per dry g) and pKa distributions for all conditions investigated. Values are the average of five independently modeled titrations. Uncertainties are 1 standard error of the mean, where available.

[1] Values are the average of parameters modeled for all 30 live titrations

[2] a wet to dry weight ratio of 10:1 was assumed

	Condition	NO_3 exp.	NO_3 stat.	N_2 exp.	N_2 stat.	NH_4 exp.	NH_4 stat.
Ligands with pK_a values 4 to 7	NO_3 exp.						
	NO_3 stat.	0.85					
	N_2 exp.	0.00	0.04				
	N_2 stat.	0.00	0.02	1.00			
	NH_4^+ exp.	0.00	0.00	0.87	0.94		
	NH_4^+ stat.	0.03	0.44	0.88	0.79	0.19	
	Average	0.00	0.19	0.65	0.48	0.03	1.00
Ligands with pK_a values 7 to 10	NO_3 exp.						
	NO_3 stat.	0.92					
	N_2 exp.	0.02	0.23				
	N_2 stat.	1.00	1.00	0.07			
	NH_4^+ exp.	0.00	0.02	0.93	0.00		
	NH_4^+ stat.	0.00	0.00	0.00	0.00	0.07	
	Average	0.01	1.00	0.98	0.06	0.29	0.00
All ligands	NO_3 exp.						
	NO_3 stat.	0.82					
	N_2 exp.	0.00	0.04				
	N_2 stat.	0.01	0.25	0.98			
	NH_4^+ exp.	0.00	0.00	0.81	0.27		
	NH_4^+ stat.	0.00	0.01	1.00	0.82	0.97	
	Average	0.00	0.14	0.75	1.00	0.03	0.36

Table 3-2. Intervals of confidence in multiple pair-wise comparisons of ligand concentration as evaluated by Tukey post-hoc analysis (two-tailed p, n = 7, df = 52).

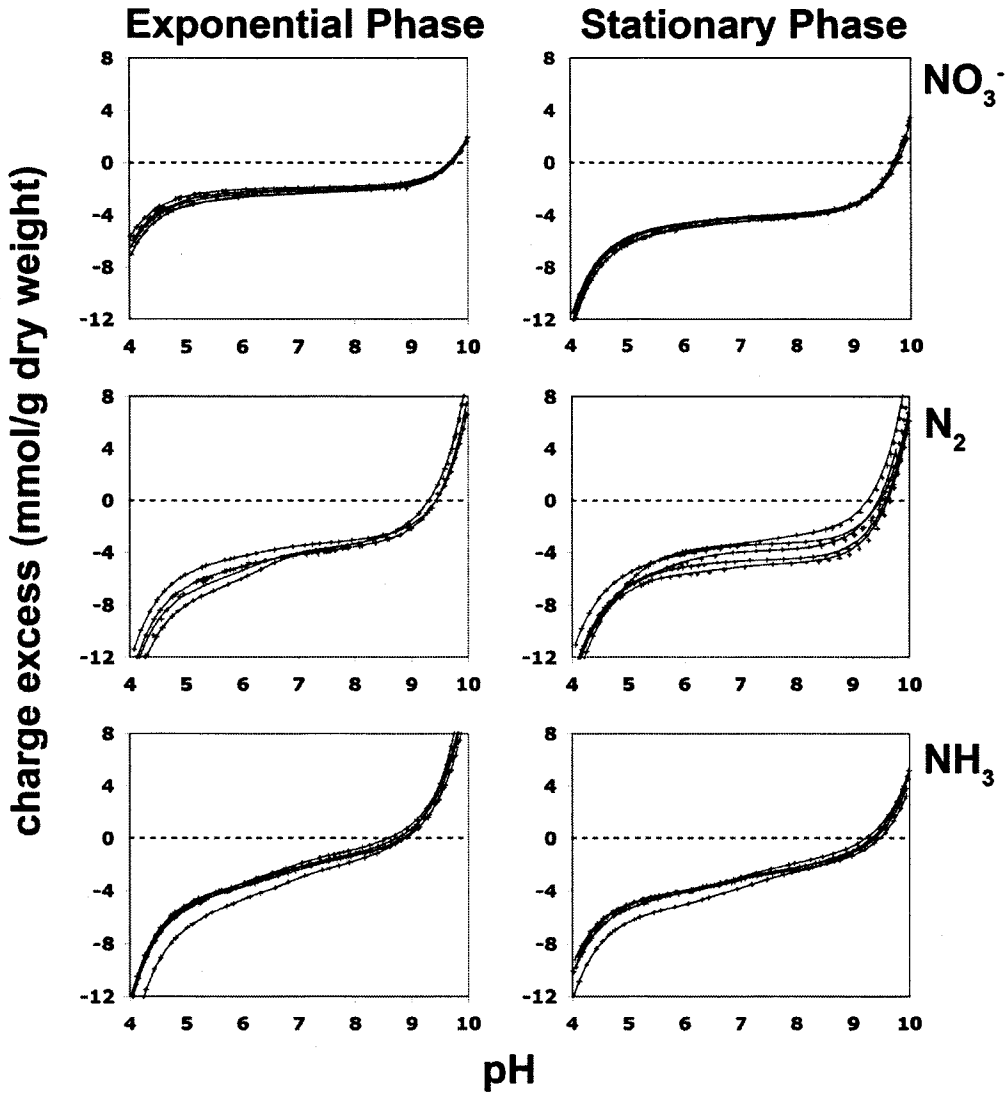

Figure 3-1. Charge excess curves grouped as a function of growth phase and nitrogen metabolism. For each condition, data points represent charge excess of five replicates as measured by titration and smooth curves represent charge excess fitted by the corresponding ligand distribution models.

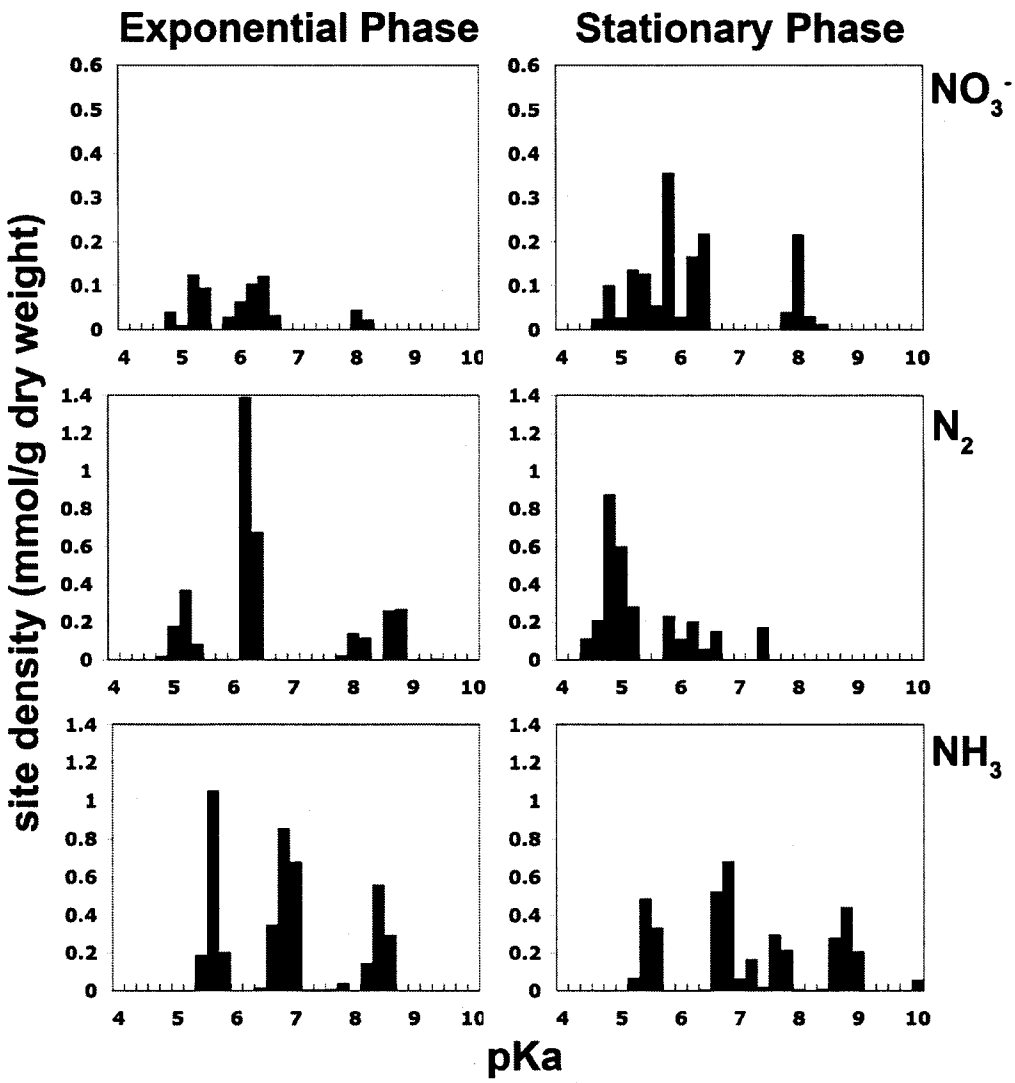

Figure 3-2. Modeled ligand distributions grouped as a function of growth phase and nitrogen metabolism. Each plot accounts for five replicate titrations, with ligand concentrations weighted by occurrence at each pK_a interval.

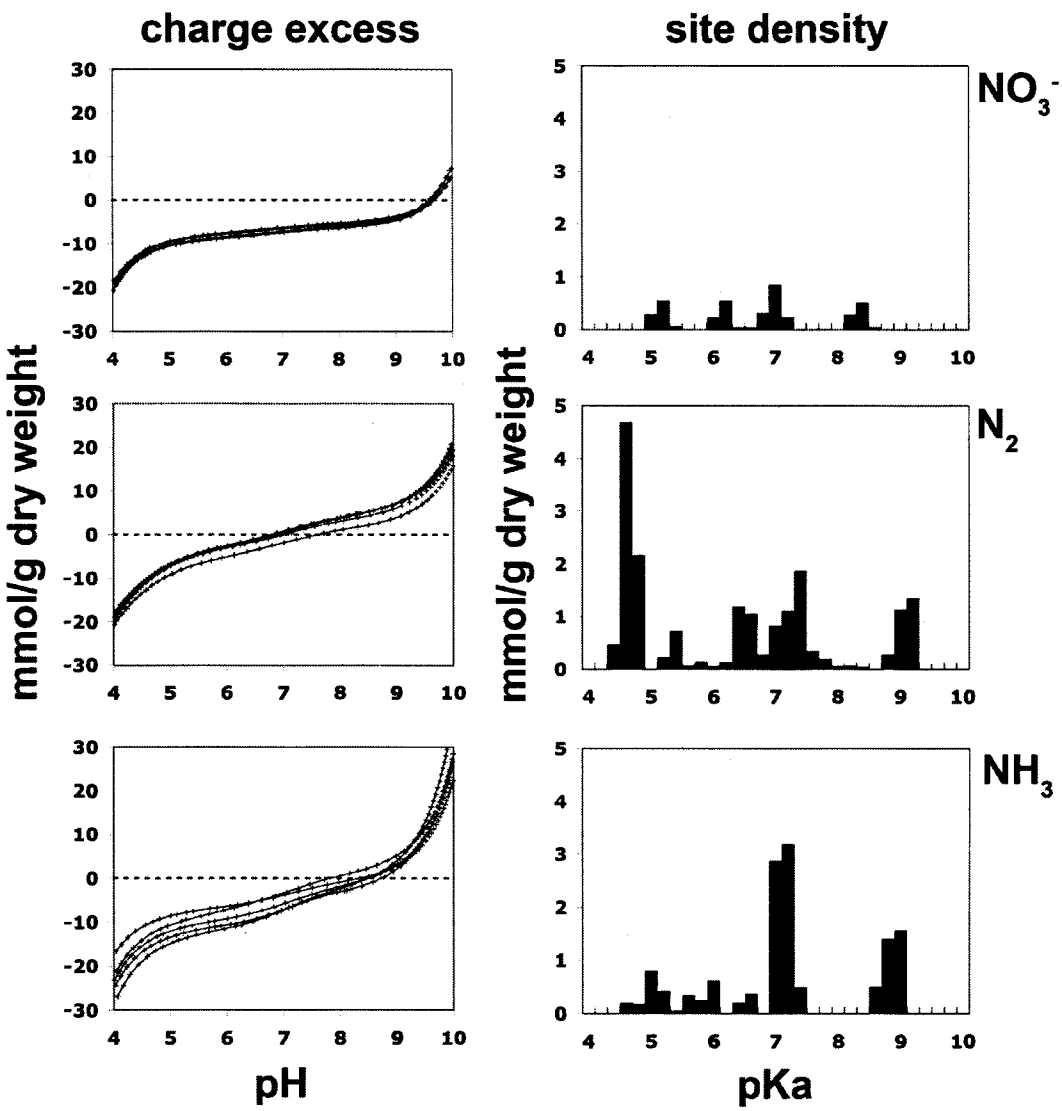

Figure 3-3. Plots of charge excess and corresponding modeled ligand distributions for stationary phase cells lysed by autoclaving. In the charge excess plots, data points represent charge excess of five replicates as measured by titration and smooth curves represent charge excess fitted by the corresponding ligand distribution models. Modeled ligand distributions accounts for five replicate titrations, and ligand concentrations weighted by occurrence at each pK_a interval.

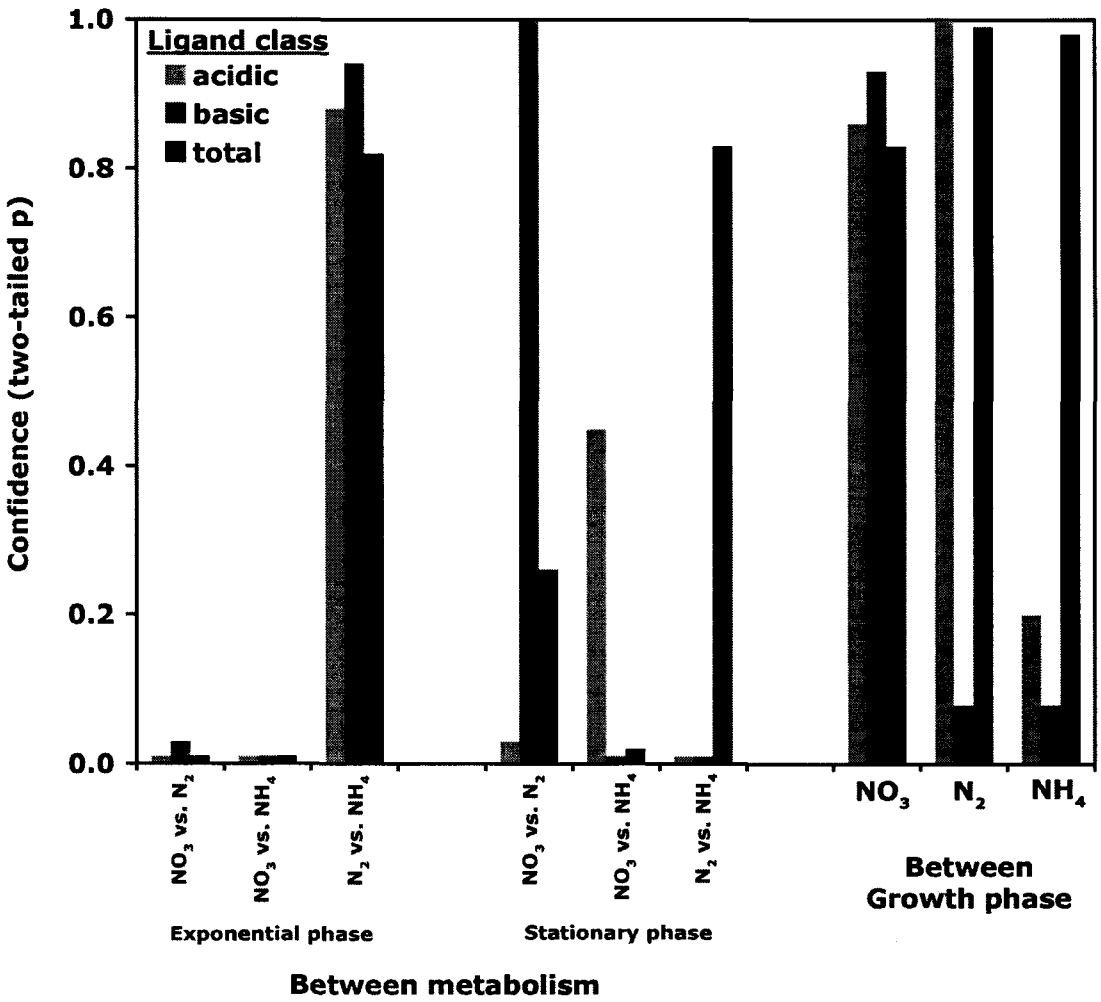

Figure 3-4. Intervals of confidence in multiple pair-wise comparisons of ligand concentration, plotted as a function of comparison type: between-metabolism exponential phase comparisons (left), between-metabolism stationary phase comparisons (center), and between growth phase metabolism comparisons (right).

3.5 References

Baughman GL and Paris DF (1981) Microbial bioconcentration of organic pollutants from aquatic systems – a critical review. *Critical Reviews in Microbiology* 8, 205-228.

Bayer ME and Sloyer Jr. JL (1990) The electrophoretic mobility of gram-negative and gram-positive bacteria: an electrokinetic analysis. *Journal of General Microbiology* 136, 867-874.

Beveridge TJ, Forsberg CW, and Doyle RJ (1982) Major sites of metal binding in *Bacillus licheniformis* walls. *Journal of Bacteriology* 150, 1438-1448.

Beveridge TJ and Koval SF (1981) Binding of metals to cell envelopes of *Escherichia coli* K-12. *Applied and Environmental Microbiology* 42, 325-335.

Beveridge TJ and Murray RG (1980) Sites of metal deposition in the cell wall of *Bacillus subtilis*. *Journal of Bacteriology* 141, 876-887.

Borrok D and Fein JB (2005) The impact of ionic strength on the adsorption of protons, Pb, Cd, and Sr onto the surfaces of Gram negative bacteria: testing non-electrostatic, diffuse, and triple-layer models. *Journal of Colloid and Interface Science* 286, 110-126

Borrok D, Fein JB, Tischler M, O'Loughlin E, Meyer, H, Liss M, and Kemner KM (2004) The Effect of Acidic Solutions and Growth Conditions on the Adsorptive Properties of Bacterial Surfaces. *Chemical Geology* 209, 107-109.

Brassard P, Kramer JR, and Collins PV (1990) Binding site analysis using linear programming. *Environmental Science and Technology*. 24, 195-201

Chamot, D and Owttrim, GW (2000) Regulation of cold shock-induced RNA helicase gene expression in the cyanobacterium *Anabaena* sp. strain PCC 7120. *Journal of Bacteriology* 182, 1251-1256.

Chang J-S, Law R, and Chang C-C (1997) Biosorption of lead, copper and cadmium by biomass of *Pseudomonas aeruginosa* PU21. *Water Research* 31, 1651-1658.

Corapcioglu MY and Kim S (1995) Modeling facilitated contaminant transport by mobile bacteria. *Water Resources Research* 31, 2693-2648.

Cox JS, Smith DS, Warren LA, and Ferris FG (1999) Characterizing heterogeneous bacterial surface functional groups using discrete affinity spectra for proton binding. *Environmental Science and Technology* 33, 4514–4521.

Daughney CJ and Fein JB (1998) The effect of ionic strength on the adsorption of H^+, Cd^{2+}, Pb^{2+}, and Cu^{2+} by *Bacillus subtilis* and *Bacilllus licheniformis*: A surface complexation model. *Journal of Colloid and Interface Science* 198, 53-77.

Daughney CJ, Fein JB and Yee, N (1998) A comparison of the thermodynamics of metal adsorption onto two common bacteria. *Chemical Geology* 144, 161-176.

Daughney CJ, Fowle DA, and Fortin DE (2001) The effect of growth phase on proton and metal adsorption by *Bacillus subtilis*. *Geochimica et Cosmochimica Acta* 65, 1025-1035.

Fein JB, Boily JF, and Yee, N (2004) Potentiometric titrations of *Bacillus subtilis* cells to low pH and a comparison of modeling approaches. *Geochimica et Cosmochimica Acta* 69, 1123-1132.

Fein JB, Daughney CJ, Yee N, and Davis TA (1997) A chemical equilibrium

model for metal adsorption onto bacterial surfaces. *Geochimica et Cosmochimica Acta* 61, 3319-3328.

Fein JB and Delea DE (1999) Experimental study of the effect of EDTA on Cd adsorption by *Bacillus subtilis*: a test of the chemical equilibrium approach. *Chemical Geology* 161, 375-383.

Fortin D, Ferris FG, and Beveridge TJ (1997) Surface-mediated mineral development by bacteria. In *Geomicrobiology: Interactions Between Microbes and Minerals* (eds. JF Banfield and KH Nealson), *Reviews in Mineralogy and Geochemistry* 35, pp. 161-180, Mineralogical Society of America, Washington, DC.

Fowle DA and Fein JB (1999) Competitive adsorption of metal cations onto two gram positive bacteria: testing the chemical equilibrium model. *Geochimica et Cosmochimica Acta* 63, 3059-3067.

Fowle DA and Fein JB (2000) Experimental measurements of the reversibility of metal-bacteria adsorption reactions. *Chemical Geology* 168, 27-36.

Fowle DA, Fein JB, and Martin AM (2000) Experimental study of uranyl adsorption by *Bacillus subtilis*. *Environmental Science and Technology* 34, 3737-3741.

Friis N and Meyers-Keith P (1986) Biosorption of uranium and lead by *Streptomyces longwoodensis*. *Biotechnology and Bioengineering* 28, 21-28.

Haas JR, Dichristina TJ, and Wade Jr. R (2001) Thermodynamics of U(VI) sorption onto *Shewanella putrefaciens*. *Chemical Geology* 180, 33-54.

Haas, JR (2004) Effects of cultivation conditions on acid-base titration properties

of *Shewanella putrefaciens*. *Chemical Geology* 209, 67-81.

Harris DC (1995) *Quantitative Chemical Analysis*. Freeman, New York, NY.

Hsu JC (1996) *Multiple Comparisons. Theory and Methods*. Chapman and Hall, London, England.

Kaneko T, Nakamura Y, Wolk CP, Kuritz T, Sasamoto S, Watanabe A, Iriguchi M, IshikawaA, Kawashima K, Kimura T, Kishida Y, Kohara M, Matsumoto M, Matsuno A, Muraki A, Nakazaki N, Shimpo S, Sugimoto M, Takazawa M, Yamada M, Yasuda M, and Tabata S (2001) Complete genomic sequence of the filamentous nitrogen-fixing cyanobacterium *Anabaena* sp. strain PCC 7120. *DNA Research* 8, 205-213.

Konhauser KO, Fyfe WS, Ferris FG, and Beveridge TJ (1993) Metal sorption and precipitation by bacteria in two Amazonian river systems: Rio Solimoes and Rio Negro, Brazil. *Geology* 21, 1103-1106.

Lindgvist R and Enfield CG (1992) Cell density and non-equilibrium sorption effects on bacterial dispersal in ground water microcosms. *Microbial Ecology* 24, 25-41.

Lourenço SO, Barbarino E, Lavin PL, Lanfer Marquez UM, and Aidar E (2004) Distribution of intracellular nitrogen in marine microalgae: Calculation of nitrogen-to-protein conversion factors. *European Journal of Phycology* 39, 17-32.

Madigan MT, Martinko JM, and Parker J (1997) *Brock Biology of Microorganisms*. 8th ed. Prentice Hall, Upper Saddle River, NJ.

Macaskie LE and Basnakova G (1988) Microbially-enhanced chemical sorption of heavy metals: A method for the bioremediation of solutions containing long-

lived isotopes of neptunium and plutonium. *Environmental Science and Tech*nology 32, 184-187.

Martinez RE and Ferris FG (2001) Chemical equilibrium modeling techniques for the analysis of high-resolution bacterial metal sorption data. *Journal of Colloid and Interface Science* 243, 73-80.

Martinez RE, Smith DS, Kulczycki E, and Ferris FG (2002) Determination of intrinsic bacterial surface acidity constants using a Donnan shell model and a continuous pKa distribution method. *Journal of Colloid and Interface Science* 253, 130-139.

McCarthy JF and Zachara JM (1989) Subsurface transport of contaminants. *Environmental Science and Technology*. 23, 496-502.

Mérida A, Candau P, and Florencio FJ (1991) Regulation of glutamine synthetase activity in the unicellular cyanobacterium *Synechocystis* sp. strain PCC 6803 by the nitrogen source: effect of ammonium. *Journal of Bacteriology* 173, 4095-4100.

Ngwenya BT, Sutherland IW, and Kennedy L (2003) Comparison of the acid-base behavior and metal adsorption characteristics of a gram-negative bacterium with other strains. *Applied Geochemistry* 18, 527-538.

Phoenix VR, Martinez RE, Konhauser KO and Ferris FG (2002) Characterization and implications of the cell surface reactivity of the cyanobacteria *Calothrix* sp. *Applied and Environmental Microbiology* 68, 4827-4834.

Plette CC, Van Riemsdijk WH, Benedetti MF, and Van der Wal A (1995) pH dependent charging behavior of isolated cell walls of a Gram-positive soil bacterium. *Journal of Colloid and Interface Science* 173, 354–363.

Rinker KD and Kelly RM (2000) Effect of carbon and nitrogen sources on growth dynamics and exopolysaccharide production for the hyperthermophilic archaeon Thermococcus litoralis and bacterium Thermotoga maritima. *Biotechnology and Bioengineering* 69, 537-547.

Rippka R, Deruelles J, Waterbury JB, Herdman M, and Stanier RY (1979) Generic assignments, strain histories and properties of pure cultures of cyanobacteria. *Journal of General Microbiology* 111, 1-61.

Smith DS, Adams NWH, and Kramer JR (1999) Resolving uncertainty in chemical speciation determinations. *Geochimica et Cosmochimica Acta* 63, 3337-3347.

Smith DS and Ferris FG (2001) Proton binding by hydrous ferric oxide and aluminum oxide surfaces interpreted using fully optimized continuous pK_a spectra. *Environmental Science and Technology* 35, 4637-4642.

Smith, DS and Kramer, JR (1999) Multi-site proton interactions with natural organic matter. *Environment International* 25, 307-314.

Sokolov I, Smith DS, Henderson GS, Gorby YA, and Ferris FG (2001) Cell surface electrochemical heterogeneity of the Fe(III)-reducing bacteria *Shewanella putrefaciens*. *Environmental Science and Technology* 35, 341-347.

Thormann KM, Saville RM, Shukla S, and Spromann AM (2005) Induction of rapid detachment in *Shewanella oneidensis* MR-1 biofilms. *Journal of Bacteriology* 187, 1014-1021.

van Loosdrecht MCM, Lyklema J, Norde W, and Zehnder AJB (1989) Bacterial adhesion: A physicochemical approach. *Microbial Ecololgy* 17, 1-15.

van Loosdrecht MCM, Norde W, Lyklema J, and Zehnder AJB (1990) Hydrophobic and electrostatic parameters in bacterial adhesion. *Aquatic Sciences* 52, 103-114.

Wandersman C and Delepelaire P (2004) Bacterial iron sources: from siderophores to hemophores. *Annual Review of Microbiology* 58, 611-647.

Warren LA and Ferris FG (1998) Continuum between sorption and precipitation of Fe(III) on microbial surfaces. *Environmental Science and Technology* 32, 2331–2337.

Wolk, CP (1996) Heterocyst formation. *Annual Review of Genetics* 30, 59-78.

Wong PK, Lam KC, and So CM (1993) Removal and recovery of Cu(II) from industrial effluent by immobilized cells of *Pseudomonas putida* II-11. *Applied Microbiology and Biotechnology* 39, 127-131.

Yee N and Fein JB (2001) Cd adsorption onto bacterial surfaces: a universal adsorption edge? *Geochimica et Cosmochimica Acta* 65, 2037–2042.

Yee N, Fein JB, and Daughney CJ (2000) Experimental study of the pH, ionic strength, and reversibility behavior of bacteria-mineral adsorption. *Geochimica et Cosmochimica Acta* 64, 609-617.

Yee N, Fowle DA, and Ferris FG (2004) A Donnan potential model for metal sorption onto *Bacillus subtilis*. *Geochimica et Cosmochimica Acta* 68, 3657-3664

CHAPTER 4

Acid-base properties of cyanobacterial surfaces II: silica as a chemical stressor influencing cell surface reactivity[1]

4.1 Introduction

As bacteria generally lack internal membrane-bound structures, they must rely on processes localized to surface membranes for a variety of homeostatic functions including metabolism, nutrient transport, signal transduction, motility, and cell division (Madigan et al., 1997). At the same time, the surface layers serve as the primary interface between bacterium and its extracellular milieu, playing a central role in a cell's ability to survive in the face of extreme chemical and physical stressors.

Furthermore, the surfaces of bacteria are highly reactive. They are studded with organic chemical functional groups that serve as efficient ligands for

[1] Lalonde SV, Smith DS, Owttrim GW, and Konhauser KO (2006) *Geochimica et Cosmochimica Acta* submission W4105, in review as of April 11th, 2006.

the sorption of metals (e.g., Beveridge and Murray, 1980; Beveridge et al., 1982; Daughney and Fein, 1998; Daughney et al., 1998), in turn affecting mineral precipitation and dissolution reactions (Konhauser et al., 1993; Fortin et al., 1997; Warren and Ferris, 1998), solute transport (e.g., McCarthy and Zachara, 1989; Lindqvist and Enfield, 1992; Corpcioglu and Kim, 1995), and redox reactions (for review, see Konhauser, 2006).

In complex solutions under laboratory conditions, the sorptive behavior of the bacterial surface has been successfully described using surface complexation modeling (e.g., Fowle and Fein, 1999). Such models have been employed to describe the bacterial surface in thermodynamic terms that are independent of experimental conditions. This enables quantitative predictions for elemental partitioning between the aqueous phase and the bacterial surface. For such models to be useful, potentiometric titrations are required to derive concentration and stability parameters for discrete proton-exchanging organic chemical functional groups (referred hereto as "ligands") comprising the bacterial surface. However, it has become apparent that titration data alone cannot provide mechanistic details of adsorption reactions at a molecular level, as different sets of ligands, modeled using different assumptions regarding how sites are affected by surface electric field effects, may provide equally good fit to potentiometric titration data (Fein et al., 2005). Despite these uncertainties, potentiometric titration remains the most practical method for enumerating the concentration of sites that may contribute to surface charge over a wide (3 - 11) pH range.

Ligand variability between bacterial species, or even inherent to a single species, should be accounted for in any modeling approach, and the extent to which a bacterium is capable of modifying its outer surface in terms of acid-base behavior is poorly understood. To date, ligand variability inherent to a single bacterial species has been quantitatively evaluated as a function of growth phase (Daughney et al., 2001; Haas, 2004; Lalonde et al., submitted), nutrient availability (Borrok et al., 2004; Haas, 2004), and metabolic pathway (Borrok et al., 2004; Haas, 2004; Lalonde et al., submitted). These factors are of special consideration because they pertain to culturing and cell harvesting procedures that

are inherent to the laboratory study of bacterial surfaces, and their influence must be accounted for. However there exist numerous other biologically relevant factors, including a wide variety of geochemical stressors, which are not typically encountered in a laboratory setting, yet may influence cell surface composition. It is the aim of this study to evaluate whether or not chemical stress, in this case growth in media at various degrees of saturation with respect to amorphous silica, may influence the acid-base properties of the cell surface as determined by potentiometric titration.

Silica was chosen as a potential stressor because numerous cyanobacteria have been observed to grow in geothermal environments where the rapid precipitation of amorphous silica results in their complete encrustation (see Konhauser et al. (2004) for review). Laboratory strains have been successfully grown in media with concentrations upwards of 300 ppm Si, where exponential phase growth proceeded concurrently with rapid silica polymerization and precipitation (Phoenix et al., 2000; Yee et al., 2003). In this study, we used potentiometric titration to examine the influence of various silica concentrations on the acid-base properties of the cyanobacterium *Anabaena* sp. strain PCC 7120. Titration data is modeled for discrete ligand concentrations and apparent pK_a constants in a non-electrostatic approach, and the results are statistically evaluated for confidence between condition parameters in a pair-wise fashion. A discrete site model was chosen over a continuous affinity approach for facility of statistical comparison, as well as applicability of discrete site data to surface complexation modeling efforts. Conditions of 300 ppm NaCl and 300 ppm Si as powdered silica are also evaluated as potential chemical stressors. As ligand variability for this organism has been reported to arise as a function of nitrogen assimilation pathway (Lalonde et al., submitted), we also conducted our experiments using different nitrogen sources for cell culturing. Finally, we considered the synergistic effects of silica concentration and nitrogen fixation pathway as determinants of cell surface reactivity.

4.2 Methods

4.2.1 Growth Procedures

The cyanobacterial strain used in this study, *Anabaena* sp. strain PCC 7120, was chosen for its capacity for nitrogen fixation, high rate of growth, and lack of sheath or S-layer (Rippka et al., 1979). The methodology of Lalonde et al. (submitted) was applied for all growth, preparation, titration, and modeling procedures.

Cultures limited to growth by ammonium assimilation, assimilatory nitrate reduction, and nitrogen fixation were separately maintained in 50 ml of nitrogen free liquid BG-11(0) media buffered to pH 8 with 10 mM Tricine and supplemented with 17.6 mM ammonium as NH_4Cl,17.6 mM nitrate as $NaNO_3$, or 17.6 mM NaCl (no fixed nitrogen source) where required. BG-11 ingredients containing fixed nitrogen (ferric ammonium citrate and cobaltous nitrate hexahydrate) were replaced with nitrogen-free equivalents (ferric citrate and cobaltous chloride hexahydrate). All cultures were grown at 30°C under a constant illumination of ~100 microeinsteins/m^2/s, bubbled with humidified air, and orbitally shaken (50 ml cultures) or magnetically stirred (1 L cultures) at 150 rpm (Chamot and Owttrim, 2000). Cultures limited to a single nitrogen source over at least three transfers were prepared as a source of inoculum (10% v/v) for larger 1 L cultures representing each nitrogen source and prepared to contain mineralizing and control compounds. For all three nitrogen sources, 1 L silica-treated cultures were prepared by the addition of sodium metasilicate to concentrations of 55 and 300 ppm Si. For nitrate-reducing growth only, conditions of 300 ppm NaCl and 300 ppm Si as powdered silica (powdered silicic acid, Fisher Scientific) were also prepared. For all relevant conditions, powdered silica or the appropriate salt was added prior to autoclaving, and cultures containing silica were adjusted to pH 8 with KOH immediately prior to inoculation. In the case of 300 ppm sodium metasilicate conditions, neutralization induced a state of supersaturation such that amorphous silica precipitated in solution and onto organic surfaces, with monomeric silica concentrations approaching 70 ppm Si after 36 hours. Cultures with 55 ppm Si were just below

saturation with respect to amorphous silica, and remained stable in monomeric silica concentration over time. Media containing powdered silica was allowed to equilibrate for 3 days after neutralization and prior to inoculation, and contained stable clay-sized silica particles throughout the experimental duration. All cultures were harvested at stationary phase growth, indicated by an absorbance of 0.6 ± 0.03 (~ 0.24 g dry bacteria/L), in order to better approximate natural conditions.

All biomass was washed immediately upon harvesting, stored at room temperature and titrated within 18 hours of harvesting. Cells centrifuged from each liter of culture were washed three times with 200 ml of 18 MΩ water, four times with 0.01 M KNO_3 titration electrolyte, and resuspended in 0.01M KNO_3 to a final volume of 50 ml. For each condition, the final 50 ml of concentrated (~4 g dry bacteria/L) biomass was divided to provide 5 replicate titrations.

4.2.2 Potentiometric titrations

Solutions were prepared using standard analytical methods (Harris, 1995) and glassware was prewashed according the methodology of Cox et al. (1999). A 0.01 M titration electrolyte was prepared using KNO_3 salt, while 0.01 M NaOH and 0.2 M HNO_3 solutions were prepared from concentrate and standardized by titration against dried KHP prior to use. All solutions were prepared using water purged of dissolved CO_2 with $N_2(g)$ for at least 30 minutes and maintained under a nitrogen atmosphere.

Titration suspensions were prepared by weight with the addition of ~10 g of concentrated, electrolyte-washed biomass suspension to ~40 g of electrolyte solution in a titration flask under a constant purge of N_2 gas. A Ross-type glass pH electrode (Man-Tech Associates Inc., Guelph, ON) was calibrated using three commercial buffers and installed in the flask along with a thermocouple, magnetic stir bar, bubbler, and titrant dispenser. After acidification of the titration suspension to pH ~3.2 with 200 µl 0.2 M HNO_3, and upon 30 minutes of equilibration, titrations were performed alkalimetrically from pH ~3.2 to pH 11 using a QC-Titrate autotitrator (Man-Tech Associates Inc., Guelph, Ontario) delivering CO_2-free 0.01 M NaOH. pH resolution was set to 0.1 and electrode

stability criteria to <1 mV/s for each step. Titration suspensions were filtered onto preweighed Whatman GF/C #42 filters (Whatman Inc, Florham park, New Jersey) immediately after titration, and oven dried at 70 °C for 48 hours prior to weighing. All conditions were represented by 5 replicate titrations, and in each case cellular integrity was confirmed by pigment autofluorescence using a Zeiss Axioskop 2 epi-fluorescent light microscope. Titration data presented by Lalonde et al. (submitted) for stationary phase *Anabaena* cultures was obtained using identical protocols and is used here to represent silica-free controls.

4.2.3 Modeling of surface ligand concentrations

Discrete bacterial surface site concentrations were fit to the titration data using a non-electrostatic linear-programming pK_a spectrum approach described in detail by Lalonde et al. (submitted) and previously applied to a variety of potentiometric titration studies (Brassard et al., 1990; Smith and Kramer, 1999; Smith et al., 1999; Cox et al., 1999; Martinez and Ferris, 2001; Martinez et al., 2002; Phoenix et al., 2002; Fein et al., 2005). It was determined by replicate blank titration that experimental error had a negligible effect on system charge balance between pH ~3.5 and pH~10.3, and data was selected in the 4 to 10 pH range for the modeling of ligand concentrations over a pK_a range of 3 to 11 in 0.2 increments. Excess in the charge balance of the system is assumed to result solely by the speciation of proton-exchanging ligands on the bacterial surface by the following charge balance:

$$\sum_{j=1}^{n}[L_j^-] - [ANC] = Cb_i - Ca_i + [H^+]_i - [OH^-]_i \qquad (1)$$

where, for the i^{th} addition of titrant, Cb and Ca are the concentrations of base and acid, respectively, $[H^+]$ and $[OH^-]$ are measured by the pH electrode, $[L_j^-]$ is the concentration of deprotonated functional groups for the j^{th} monoprotic site of n possible sites set by the pK_a spectrum, and the acid neutralizing capacity (ANC) functions as a constant offset in charge excess. The bacterial ligand concentrations and ANC that provide the best fit to the measured charge excess (right hand side of equation (1)) is determined iteratively by minimizing the absolute error

between measured and fitted charge excess (left hand side of equation (1)). The number of distinct-pK_a sites that are required to describe the data is minimized as the linear-programming approach emphasizes zero as a possible solution, and pK_a values were not corrected for surface electrostatic potential in order to avoid assumptions regarding uniformity in cell surface area and specific capacitance. All replicate titrations were modeled independently in order to provide estimates of variance for statistical purposes.

4.3 Results and Discussion

4.3.1 Charge Excess

Measured and fitted charge excess curves representing sodium metasilicate conditions and silica-free controls are plotted as a function of nitrogen source and silica concentration in Figure 4-1. Rapid changes in charge excess, corresponding to increased surface buffering capacity, occurred at pH extremes for all conditions tested and have been previously reported for titrations of Gram-negative bacterial surfaces (Haas et al., 2001; 2004; Lalonde et al., submitted). Significant concentrations of ligands with extreme dissociation constants, including acidic carboxyl and basic hydroxyl functional groups, are likely responsible for buffering in this region, although increasing uncertainty in measured charge excess at extreme pH (Smith et al., 1999), and a lack of charge excess inflection within the titration range, prevents their accurate quantification. Modeling performed over a pK_a range of 3 to 11 allowed for the inclusion of these hypothesized ligands to provide better fit to excess charge without significantly affecting ligand distributions in the 4 to 10 pK_a range (as per Lalonde et al., submitted).

Uncertainty in charge excess at low pH (<3) prevents knowledge of a zero proton condition ($T_H°$), and the charge balance expression ignoring $T_H°$ implicitly assigns a value of zero to the pH of the titration suspension prior to acidification (pH ~7) (Fein et al., 2005; Lalonde et al., submitted). It is clear from Figure 4-1 that the point of zero charge (PZC) varies between conditions where it should be fixed. In other words, variable degrees of hysteresis have occurred as the result of

non-reversible speciation reactions. The irreversible desorption of structurally bound Mg and Ca due to rapid acidification of bacterial suspensions prior to titration may account for some hysteretic effects (Borrok et al., 2004), and reverse titration of selected samples confirmed that hysteretic effects were incurred as the result of rapid acidification (data not shown). It should be noted that two directions of hysteresis were observed; for most conditions, including all 0 ppm Si conditions, more equivalents of base were required to return to initial electrolyte pH (~7) than the amount of acid equivalents added during initial acidification, while for others (i.e., N_2 and NH_4 conditions at 55 ppm), the reverse occurred. The former would be expected with the exposure of previously unavailable ligands by acidification, and the latter with the unavailability of previously exposed ligands after acidification. Organic compounds also display true hysteresis during sorption onto soils and sediments, where hysteresis is the result of the irreversible structural expansion of the sorbant rather than the entrapment of sorbate (Sander et al. 2005; 2006), and it is not unreasonable that similar processes acting on the microbial surface during acidification may have contributed to hysteresis in either direction. Variability in the direction and degree of hysteresis between conditions is difficult to reconcile with the repeatability of hysteretic effects between replicates, and considered together they indicate differences in cell surface composition between conditions rather than experimental error.

Hysteresis is accounted for during modeling by the acid-neutralizing capacity term representing vertical offset of the charge excess fit, and therefore does not affect the modeling of ligand distributions over the reversible (pH 3.2 to 11) titration range. The charge excess curves are presented in Figure 4-1 for the qualitative assessment of replicate repeatability and the evaluation of condition-specific charging profiles.

4.3.2 Modeled parameters

Modeled parameters for all conditions are presented in Table 4-1, and sodium metasilicate conditions are summarized by composite pK_a distribution plots in Figure 4-2. As evident in Figure 4-2, ligand distributions varied

sufficiently between conditions as to preclude the assignment of specific sites that are conserved between all conditions. For this reason, data is grouped into acidic (ligands with pK_a values between 4 and 7) and basic (ligands with pK_a values between 7 and 10) categories in Table 4-1, enabling pair-wise comparison and statistical correlation between conditions (discussed below).

Data supporting Table 4-1 is displayed graphically in Figure 4-2 in the form of ligand pK_a distribution plots that present for each condition the modeling results compounded over all five conditions and weighted by occurrence on a dry weight basis, as described by Lalonde et al. (submitted). All conditions return non-zero concentrations for both acidic and basic ligand categories, and variability is evident between all conditions in ligand concentration, pK_a distribution, and the number of distinct sites invoked by the pK_a spectrum model.

Several general, qualitative observations can be made regarding the composite plots shown in Figure 4-2. For conditions with 300 ppm Si, ligands with pK_a values below ~6 are noticeably absent and the concentration of basic ligands increases relative to conditions with 55 or 0 ppm Si. It is unlikely that these basic ligands represent the ionization of silicic acid that may have been transferred or unremoved by the washing procedure; although soluble silicic acid has a pK_a of 9.8 (Iler, 1979), surface sites on colloidal and particulate silica have ionization constants of ~7.5 (Kobayashi et al., 2005), and such sites are absent in the composite plots for 300 ppm Si even though the colloidal or particulate silica is more likely to have been transferred during washing than the soluble silicic acid.

Conditions with 0 and 55 ppm Si generally indicate cell surfaces dominated by acidic ligands, in concurrence with the overall negative surface charge typically displayed by both Gram-negative and Gram-positive bacteria (Bayer and Sloyer, 1990). Electrophoretic assessment of surface charge was attempted over the course of this study, however, the filamentous nature of *Anabaena* introduced chain-length effects and other random errors that prevented any conclusions beyond a neutral to negatively charged surface for all conditions assessed (data not shown). Although effective surface charge is partially

determined by ligands outside of the titration range, the balance of acidic ligands conferring negative charge at neutral pH, and those basic ligands conferring positive charge at neutral pH, will to some extent control effective surface charge.

Based on previous spectroscopic investigations (Yee et al., 2004; Jiang et al., 2004), ligands with pK_a values between 8 and 10 likely represent amine functional groups contributing positive charge at neutral pH, as phenolic hydroxyl functional groups display dissociation constants between 9.9 and 10.8 (Martell and Smith, 1974) and at least for Gram-positive bacteria, have not been considered important constituents of major cell wall components (Cox et al., 1999). Within the Gram-negative cell wall, peptidoglycan, proteins, and lipoproteins all possess amine functional groups, sometimes at more than one location per polymer unit, and spectroscopic methods confirm their abundance on the bacterial surface (Yee et al., 2004; Jiang et al., 2004). As protonated amine functional groups are the only proton-exchanging ligands conferring positive charge to the bacterial surface, it follows that the direction and degree of electrical charge on a bacterial surface free of sorbed contaminants is primarily determined at any pH by the balance in concentration between protonated amine functional groups and deprotonated acidic functional groups conferring negative charge. Variability in ligand distribution between conditions is discussed in this context after statistical treatments outlined below.

4.3.3 Sodium chloride and particulate silica stress

Conditions of 300 ppm NaCl and 300 ppm Si as particulate silica were also investigated for nitrate-reducing cultures, and the results are included in Table 4-1 and summarized graphically in Figure 4-3. These conditions were performed on nitrate-reducers out of consideration for the large body of genetic knowledge regarding the cyanobacterial salt stress response (discussed below).

For nitrate-reducing conditions of 300 ppm NaCl, while charge excess curves resemble those obtained for 0 and 55 ppm Si nitrate-reducing conditions, significant hysteresis was observed. The direction of hysteresis is opposite to that observed for most conditions; for conditions of 300 ppm NaCl, titratible

functional groups were rendered unavailable by rapid acidification. This may be, in part, reconciled by previous efforts that have revealed expressional changes in both membrane and cytoplasmic proteins that are induced by osmotic and salt stress. For the halotolerant cyanobacterium *Anabaena torulosa*, as many as 90 genes are induced in response to salt-stress (Apte and Bhagwat, 1989; Apte and Haselkorn, 1990), and for *Synechocystis* sp. strain PCC 6803, about 240 genes are upregulated 3-fold within the first 30 min of exposure to salt, decreasing to 39 after 24 hours (Marin et al., 2004). Detailed study has demonstrated that overexpression of a Na^+/H^+ antiporter confers salt tolerance to *Synechococcus* sp. strain PCC 7942 (Waditee et al., 2002). While the influence of changes in membrane protein expression on bulk acid-base microbial surface characteristics remains unknown, the increased importance of transmembrane structures whose function or conformation is dependant on pH, as is the case with the Na^+/H^+ transporter (Putney et al., 2002), could account for the significant hysteresis observed for conditions of 300 ppm NaCl, and similar processes might account for the variability in hysteresis between conditions. The composite plot of ligand distribution for the 300 ppm NaCl condition shows a total ligand concentration comparable to stressor-free controls, however the majority of ligands have a pK_a around 7. Interestingly, salt-stress-induced proteins previously identified from two different strains of *Anabaena* have isoelectric points between 5.8 and 7.5 (Apte and Bhagwat, 1989).

Results obtained from conditions of 300 ppm Si (as particulate silica) are also presented in Figure 4-3, and display the largest deviation from other conditions in both charge excess and ligand distribution. Hysteresis was minimal for this condition, and the charge excess curve shows increased buffering over the entire titration range. Modeled ligand concentrations were in total approximately 6 times higher than other conditions, and largely distributed between equally large peaks at pK_a 7 and 9. It should be noted that the mode of growth in the presence of particulate silica was different relative to all other conditions; silica particles were rapidly covered by *Anabaena* cells, and the cultures were dominated by clumps of bacteria-silica aggregates, in contrast to the well-dispersed nature of

Anabaena cells grown under all other conditions. The incomplete separation of bacteria from silica during washing is likely responsible for the elevated ligand concentrations observed for this condition. An intrinsic ionization constant of 7.5 has been predicted for surface sites of particulate silica on the basis of the multisite surface complexation (MUSIC) model and estimated by potentiometric titration to be 7.6 (Kobayashi et al., 2005), and the first deprotonation of monosilicic acid occurs ~9.8 (Iler, 1979). As discussed above, the titrations of this condition (SiO_2, Fig. 4-3) were likely controlled by the presence of particulate silica that could not be removed from the bacterial surfaces or was consistently transferred along with the bacteria after centrifugation and between washes.

4.3.4 Sources of ligand variability

In order to ascertain the sources of variability between the examined conditions, pair-wise indices of confidence in comparisons between ligand concentrations were generated using the Tukey-Kramer test in ANOVA post-hoc analysis. The Tukey-Kramer test, a variant of the Tukey HSD test that utilizes harmonic means to account for unequal sample sizes, allows for a large number of pair-wise comparisons to be made while maintaining an overall type I error rate at the desired level of significance (0.05 in this case) (Hsu, 1996). Previous titration studies revealing variability in ligand distribution between growth conditions (Daughney et al., 2001; Haas, 2004) have employed independent pair-wise comparisons plagued by an overall type I error rate that increases with the number of comparisons made (see Lalonde et al., submitted). The Tukey-Kramer test accounts for an increasing number of pair-wise comparisons by decreasing the confidence in difference between pairs according to the studentized range distribution.

Modeled parameters were broadly classified as acidic (pK_a <7) or basic (pK_a >7) in order to simplify the comparison of ligands between conditions and to select for only important changes with respect bulk acid-base surface properties. The average parameters from conditions of 300 ppm Si as particulate silica were considered outliers and excluded from Tukey-Kramer analysis. Three distinct

rounds of Tukey-Kramer analysis were performed, one for each class of ligand concentration (acidic or basic) and one for total ligand concentration, and each round comprised all pair-wise comparisons between 11 mean concentrations (mean concentrations from 10 conditions of n=5, and the mean of those concentrations with n=50). Two-tailed confidence intervals for all pair-wise concentration comparisons are presented for reference in Table 4-2.

In order to distinguish trends in the similarity of parameters across conditions, two-tailed confidence intervals obtained by Tukey-Kramer analyses are grouped by comparison type in Figure 4-4. Pairwise-comparisons between metabolic conditions indicate that differences in ligand distributions resulting from differential metabolism are greatest at 0 ppm Si, less important at 300 ppm Si, and least important at 55 ppm. In other words, metabolic pathway appears to affect ligand distribution most importantly at 0 ppm Si and least importantly at 55 ppm Si. From comparisons between Si concentrations, it is apparent that variability in ligand distribution incurred as the result of silica concentration affected ammonium-assimilating cultures most significantly, while nitrate-reducing cultures were least affected by increasing silica concentration. Interestingly, confidence in comparisons between silica concentrations was often higher for total ligand concentrations than for the concentration of one or both ligand classes, in contrast to metabolic comparisons where confidence in total ligand concentrations was generally accompanied by confidence in individual ligand classes. As a re-distribution of ligands between pK_a classes may not affect total ligand concentration, it would appear that the presence of silica at times induced a redistribution of ligands in pK_a space with lesser affect on total ligand concentration. The above observations are generalizations to which exceptions occur in essentially every case, usually with respect to one or more ligand classes, and should be considered preliminary; it is however clear that the interplay between metabolism and geochemical stressor in determining bacterial surface properties is complex.

4.3.5 Trends in ligand distribution

Mean ligand concentrations are plotted for all sodium metasilicate conditions as a function of ligand grouping (acidic, basic, total) and Si concentration in Figure 4-5. For the purposes of this figure (and in contrast to Tukey-Kramer analysis) conditions of 300 ppm NaCl were omitted along with the conditions of 300 ppm Si as particulate silica. The mean ligand concentrations for each condition were plotted, and a linear regression was applied between Si concentration and the corresponding mean ligand concentration. On average, the concentration of acidic ligands decreased with increasing Si concentration with excellent fit to the linear regression ($R^2 = 0.9997$), while the average concentration of basic ligands generally increased with higher Si concentrations ($R^2 = 0.5221$). A plot of the average concentration ratio of acidic to basic ligands vs. Si concentration highlights the covariance; the average ratio of acidic to basic ligands decreases from over 7:1 to nearly 1:1, with good fit ($R^2 = 0.9693$). One major consequence of such ligand pK_a redistribution is the alteration of effective surface charge; as proton-exchanging ligands are the sole providers of effective surface charge on bacterial surfaces under ideal conditions (Fein et al., 2005), the increased concentration of amine functional groups conferring positive charge at pH values below 8 and decreased contribution of ligands contributing negative charge at pH values below 7 (i.e. carboxyl and phosphoryl) will result in neutralization of the inherent negative charge of the Gram-negative cell wall.

On average, the total ligand concentration also decreased with increasing silica concentration ($R^2 = 0.5967$), and growth of *Anabaena* in supersaturated silica solutions resulted in a cell surface that was on average 20% less reactive over the titration range.

The decrease in the degree and density of negative charge on the cyanobacterial surface has important implications for substrate adherence and colloidal attachment. Microbial adhesion is determined over larger (> 1 nm) separation distances by a combination of universally attractive Van der Waals and generally repulsive electrostatic forces, the former of which largely constitutes hydrophobicity, while the latter arises from electrical interactions between

negatively charged bacterial cells and natural surfaces which tend to possess negative charges (Van Loosdrecht et al., 1989). For hydrophobic surfaces, Van der Waals forces will determine bacterial adhesion; however, for more hydrophilic cell surfaces, such as the case for planktonic cyanobacteria (Fattom and Shilo, 1984), electrostatic forces become more influential on the adhesion process (Van Loosdrecht et al., 1987). For instance, Zita and Hermansson (1997) showed a strong correlation between positive charges on the bacterial surface and cell surface hydrophobicity using 6 different strains of *E. Coli*, however their findings remain unconfirmed. The methods utilized in the present study do not allow for conclusions regarding cell surface hydrophobicity, and for the purposes of discussion we assume that hydrophobicity remains unchanged between growth conditions, although this is unlikely the case (Van Loosdrecht et al., 1987; Fattom and Shilo, 1984), and that cells of *Anabaena* are likely hydrophilic, as inferred their planktonic habit of growth (Fattom and Shilo, 1984). The net result of decreasing negative surface charge on the hydrophilic cyanobacterial surface with increasing silica concentration should facilitate attachment to negatively charged surfaces, such as those displayed by particulate and colloidal silica. Walker et al. (2005) similarly indicated that for Gram-negative bacteria, non-specific adhesion is facilitated by changes in cell surface electrical potential and surface charge heterogeneity provided by membrane proteins and lipoproteins.

This trend is not particularly well-suited for the growth of a cyanobacterium in a silicifying solution; lower electrostatic repulsion between negatively-charged silica species and the negatively-charged bacterial surface will promote the adsorption of silica species to the cell surface. As cyanobacteria have been experimentally grown in silicifying solutions at concentrations significantly higher than typically found in natural waters, and have been observed to flourish in silica-depositing geothermal springs (see Konhauser et al., 2004 for review), it is apparent that the adsorption of silica species is not immediately detrimental to many species of cyanobacteria. In fact, the benthic style of growth observed for conditions of 300 ppm Si (as particulate silica) points to an alternative purpose for the modification of ligand distribution; that of surface attachment. As highlighted

by Van Loosdretch et al. (1987), benthic and planktonic bacteria modify their surface properties differently in the face of nutrient stress; benthic bacteria become more hydrophilic, promoting surface detachment and recolonization (Fattom and Shilo, 1984; Malmqvist, 1983; Wrangstadh et al., 1986), while starvation promotes surface attachment amongst planktonic bacteria (Kjelleberg and Hermansson, 1984; Dawson et al., 1981). For planktonic bacteria, it is assumed that attachment to suspended solids will increase mobility and favor recolonization (Van Loosdretch et al., 1987). We consider it likely that the results reported here represent a similar survival strategy on the part of *Anabaena*; the cell is capable of modifying the surface concentration of charge-conferring functional groups in response to geochemical stress in order to facilitate potential transport and recolonization. For a planktonic organism such as *Anabaena*, such a response may be poorly suited to survival in hot spring system rapidly precipitating amorphous silica, and it is likely that surface characterization of cyanobacterial strains more typical of hot spring settings, (i.e. mat-forming *Calothrix* and *Phormidium* species) will reveal alternative strategies for survival during silica encrustation (e.g., production or thickening of sheath material, as indicated by Benning et al. (2004)). Nonetheless, our results indicate that the cell surface is dynamic, where as a consequence of biological demand a cell may modify its surface properties during growth as a function of stressor concentration. While such changes have been previously indicated using hydrophobicity data (see Van Loosdretch, 1987 for summary), we show for the first time that such changes are discernable from potentiometric titration data alone, in such a way that may be accounted for in a surface complexation modeling approach.

4.4 Conclusion

The concentration and pK_a distributions of proton-exchanging ligands on the surface of *Anabaena* sp. strain PCC 7120 were modeled from the potentiometric titration of pure cultures and used to investigate the role of silica as a geochemical stressor determining acid-base properties of the bacterial surface. Experiments were performed using stationary phase cells grown under a variety of dissolved silica concentrations and nitrogen assimilation pathways. It was determined that variability in acid-base surface properties attributable to nitrogen metabolism were greatest at 0 ppm Si, and decreased in importance for conditions both undersaturated and supersaturated with respect to amorphous silica. Cultures grown by ammonium assimilation were most sensitive to the presence of silica in terms of acid-base surface properties, while cultures grown by nitrate reduction were the least sensitive to the presence of silica. On average, ligands with pK_a values between 4 and 7 (ligands typically contributing negative charge at circumneutral pH) decreased in concentration with increasing silica concentration, while ligands with pK_a values between 7 and 10 (including amine functional groups contributing positive charge at circumneutral pH) increased with increasing silica concentration. The total site density decreased with increasing silica concentration, and the net effect of exposure to silicifying solutions during growth is postulated to be facilitated non-specific adhesion. These results indicate that a single bacterial species subtly controls surficial acid-base properties in response to geochemical stressors that are independent of nutrition, and that potentiometric titration may be used to quantify such changes within a thermodynamic framework applicable to surface complexation modeling.

pK_a	4 to 7	7 to 10	Ratio (acidic to basic)	Total
NO_3 0 ppm Si	1.24±0.08	0.30±0.05	4.11	1.55±0.10
NO_3 55 ppm Si	1.58±0.19	0.20±0.05	7.74	1.79±0.20
NO_3 300 ppm Si	1.10±0.08	0.99±0.13	1.10	2.09±0.15
NO_3 300 pm NaCl	2.13±0.15	0.42±0.06	5.05	2.55±0.15
NO_3 300 ppm Si[1]	4.00±0.39	8.26±0.69	0.48	12.25±0.54
N_2 0 ppm Si	2.85±0.49	0.18±0.18	16.19	3.02±0.65
N_2 55 ppm Si	1.93±0.09	0.57±0.11	3.40	2.50±0.18
N_2 300 ppm Si	1.39±0.07	1.97±0.22	0.71	3.36±0.18
NH_4 0 ppm Si	2.18±0.23	1.70±0.10	1.28	3.88±0.31
NH_4 55 ppm Si	2.29±0.12	0.55±0.03	4.14	2.85±0.11
NH_4 300 ppm Si	1.12±0.08	0.69±0.10	1.63	1.81±0.14
Average[2]	1.79±0.10	0.71±0.10	2.54	2.50±0.15

Table 4-1. Modeled ligand concentrations (in mmol per dry g) and pK_a distributions for all conditions tested. Si concentrations describe cultures supplemented with sodium metasilicate unless otherwise noted. Values are the average of five independently modeled titrations. Uncertainties are 1 standard error of the mean.

[1] Si as particulate silica

[2] Average values reported here exclude 300 ppm NaCl and colloidal silica conditions.

ligands with pK_a from 4 to 7

Nitrogen metabolism		NO_3			N_2			NH_4			NO_3
	geochemical stressor	0 ppm Si	55 ppm Si	300 ppm Si	0 ppm Si	55 ppm Si	300 ppm Si	0 ppm Si	55 ppm Si	300 ppm Si	300 ppm NaCl
NO_3	55 ppm Si	0.98									
	300 ppm Si	1.00	0.80								
N_2	0 ppm Si	0.00	0.00	0.00							
	55 ppm Si	0.33	0.97	0.10	0.05						
	300 ppm Si	1.00	1.00	0.99	0.00	0.69					
NH_4	0 ppm Si	0.04	0.53	0.01	0.36	1.00	0.16				
	55 ppm Si	0.01	0.28	0.00	0.64	0.96	0.06	1.00			
	300 ppm Si	1.00	0.85	1.00	0.00	0.13	1.00	0.01	0.00		
NO_3	300 ppm NaCl	0.06	0.66	0.01	0.26	1.00	0.23	1.00	1.00	0.02	
	Average	0.19	0.99	0.03	0.00	1.00	0.63	0.77	0.40	0.04	0.89

ligands with pK_a from 7 to 10

Nitrogen metabolism		NO_3			N_2			NH_4			NO_3
	geochemical stressor	0 ppm Si	55 ppm Si	300 ppm Si	0 ppm Si	55 ppm Si	300 ppm Si	0 ppm Si	55 ppm Si	300 ppm Si	300 ppm NaCl
NO_3	55 ppm Si	1.00									
	300 ppm Si	0.00	0.00								
N_2	0 ppm Si	1.00	1.00	0.00							
	55 ppm Si	0.89	0.54	0.30	0.42						
	300 ppm Si	0.00	0.00	0.00	0.00	0.00					
NH_4	0 ppm Si	0.00	0.00	0.00	0.00	0.00	0.89				
	55 ppm Si	0.92	0.60	0.25	0.48	1.00	0.00	0.00			
	300 ppm Si	0.44	0.15	0.77	0.10	1.00	0.00	0.00	1.00		
NO_3	300 ppm NaCl	1.00	0.97	0.04	0.93	1.00	0.00	0.00	1.00	0.88	
	Average	0.09	0.01	0.32	0.00	1.00	0.00	0.00	0.99	1.00	0.56

All ligands

Nitrogen metabolism		NO_3			N_2			NH_4			NO_3
	geochemical stressor	0 ppm Si	55 ppm Si	300 ppm Si	0 ppm Si	55 ppm Si	300 ppm Si	0 ppm Si	55 ppm Si	300 ppm Si	300 ppm NaCl
NO_3	55 ppm Si	1.00									
	300 ppm Si	0.92	1.00								
N_2	0 ppm Si	0.00	0.04	0.28							
	55 ppm Si	0.26	0.68	0.99	0.93						
	300 ppm Si	0.00	0.00	0.03	1.00	0.40					
NH_4	0 ppm Si	0.00	0.00	0.00	0.40	0.01	0.94				
	55 ppm Si	0.02	0.14	0.60	1.00	1.00	0.94	0.16			
	300 ppm Si	1.00	1.00	1.00	0.05	0.72	0.00	0.00	0.16		
NO_3	300 ppm NaCl	0.19	0.58	0.97	0.97	1.00	0.49	0.02	1.00	0.62	
	Average	0.03	0.25	0.92	0.67	1.00	0.06	0.00	0.96	0.30	1.00

Table 4-2. Confidence intervals in pair-wise comparisons of ligand concentration evaluated by Tukey post-hoc analysis (two-tailed p, n = 11, df = 89).

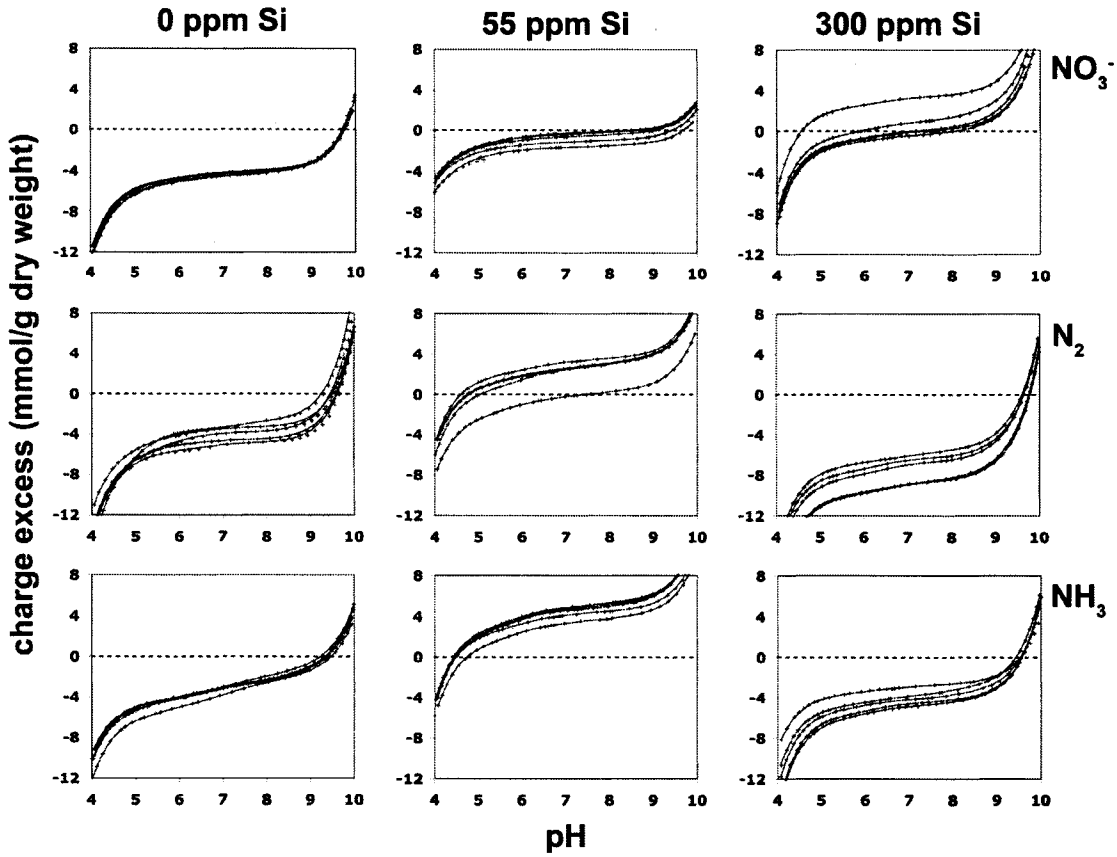

Figure 4-1. The pH dependence of *Anabaena* surface charge excess, plotted as a function of media nitrogen source and silica concentration. Silica was provided as sodium metasilicate, and conditions of 55 ppm Si were approximately saturated with respect to amorphous silica. Conditions of 300 ppm Si were rendered supersaturated with respect to amorphous silica such that the rapid polymerization of silica occurred during growth. For each condition, data points represent charge excess data from five replicate titrations, and smooth curves represent charge excess as fit by discrete ligand modeling.

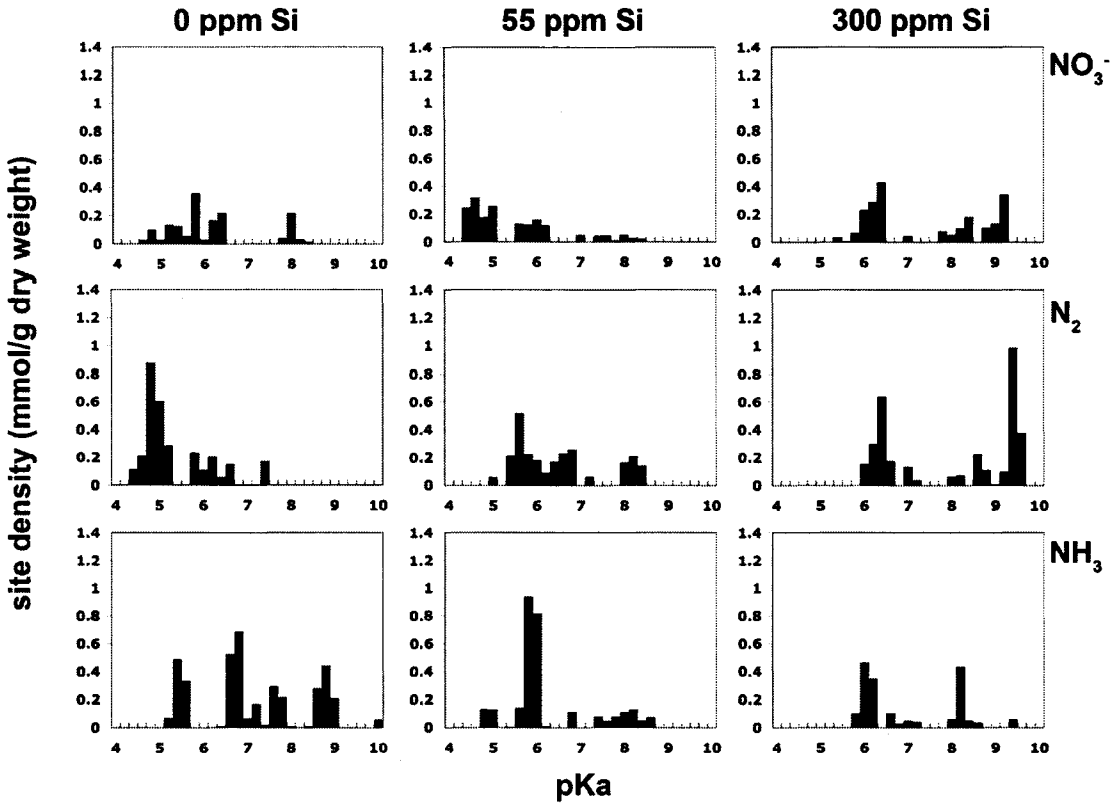

Figure 4-2. Modeled ligand distributions grouped as a function of media nitrogen source and silica concentration. Silica conditions correspond to those describe for Figure 1. Each plot accounts for five replicate titrations, with ligand concentrations weighted by occurrence at each pK_a interval.

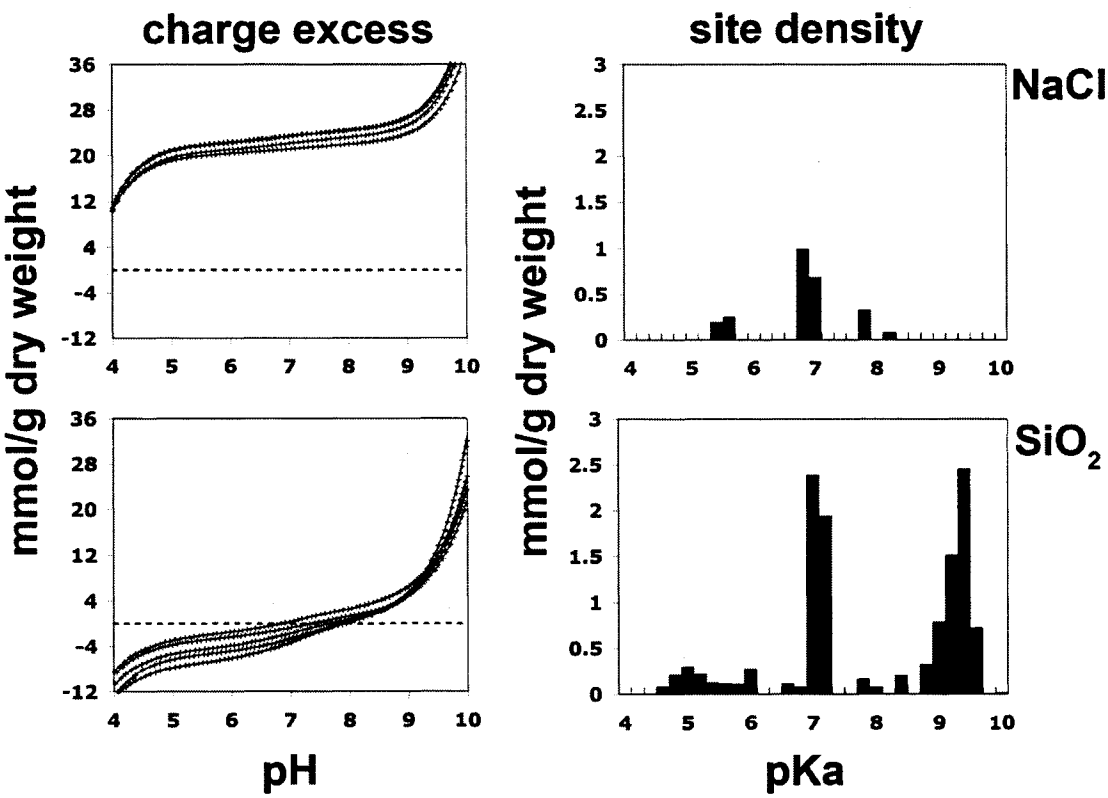

Figure 4-3. Plots of charge excess and corresponding modeled ligand distributions for *Anabaena* grown under nitrate-reducing conditions with 300 ppm NaCl and 300 ppm Si as particulate silica. Both measured (data points) and fitted (smooth curves) charge excess is presented for five replicates, and ligand distributions are weighed by occurrence and compounded over five replicates.

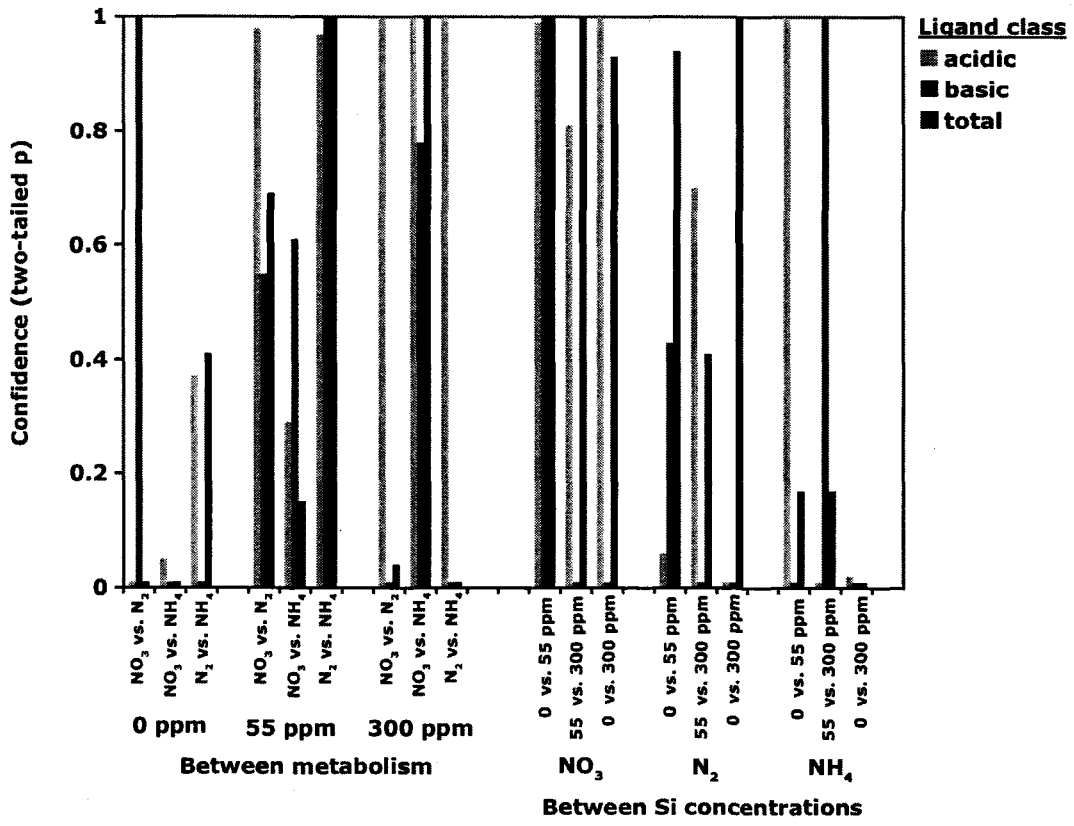

Figure 4-4. Confidence intervals in multiple pair-wise comparisons of ligand concentration, plotted as a function of comparison type: between-metabolism comparisons grouped as a function of Si concentration (left) and between-Si concentration comparisons grouped as a function of nitrogen metabolism (right).

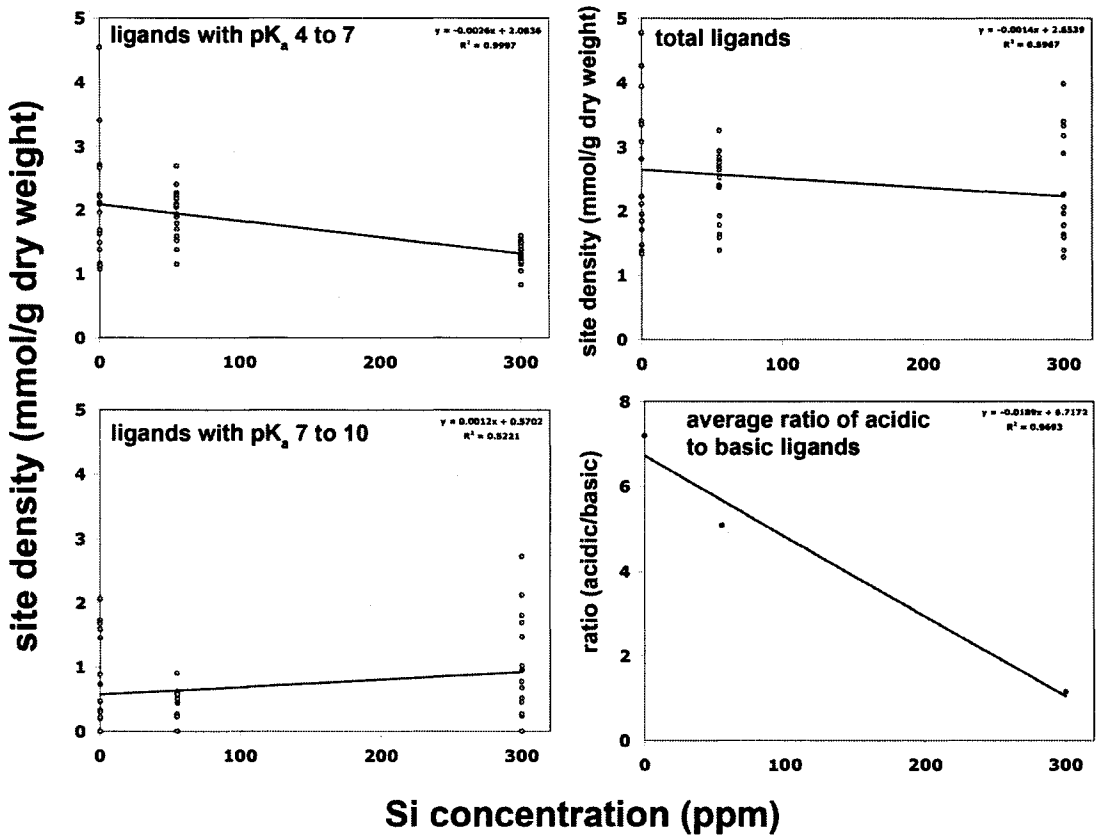

Figure 4-5. Average ligand concentrations as a function of ligand class and Si concentration. Also plotted is the average ratio of acidic to basic ligands as function of Si concentration. Grey points represent average ligand concentrations for individual conditions (n=5 at each point) and dark points represent the overall average ligand concentration at that Si concentration (n=15 at each point). Conditions of 300 ppm NaCl and 300 ppm Si as particulate silica are omitted.

4.5 References

Apte SK and Haselkorn R (1990) Cloning of salinity stress-induced genes from the salt-tolerant nitrogen-fixing cyanobacterium *Anabaena torulosa*. *Plant Molecular Biology* 15, 723–733.

Apte SK and Bhagwat AA (1989) Salinity-stress-induced proteins in two nitrogen-fixing *Anabaena* strains differentially tolerant to salt. *Journal of Bacteriology* 171, 909–915.

Baughman GL and Paris DF (1981) Microbial bioconcentration of organic pollutants from aquatic systems – a critical review. *Critical Reviews in Microbiology* 8, 205-228.

Bayer ME and Sloyer Jr. JL (1990) The electrophoretic mobility of gram-negative and gram-positive bacteria: an electrokinetic analysis. *Journal of General Microbiology* 136, 867-874.

Benning LG, Phoenix VR, Yee N, and Konhauser KO (2004) The dynamics of cyanobacterial silicification: an infrared micro-spectroscopic investigation. *Geochimica et Cosmochimica Acta* 68, 743–757.

Beveridge TJ, Forsberg CW, and Doyle RJ (1982) Major sites of metal binding in *Bacillus licheniformis* walls. *Journal of Bacteriology* 150, 1438-1448.

Beveridge TJ and Murray RG (1980) Sites of metal deposition in the cell wall of *Bacillus subtilis*. *Journal of Bacteriology* 141, 876-887.

Borrok D, Fein JB, Tischler M, O'Loughlin E, Meyer, H, Liss M, and Kemner KM (2004) The Effect of Acidic Solutions and Growth Conditions on the Adsorptive Properties of Bacterial Surfaces. *Chemical Geology* 209, 107-109.

Boyanov MI, Kelly SD, Kemner KM, Bunker BA, Fein JB, and Fowle DA (2003) Adsorption of cadmium to *B. subtilis* bacterial cell walls - a pH-dependent XAFS spectroscopy study. *Geochimica et Cosmochimica Acta* 67, 3299-3311.

Brassard P, Kramer JR, and Collins PV (1990) Binding site analysis using linear programming. *Environmental Science and Technology* 24, 195-201.

Chamot, D and Owttrim, GW (2000) Regulation of cold shock-induced RNA helicase gene expression in the cyanobacterium *Anabaena* sp. strain PCC 7120. *Journal of Bacteriology* 182, 1251-1256.

Corapcioglu MY and Kim S (1995) Modeling facilitated contaminant transport by mobile bacteria. *Water Resources Research* 31, 2693-2648.

Cox JS, Smith DS, Warren LA, and Ferris FG (1999) Characterizing heterogeneous bacterial surface functional groups using discrete affinity spectra for proton binding. *Environmental Science and Technology* 33, 4514–4521.

Daughney CJ and Fein JB (1998) The effect of ionic strength on the adsorption of H^+, Cd^{2+}, Pb^{2+}, and Cu^{2+} by *Bacillus subtilis* and *Bacilllus licheniformis*: A surface complexation model. *Journal of Colloid and Interface Science* 198, 53-77.

Daughney CJ, Fein JB and Yee, N (1998) A comparison of the thermodynamics of metal adsorption onto two common bacteria. *Chemical Geology* 144, 161-176.

Daughney CJ, Fowle DA, and Fortin DE (2001) The effect of growth phase on proton and metal adsorption by *Bacillus subtilis. Geochimica et Cosmochimica Acta* 65, 1025-1035.

Fein JB, Boily JF, and Yee, N (2004) Potentiometric titrations of *Bacillus subtilis*

cells to low pH and a comparison of modeling approaches. *Geochimica et Cosmochimica Acta* 69, 1123-1132.

Dawson MP, Humphrey BA, and Marshall KC (1981) Adhesion: a tactic in the survival strategy of marine *vibrio* during starvation. *Current Microbiology* 6, 195-199.

Fattom A and Shilo M (1984) Hydrophobicity as an adhesion mechanism of benthic cyanobacteria. *Applied and Environmental Microbiology* 47, 135-143.

Fein JB and Delea DE (1999) Experimental study of the effect of EDTA on Cd adsorption by *Bacillus subtilis*: a test of the chemical equilibrium approach. *Chemical Geology* 161, 375-383.

Fein JB, Boily J-F, Yee N, Gorman-Lewis D, and Turner, BF (2005) Potentiometric titrations of *Bacillus subtilis* cells to low pH and a comparison of modeling approaches. *Geochimica et Cosmochimica Acta.* 69, 1123-1132.

Fortin D, Ferris FG, and Beveridge TJ (1997) Surface-mediated mineral development by bacteria. In: JF Banfield and KH Nealson (eds), *Geomicrobiology: Interactions Between Microbes and Minerals. Reviews in Mineralogy and Geochemistry* 35, pp. 161-180, Mineralogical Society of America, Washington, DC.

Fowle DA and Fein JB (1999) Competitive adsorption of metal cations onto two gram positive bacteria: testing the chemical equilibrium model. *Geochimica et Cosmochimica Acta* 63, 3059-3067.

Haas JR, Dichristina TJ, and Wade Jr. R (2001) Thermodynamics of U(VI) sorption onto *Shewanella putrefaciens. Chemical Geology* 180, 33-54.

Haas, JR (2004) Effects of cultivation conditions on acid-base titration properties of *Shewanella putrefaciens*. *Chemical Geology* 209, 67-81.

Harris DC (1995) *Quantitative Chemical Analysis*. Freeman, New York, NY.

Hsu JC (1996) *Multiple Comparisons. Theory and Methods*. Chapman and Hall, London, England.

Iler RK (1979) *The Chemistry of Silica: Solubility, Polymerization, Colloidal and Surface Properties, and Biochemistry of Silica*. John Wiley and Sons, New York, NY.

Jiang W, Saxena A, Song B, Ward BB, Beveridge TJ, and Myneni SCB (2004) Elucidation of functional groups on Gram-positive and Gram-negative bacterial surfaces using infrared spectroscopy. *Langmuir* 20, 11433-11442.

Kelly SD, Kemner KM, Fein JB, Fowle DA, Boyanov MI, Bunker BA, and Yee N (2002) X-ray absorption fine-structure determination of pH dependent U-bacterial cell wall interactions. *Geochimica et Cosmochimica Acta*, 66, 3875-3891.

Kjelleberg, S and Hermansson M (1984) Starvation-induced effects on bacterial surface characteristics. *Applied and Environmental Microbiology* 48, 497-503.

Kobayashi M, Juillerat F, Galletto P, Bowen P, and Borkovec M (2005) Aggregation and charging of colloidal silica particles: effect of particle size. *Langmuir* 21, 5761-5769.

Konhauser KO, Fyfe WS, Ferris FG, and Beveridge TJ (1993) Metal sorption and precipitation by bacteria in two Amazonian river systems: Rio Solimoes and Rio Negro, Brazil. *Geology* 21, 1103-1106.

Konhauser KO, Jones B, Phoenix VR, Ferris G, and Renaut RW (2004) The Microbial Role in Hot Spring Silicification. *Ambio.* 33, 552-558.

Konhauser KO (2006) *Introduction to Geomicrobiology.* Blackwell Scientific Publications, Oxford, England.

Lalonde SV, Smith DS, Owttrim GW, and Konhauser KO (submitted) Acid-base properties of cyanobacterial surfaces I: influences of growth phase and nitrogen metabolism on cell surface reactivity. *Submitted to Geochimica et Cosmochimica Acta 03/2006, manuscript W4104.*

Lindgvist R and Enfield CG (1992) Cell density and non-equilibrium sorption effects on bacterial dispersal in ground water microcosms. *Microbial Ecology* 24, 25-41.

Madigan MT, Martinko JM, and Parker J (1997) *Brock Biology of Microorganisms.* 8th ed. Prentice Hall, Upper Saddle River, NJ.

Malmqvist T (1983) Bacterial hydrophobicity measured as partition of palmitic acid between the two immiscible phases of cell surface and buffer. *Acta Pathol Microbiol. Immunol. Scand. Sect. B.* 91, 69-73.

Marin K, Kanesaki Y, Los DA, Murata N, Suzuki I, and Hagemann M (2004) Gene expression profiling reflects physiological processes in salt acclimation of *Synechocystis* sp. strain PCC 6803. *Plant Physiology* 136, 3290-3300.

Martell AE and Smith RM (1977) *Critical stability constants.* Plenum Press, New York, NY.

Martinez RE and Ferris FG (2001) Chemical equilibrium modeling techniques for the analysis of high-resolution bacterial metal sorption data. *Journal of Colloid and Interface Science* 243, 73-80.

Martinez RE, Smith DS, Kulczycki E, and Ferris FG (2002) Determination of intrinsic bacterial surface acidity constants using a Donnan shell model and a continuous pKa distribution method. *Journal of Colloid and Interface Science* 253, 130-139.

McCarthy JF and Zachara JM (1989) Subsurface transport of contaminants. *Environmental Science and Technology*. 23, 496-502.

Phoenix VR, Adams DG, and Konhauser KO (2000) Cyanobacterial viability during hydrothermal biomineralization. *Chemical Geology* 169, 329-338.

Phoenix VR, Martinez RE, Konhauser KO and Ferris FG (2002) Characterization and implications of the cell surface reactivity of the cyanobacteria *Calothrix* sp. *Applied and Environmental Microbiology* 68, 4827-4834.

Putney, LK, Denker, SP, and Barber, DL (2002) The changing face of the Na^+/H^+ exchanger, NHE1: structure, regulation, and cellular actions. *Annual Review of Pharmacology and Toxicology* 42, 527-552.

Rippka R, Deruelles J, Waterbury JB, Herdman M, and Stanier RY (1979) Generic assignments, strain histories and properties of pure cultures of cyanobacteria. *Journal of General Microbiology* 111, 1-61.

Sander M, Lu Y, and Pignatello JJ (2005) A Thermodynamically Based Index for Quantifying True Sorption Hysteresis. *Journal of Environmental Quality* 34, 1063-1072.

Sander M, Lu Y, and Pignatello JJ (2006) Conditioning-Annealing Studies of Natural Organic Matter Solids Linking Irreversible Sorption to Irreversible Structural Expansion. *Environmental Science and Technology* 40, 170-178.

Smith DS, Adams NWH, and Kramer JR (1999) Resolving uncertainty in chemical speciation determinations. *Geochimica et Cosmochimica Acta* 63, 3337-3347.

Smith, DS and Kramer JR (1999) Multi-site proton interactions with natural organic matter. *Environment International* 25, 307-314.

van Loosdretch MCM, Lyklema J, Norde W, and Zehnder AJB (1989) Bacterial adhesion: a physicochemical approach. *Microbial Ecology* 17, 1-15.

van Loosdrecht MCM, Lyklema J, Norge W, Schraa G, and Zehnder AJB (1987) Electrophoretic mobility and hydrophobicity as a measure to predict the initial steps of bacterial adhesion. *Applied and Environmental Microbiology* 53, 1898-1901.

Vadillo-Rodriguez V, Busscher HJ, Norde W, de Vries J, and van der Mei HC (2004) Relations between macroscopic and microscopic adhesion of *Streptococcus mitis* strains to surfaces. *Microbiology* 150,1015-1022.

Waditee R, Hibino T, Tanaka Y, Nakamura T, Incharoensakdi A, and Takabe T (2002) Overexpression of Na^+/H^+ antiporter confers the salt tolerance of freshwater cyanobacterium capable of growth in sea water. *Proceedings of the Natural Academy of Sciences of the USA* 99, 4109-4114.

Walker SL, Hill JE, Redmon JA, and Menachem E (2005) Influence of growth phase on adhesion kinetics of *Escherichia coli* D21g. *Applied and Environmental Microbiology* 71, 3093-3099.

Warren LA and Ferris FG (1998) Continuum between sorption and precipitation of Fe(III) on microbial surfaces. *Environmental Science and Technology* 32, 2331–2337.

Wrangstadh M, Conway PL, and Kjelleberg S (1986) The production of an extracellular polysaccharide during starvation of a marine *Pseudomonas* sp. and the effect thereof on adhesion. *Archives of Microbiol*ogy 14, 220-227.

Zita A and Hermansson M (1997) Effects of bacterial cell surface structures and hydrophobicity on attachment to activated sludge flocs. *Applied and Environmental Microbiology* 63, 1168–1170.

Chapter 5

Summary

Fossils in the form of silicified microbes provide some of the oldest physical evidence for life on Earth, yet the molecular mechanisms underpinning the silicification process are poorly understood. Of particular interest are species-specific rates of silicification, indicated by previous laboratory investigations (see Chapter 1), that may give rise to preservational biases in the rock record. In order to better understand the inorganic and organic chemical basis for such species-specificity, laboratory silicification experiments were performed using both thermophilic *Aquificales* and mesophilic cyanobacterial genera.

As outlined in Chapter 2, *Sulfurihydrogenibium azorense*, a thermophilic, chemolithoautotrophic member of the deeply-branching bacterial order *Aquificales* was chosen for study due to its unique phylogenetic position,

metabolic capabilities, biofilm-forming habit, and propensity to live in hydrothermal waters rich in mineralizing agents. Batch culture silicification experiments revealed that:

(1) whether dead or actively metabolizing, *S. azorense* had a negligible affect on the rate and extent of monomeric silica polymerization under all conditions studied,

(2) during growth by hydrogen-oxidation, up to 7% of the total silica was immobilized from solution in the form of large silica polymers and colloids,

(3) the extensive EPS matrix produced under conditions of H_2-oxidation were compositionally rich in surface amine functional groups conferring positive charge to this biological interface, and that these functional groups were likely responsible for the silica sorptive capacity observed for this organism,

(4) minimal EPS production, and correspondingly, negligible silica adsorption, occurred under conditions of elemental sulfur oxidation,

(5) cells of *S. azorense* remained viable in culture media containing 300 ppm Si, and responded to increasing media silica concentration by entering exponential phase more rapidly, and attaining higher soluble protein concentrations.

Together, these results establish metabolic pathway as a factor affecting the silicification process of a single bacterial species, and thus as a variable potentially responsible, to some degree, for species-specific silicification patterns. Furthermore, the results have strong implications for preservation bias in the rock record, demonstrating for the first time that metabolically versatile bacterial species such as *S. azorense* may have organic structures that are better preserved under conditions more conducive to one metabolic pathway over another, and

given the fact that the cell itself is not silicified, only the biofilm would be retained in the rock record.

As discussed in Chapter 2, metabolic specificity in the silicification process is unlikely to have been the result of metabolic reactions affecting the bulk media or cell-microenvironment chemistry, but rather appears to be the result of differential EPS production by this bacterium when grown under different culture conditions. It is clear from Chapter 2 that the surface chemistry of the bacterial interface in question (EPS in the case of Chapter 2) is an important determinant in the initial stages of microbe-mineral interaction. In order to further explore the ability for a single bacterial species to modify the surface chemical properties of its own solid-liquid interface over short (non-evolutionary) timescales, a bacterial system of less complicated surface composition was required.

The cyanobacterium *Anabaena* sp. strain PCC 7120 was selected for its exposed Gram-negative cell wall (i.e., free of extracellular surface layers such as EPS), metabolic versatility, ease of culture, and available genomic data. In order to fully understand the dynamic nature of this organism's surface chemistry, special consideration of batch culture growth conditions was first required. Chapter 3 examines, by potentiometric titration, variations in cell surface chemistry that arise over the course of the batch culture life cycle, and as a function of the three nitrogen acquisition pathways available to this organism. The surface chemical parameters averaged over all conditions investigated are statistically evaluated in a pair-wise manner for their ability to describe the parameters obtained for each condition, and it was found that the average surface chemical parameters are inadequate for the accurate description of this microbial surface. In other words, sufficient variability in cell surface chemistry may arise as a function of this organism's batch culture growth conditions as to warrant separate surface chemical descriptions that are specific to each growth condition. Chapter 3 confirms that variations in cell surface reactivity may indeed arise as a function of metabolic pathway by evaluating and reporting such variations in a quantitative surface chemical framework directly applicable to surface

complexation modeling efforts. It is clear from the data presented in Chapter 3 that the experimental study of biomineralization may be optimized by the use of cultured biomass whose cell surface properties have been carefully considered in light of potential growth conditions.

The cell surface chemistry of *Anabaena* sp. was further evaluated after growth in the presence of various geochemical stressors (NaCl, particulate SiO_2, H_4SiO_4), and as a function of nitrogen source, in Chapter 4. Cell cultures were grown in both silica-undersaturated and silica-supersaturated culture media, the latter of which was neutralized immediately prior to inoculation such that monosilicic acid condensed to precipitate colloidal silica on and around the growing cells. Surface chemical parameters were assessed by potentiometric titration, statistically evaluated for confidence between conditions in a pair-wise manner, and analyzed independently as functions of silica concentration and nitrogen source. It was determined that at high (300 ppm Si) silica concentrations, surface chemical differences arising as a consequence of nitrogen source become small to insignificant, and specific patterns emerge in the distribution of cell surface functional groups. At high silica concentration, low pK_a functional groups, responsible for the bulk of the negative-charge on the bacterial surface at circumneutral pH, decrease in surface concentration, while high pK_a functional groups, typically conferring positive-charge to the bacterial surface, increase in concentration. Furthermore, the average total site density decreases by ~20% as the result of growth in silica-supersaturated solution.

In this Chapter, biological response of *Anabaena* sp. to the silicification processes is quantified in chemical terms that are directly applicable surface complexation theory, and allow for the results to be interpreted within prevailing physico-chemical models. In this regard, decreased anionic surface charge and total charge density will promote facilitated, non-specific surface adhesion and inhibit metal cation adsorption. In a broader scope, the results of Chapter 4 emphasize a characteristic of microbial life that has been largely ignored to date, that being the ability of a bacterium to modify the chemical composition of its own surface, over several generations, as a survival strategy. Previous studies of

microbial surface chemistry relying on a paradigm of unwavering surface chemical parameters may need reassessment.

The aim of this project was to investigate the nature of the microbial surface as it pertains to silicification, and inextricably, to biomineralization as a whole. After the silicification experiments detailed in Chapter 2, it became apparent that the biological surfaces upon which biomineralization reactions such as silicification occur are in fact dynamic in chemical composition. In follow-up experiments detailed in Chapters 3 and 4, this dynamic nature was evaluated in a quantitative framework pertinent not only to the study of silicification, but also to the study of biomineralization at large. The research conducted during this MSc program reveals the complexity of microbe-metal-mineral interactions, and highlights the need to fully consider how the cell might respond to varying environmental conditions. In this regard, previous assumptions made for Precambrian fossils, based solely on a few experimental studies, will have no doubt led to misinterpretations of the palaeoenvironmental conditions in which the ancient species grew.

Appendix 1: Matlab script developed for the discrete site modeling of potentiometric titration data by linear programming

----- start script -----

```
clc;
clear;
format long;
warning off MATLAB:divideByZero;
disp 'Welcome to pKa Spectrum Titration Cruncher v1.0';
disp 'By Stefan Lalonde, University of Alberta, 10/21/05';
disp 'Linear Programming Optimization courtesy of Scott Smith, Wilfred Laurier
University';

%nomenclature
%"org"b,pH,etc - original data preserved through any selection criteria
%"std"b,pH,etc - standardized to dry weight

%set figure preferences
set(0,'defaultaxesfontsize',14);
set(0,'defaultlinelinewidth',2);

% Data Preparation - select and read input file, input concentrations and weights,
% and calculate excess charge (b) from raw titration data

disp ' ';
filename = input('filename: ','s');
%weightinitial=input('initial weight (g): ');
KNO=input('KNO3 (g): ');
%BAC=input('Bac. suspension (g): ');
weightinitial=KNO;
dryweight= input('dry weight (g): ');
%set titration direction (up or down)
%direction = input('direction (u/d):','s');
direction = 'u';
Kw=1e-14;
%set MW of titrant and buffer (buffer=initial addition of acid/base)
%we use NaOH (MW=40) and HNO3 (MW=63)
if direction=='u',
        MWbuffer=63;
        MWtitrant=40;
        %molesbufferadded=input ('moles H+ added at start: ');
```

```
        molesbufferadded=0.00000;
        weightbufferadded=0.00;
        else
        MWbuffer=40;
        MWtitrant=63;
        weightbufferadded=0;
        molesbufferadded=0;
end
MWelectrolyte=101.11; conc=0.01;
%MWelectrolyte = input('electolyte MW: ');
%conc = input('conc: ');

%read raw data file OR...(see next paragraph)
%add additional %q and corresponding variable as needed to textread raw data
file
%[SampleID,Vol,pH]=textread(filename,'%q %q
%q','whitespace','','delimiter',',','headerlines',1);
%filename=strrep(filename,'.TXT','');
%SampleID=char(SampleID); %Vol=char(Vol); %pH=char(pH);
%Vol=str2num(Vol); %pH=str2num(pH);

% ...open excel data from dataholder.txt
[Vol,pH]=textread('dataholder.txt','%s %s');
Vol=char(Vol); pH=char(pH); clear temp;
Vol=str2num(Vol); pH=str2num(pH);
SampleID=[];

%calculate weights
%titrant and buffer are added by volume, so total weight should include weight of
their dissolved constituents
molestitrantadded=(conc*(Vol/1000));
weightinitial=(weightinitial/1000)+weightbufferadded;
weightwater=Vol/1000;
weighttotal=weightinitial+weightwater+weightbufferadded+(molestitrantadded*
MWtitrant/1000)+(molesbufferadded*MWbuffer/1000);
conctitrant=(molestitrantadded./weighttotal);
concbuffer=(molesbufferadded./weighttotal);

orgpH=pH;
low=4;
up=10;
conctitrant(pH>up)=[];
pH(pH>up)=[];
conctitrant(pH<low)=[];
pH(pH<low)=[];
```

```
%charge balance
H=10.^(-1*pH);
OH=(Kw*ones(size(H)))./H;

% calculate b and force b=0 at start (or end in the case of down titration) if
desired
if direction=='d',
        concbuffer=0;
        b=conctitrant-concbuffer+H-OH;
        %force zero
        b=-1*b+b(size(b,1),:);
        else
        concbuffer=0;
        b=conctitrant-concbuffer-H+OH;
        %force zero
        b=b-b(1,1);
end

% automated data selection - either by pH range or by 1st deriv. filter

% Select data based on first derivative of b (and calculate first deriv. stdorgb)
% format: db/dpH = (b2-b1)/(pH2-pH1), plotted at (pH1+pH2)/2
u=1:(size(pH,1)-1); u=u';
v=2:(size(pH,1)); v=v';
deriv(u,1)=(b(v,1)-b(u,1))./(pH(v,1)-pH(u,1));
derivpH(u,1)=(pH(v,1)+pH(u,1))/2;

%preserve original values and standardize some values
orgb=b;
stdorgb=orgb./dryweight;
stdderiv(u,1)=(stdorgb(v,1)-stdorgb(u,1))./(pH(v,1)-pH(u,1));

% Derivative criteria:
%derivcut=input('1st derivative cutoff: ');
derivcut=-.00015;
abs_derivcut=abs(derivcut);
abs_deriv=abs(deriv);
abs_stdderiv=abs_deriv/dryweight;

% cut last points on pH, b, and H to make deriv same size (preserving original
pH,H as org)

b(size(b,1),:)=[];
pH(size(pH,1),:)=[];
H(size(H,1),:)=[];
```

```
% cut b, H, and pH for deriv criteria
%b(abs_deriv>abs_derivcut)=[];
%pH(abs_deriv>abs_derivcut)=[];
%H(abs_deriv>abs_derivcut)=[];


% or

% cut b, H, pH for low<pH<up
low=4;
up=10;

b(pH>up)=[];
H(pH>up)=[];
pH(pH>up)=[];
H(pH<low)=[];
b(pH<low)=[];
pH(pH<low)=[];

% remove values with negative 1st derivatives (which indicates major problems,
ie. bumped electrode, etc!)
%b(deriv<0)=[];
%H(deriv<0)=[];
%pH(deriv<0)=[];


% Dr. Scott Smith's pKa spectrum linear programming model

% this will take data and fit it to Lts given a fixed
% pKas distribution

% set pKa range and interval
%lowend=input('lowest pKa: ');
%highend=input('highest pKa: ');
%interval=input('interval: ');
%lowend=round(min(pH)); highend=round(max(pH)); interval=.2;
%pKas=[lowend:interval:highend];
pKas=[3:.2:11];


% now a nested loop of size i and j to make matrix A of alphas
% and make vector b of values to be fit = charge excess

K=10.^(-1*pKas);
```

```
for i=1:size(pH,1)
   for j=1:size(pKas,2)
      A(i,j)=K(j)/(K(j)+H(i));
   end
end

[m,n]=size(A);

% now setup the dual problem as in Kramer and Brassard 1992

Ad=[A' 0.5*diag(ones(1,n))];
Ad(size(Ad,1)+1,:)=[ones(1,size(A',2)) zeros(1,n)];

bd=.5*sum(A); bd(size(bd,2)+1)=m/2;

fd=[-1*b' zeros(1,n)];

vlb=zeros(size(fd)); %vub=1*ones(size(fd));
vub=[];

N=length(bd);

Aeq = Ad(1:N,:);
beq = bd(1:N);
Ad = Ad(N+1:end,:);
bd = bd(N+1:end,:);

[X,FVAL,EXITFLAG,OUTPUT,LAMBDA]=linprog(fd,Ad,bd,Aeq,beq,vlb,vub,[
]);

solv=LAMBDA.eqlin(1:N-1);
Canc=-1*LAMBDA.eqlin(N);

% also calculate error
bcalc=A*solv-Canc;
err=bcalc-b;

% end Dr. Scott Smith's linear program model

% standardize by dry weight for output
stdb=b/dryweight;
stdorgb=orgb/dryweight;
stdbcalc=bcalc/dryweight;
stdsolv=solv/dryweight;
stderr=err/dryweight;
stdCanc=Canc/dryweight;
```

```
%sum ligands over 4-10 range
stdtotal=sum(stdsolv(6:36));

%print modeled results as desired
%stdsolv
%stdCanc

% observed (calc) and modeled (model) buffering capacity
% do this for all ligands (set by y) as well as ligands in range of interest (set by z)
calcbuffcap=stdderiv;
calcbuffcappH=derivpH;
%calcbuffcap(abs_deriv>abs_derivcut)=[];
%calcbuffcappH(abs_deriv>abs_derivcut)=[];
clear ligandbuffcap modelbuffcap sumligandbuffcap
for x=(1:size(H,1));
        for y=(1:size(pKas,2));
                for z=(6:36);
                        ligandbuffcap1(x,y)=((10.^(-
pKas(1,y))).*stdsolv(y,1).*H(x,1))./(((10.^(-pKas(1,y)))+H(x,1)).^2);
                        sumligandbuffcap1=sum(ligandbuffcap1')';

        modelbuffcap(x,1)=2.3.*(H(x,1)+(Kw/H(x,1))+(sumligandbuffcap1(x,1)))
;
% do this for pKa range specified by z (rangebuffcap) - ie. eliminate dubious
ligands
                        ligandbuffcap2(x,z)=((10.^(-
pKas(1,z))).*stdsolv(z,1).*H(x,1))./(((10.^(-pKas(1,z)))+H(x,1)).^2);
                        sumligandbuffcap2=sum(ligandbuffcap2')';

        rangebuffcap(x,1)=2.3.*(H(x,1)+(Kw/H(x,1))+(sumligandbuffcap2(x,1)));
                end
        end
end

%convert some units and determine some ranges for plots
calcbuffcap=calcbuffcap*1000;
modelbuffcap=modelbuffcap*1000;
rangebuffcap=rangebuffcap*1000;
rangebuffcappH=pH;
rangebuffcappH(rangebuffcappH>10)=[];
buffplotmax=calcbuffcap;
buffplotmax(derivpH>10)=[];
plotmaxpH=derivpH; plotmaxpH(derivpH>10)=[];
buffplotmax(plotmaxpH<4)=[]; clear plotmaxpH;
rangebuffcap(pH>10)=[];
rangebuffcap(rangebuffcappH<4)=[];
```

```
rangebuffcappH(rangebuffcappH<4)=[];

% plot data
figure(1); plot (Vol,orgpH,'.'); title(['Titration curve - ',
filename],'FontSize',16,'FontWeight','bold'); xlabel('titrant added
(ml)','FontSize',16,'FontWeight','bold');
ylabel('pH','FontSize',16,'FontWeight','bold'); figure(1);
figure(2); plot(derivpH,deriv,'x',pH,b,'.',pH,b); axis([4 10 min(orgb)
max(orgb)]);title(['Data selection and first derivative - ',
filename],'FontSize',16,'FontWeight','bold'); ylabel('b and db/dpH (mol/dry g and
per pH)','FontSize',16,'FontWeight','bold');
xlabel('pH','FontSize',16,'FontWeight','bold');figure(2);
figure(3); plot(pH,stdb,'.',pH,stdbcalc); title(['Measured and Fitted Charge Excess
- ', filename],'FontSize',16,'FontWeight','bold'); ylabel('charge excess (mol/dry
g)','FontSize',16,'FontWeight','bold');
xlabel('pH','FontSize',16,'FontWeight','bold');figure(3);
figure(4); bar(pKas,stdsolv); axis([3 11 min(stdsolv) max(stdsolv)]); title(['pKa
distribution - ', filename],'FontSize',16,'FontWeight','bold'); ylabel('site
concentration (mol/dry g)','FontSize',16,'FontWeight','bold');
xlabel('pKa','FontSize',16,'FontWeight','bold');figure(4);
figure(8); bar(pKas,stdsolv); axis([4 10 min(stdsolv) max(stdsolv(6:36,:))]);
title(['pKa distribution - ', filename],'FontSize',16,'FontWeight','bold'); ylabel('site
concentration (mol/dry g)','FontSize',16,'FontWeight','bold');
xlabel('pKa','FontSize',16,'FontWeight','bold');figure(8);
figure(5); plot(pH,stdb,'.',pH,stdbcalc); axis([4 10 (min(stdorgb))
(max(stdorgb))]); title(['Measured and Fitted Charge Excess - ',
filename],'FontSize',16,'FontWeight','bold'); ylabel('charge excess (mol/dry
g)','FontSize',16,'FontWeight','bold');
xlabel('pH','FontSize',16,'FontWeight','bold');figure(5);
figure(6); plot(pH,stderr,'.'); title(['Modeled Charge Relative Error - ',
filename],'FontSize',16,'FontWeight','bold'); ylabel('error (moles/L per dry
g)','FontSize',16,'FontWeight','bold');
xlabel('pH','FontSize',16,'FontWeight','bold');figure(6);
figure(7);
plot(calcbuffcappH,calcbuffcap,'.',pH,modelbuffcap,rangebuffcappH,rangebuffca
p,'o'); axis([4 10 min(rangebuffcap) max(buffplotmax)]);title(['Measured and
Modeled Buffer capacity - ', filename],'FontSize',16,'FontWeight','bold');
ylabel('db/dpH (mmol/pH per dry g)','FontSize',16,'FontWeight','bold');
xlabel('pH','FontSize',16,'FontWeight','bold');figure(7);

% save output to .mat and .txt file
% all variables must be row vectors for output
% all strings must be one row large
% no structures or cell arrays
SampleID=[];
pKas=pKas';
```

```
clear LAMBDA OUTPUT i j;
save (['data_',filename,'.mat'],
'stdtotal','pH','orgb','b','bcalc','pKas','SampleID','calcbuffcappH','calcbuffcap','mod
elbuffcap','rangebuffcap','stdorgb','stdsolv','stdb','stdbcalc','stderr','stdderiv','stdCan
c','weightwater','weighttotal','weightbufferadded','Vol','H','OH', 'Canc', 'err',
'MWbuffer', 'deriv', 'derivcut', 'derivpH', 'direction', 'filename', 'weightinitial',
'molesbufferadded', 'molestitrantadded', 'orgpH', 'solv', 'MWtitrant', 'MWbuffer',
'MWelectrolyte');
save ('datatemp.mat',
'pH','pKas','SampleID','stdtotal','calcbuffcappH','calcbuffcap','modelbuffcap','rang
ebuffcap','stdorgb','stdsolv','stdb','stdbcalc','stderr','stdderiv','stdCanc','weighttotal','
Vol','H','err','derivcut','derivpH','direction', 'filename', 'orgpH', 'solv');
disp 'Exporting Data:';
disp ' ';
save_ascii(['datatemp.mat'],['out_',filename,'.txt'],'%22.20f',',');


% save some .ps graphs
print ('-f1', '-deps2', ['titratecurve_',filename,'.ps']);
print ('-f2', '-deps2', ['derivcut_',filename,'.ps']);
print ('-f4', '-deps2', ['pKaspectrum_',filename,'.ps']);
print ('-f5', '-deps2', ['bfit_',filename,'.ps']);
print ('-f6', '-deps2', ['err_',filename,'.ps']);
print ('-f7', '-deps2', ['buffcap_',filename,'.ps']);
print ('-f8', '-deps2', ['centralpKas_',filename,'.ps']);

% fini
```

----- **end script** -----